

UNIVERSIDAD DE SALAMANCA

Departamento de Ingeniería Cartografía y del terreno



**VNiVERSiDAD
DE SALAMANCA**

TESIS DOCTORAL

Aplicación de métodos de Correlación Digital de Imágenes y enfoques probabilísticos en el diseño de soluciones presurizadas elaboradas con materiales compuestos

Roberto José García Martín

Ávila, 2020

Departamento de Cartografía e Ingeniería del terreno
Escuela Politécnica Superior de Ávila
Universidad de Salamanca

Autor:

Roberto José García Martín

Directores Tesis

Dr. José Luis González Fueyo

Dr. Luis Javier Sánchez Aparicio

Tutor Académico

Dr. Diego González Aguilera

Programa de Doctorado:

Geotecnologías aplicadas a la Construcción, Energía e Industria

2020

“Aplicación de métodos de Correlación Digital de Imágenes y enfoques probabilísticos en el diseño de soluciones presurizadas elaboradas con materiales compuestos”

Tesis Doctoral presentada por Roberto José García Martín

Informe de los Directores de Tesis

La presente Tesis Doctoral se enmarca en la línea de investigación: *Caracterización de materiales y soluciones industriales mediante enfoques basados en la correlación digital de imágenes*, del grupo de investigación reconocido de la Universidad de Salamanca TIDOP (<http://tidop.usal.es>). Línea que se ha visto mejorada con los resultados que en este documento se exponen.

La actividad investigadora aquí presentada plantea el uso de técnicas propias de la Geomática, como es la fotogrametría y visión computacional, al campo de la ingeniería industrial, concretamente al diseño de soluciones para el almacenamiento y transporte de fluidos presurizados basadas en materiales compuestos. Enfoque que queda fortalecido con el uso de técnicas de simulación numérica avanzada, métodos probabilísticos y optimizaciones robustas, dando como resultado una hibridación que augura un horizonte muy prometedor y competitivo en diferentes ámbitos y especialmente en la aplicación que aquí se sugiere.

En lo que respecta al documento, éste arranca con un adecuado estado del arte, lo que permite identificar, de forma clara y unívoca, las potenciales líneas de investigación. Cerrado el estado del arte, el documento expone un objetivo general y varios objetivos específicos que van cumpliéndose a lo largo del desarrollo de un total de tres artículos científicos en revistas indexadas de alto factor de impacto, todas ellas pertenecientes al primer cuartil (Q1): *Sensors*, *Construction and Building Materials* y *Archives of Civil and Mechanical Engineering*, quedando así validadas las metodologías, resultados y conclusiones presentadas en este documento. Contribuciones que han sido sometidas a procesos de evaluación crítica y revisión por parte de expertos internacionales de trayectoria reconocida en la materia, lo cual pone de manifiesto la calidad e interés científico de la investigación planteada.

La Tesis Doctoral concluye con el correspondiente apartado de conclusiones en el que de forma precisa y concreta se especifican las citadas aportaciones de manera que puedan ser objeto de crítica y proyección hacia el desarrollo de trabajos futuros integrados en la línea de investigación mencionada.

Resulta también necesario remarcar el amplio interés por parte del sector industrial en los procedimientos aquí desarrollados, siendo estos empleados en el proyecto europeo

liderado por la Universidad de Salamanca: COMPRESSer (SOE2/P1/E0643) del programa Interreg V-B Europa; así como en un proyecto nacional FaTIMA (RTI2018-099850-B-I00) del programa Retos Investigación.

Desde un punto de vista formal, la Tesis Doctoral aquí expuesta cumple con los requisitos establecidos por la Universidad de Salamanca para la presentación de tesis por compendio de artículos.

Por todo lo expuesto anteriormente, el Director y Co-Director de esta Tesis dan el visto bueno para su presentación y defensa.

En Ávila, a 1 de septiembre de 2020



Dr. José Luis González Fueyo



Dr. Luis Javier Sánchez Aparicio

La presente Tesis Doctoral corresponde a un compendio de 3 trabajos previamente publicados que se especifican a continuación:

1. SmartFire: Intelligent platform for monitoring fire extinguishers and their building environment.

Roberto José García Martín¹, Alfonso González-Briones², Juan M. Corchado²

¹ Departamento de Ingeniería Mecánica, Escuela Politécnica Superior de Zamora, Universidad de Salamanca. toles@usal.es (R.J.G.M)

² Grupo de Investigación BISITE, Edificio I+D+i, Universidad de Salamanca. alfonsogb@usal.es (A.G.-B.); corchado@usal.es (J.M.C.)

Sensors 2019; DOI: 10.3390/s19102390

2. Combining digital image correlation and probabilistic approaches for the reliability analysis of composite pressure vessels.

Roberto García-Martín¹, Álvaro Bautista-De Castro², Luis Javier Sánchez-Aparicio³, José G. Fueyo¹, Diego Gonzalez-Aguilera²

¹Departamento de Ingeniería Mecánica, Escuela Politécnica Superior de Zamora, Universidad de Salamanca. toles@usal.es (R.J.G.M), fueyo@usal.es (J.L.G.F.)

²Departamento de Ingeniería Cartográfica y del Terreno, Escuela Politécnica de Ávila, Universidad de Salamanca. alvarobautistadecastro@usal.es (A.B.C), daguilera@usal.es (D.G.A)

³Departamento de Construcción y Tecnología Arquitectónicas, Escuela Técnica Superior de Arquitectura de Madrid, Universidad Politécnica de Madrid. lj.sanchez@upm.es (L.J.S.A)

Archives of Civil and Mechanical Engineering, 2019; DOI:10.1016/j.acme.2018.10.001

3. Digital image correlation and reliability-based methods for the design and repair of pressure pipes through composite solutions

Roberto García-Martín¹, Jorge López-Rebollo², Luis Javier Sánchez-Aparicio³, José G. Fueyo¹, Javier Pisonero², Diego González-Aguilera²

¹Departamento de Ingeniería Mecánica, Escuela Politécnica Superior de Zamora, Universidad de Salamanca. toles@usal.es (R.J.G.M), fueyo@usal.es (J.L.G.F.)

²Departamento de Ingeniería Cartográfica y del Terreno, Escuela Politécnica de Ávila, Universidad de Salamanca. jorge_lopez@usal.es (J.L.R), j_pisonero@usal.es (J.P.C.), daguilera@usal.es (D.G.A)

³Departamento de Construcción y Tecnología Arquitectónicas, Escuela Técnica Superior de Arquitectura de Madrid, Universidad Politécnica de Madrid. lj.sanchez@upm.es (L.J.S.A)

Construction and Building Materials, 2020; DOI: 10.1016/j.conbuildmat.2020.118625

Agradecimientos

La culminación de la tesis cierra otra etapa formativa, la cual lejos de ser un proceso individual, se ha logrado gracias al esfuerzo y empuje de todas las personas de mi entorno, tanto a nivel profesional como personal; mi agradecimiento a todos ellos. Por lo tanto, esta página adquiere especial importancia cuando se culmina el trabajo que representa una Tesis Doctoral.

Mi agradecimiento especial a todos los que contribuyeron a las publicaciones, destacando la labor y esfuerzo de mis directores de tesis, Dr. José L. González Fueyo por su esfuerzo y confianza durante todos estos años y Dr. Luis J. Sánchez Aparicio, cercano y capaz siempre de encontrar la luz al final del túnel, así como al Dr. Diego González Aguilera por apostar por mí y por su apoyo constante. Este agradecimiento se hace extensible al grupo Bisite; en especial al Dr. Juan M. Corchado Rodríguez y sobre todo al Dr. Alfonso González Briones, que siempre ofrece el 200%.

Por último, y no menos importante, a la familia, en especial a mi pareja y a mi hijo Noé; mi agradecimiento eterno por su cariño y tiempo prestado.

Resumen

La Ciencia y la Tecnología son herramientas indispensables en la construcción de sociedades modernas. Actualmente se está inmerso en una dinámica que no sólo persigue encontrar soluciones a problemas cotidianos, si no en un esfuerzo que busca el avanzar permanentemente en el conocimiento, para afrontar nuevos retos, buscar nuevas soluciones y mejorar el nivel tecnológico de nuestra sociedad. Es esta filosofía, la que fundamenta la presente Tesis Doctoral.

Hace años se hablaba de que en algunos campos se estaban alcanzando los denominados “techos tecnológicos”, pero cuando se estaba cerca de éstos en el campo de la ingeniería se produce una revolución gracias a la aparición de los materiales compuestos. Si bien es cierto que la ingeniería actualmente está dotada de grandes técnicas y herramientas, se tiende a aplicar métodos tradicionales y conocimiento adquirido a las nuevas situaciones. En el ejemplo planteado, esta actitud no siempre arroja buenos resultados, dado el complejo comportamiento y la falta de experiencia en estos nuevos materiales.

Este trabajo, en un afán de progresar en la búsqueda de métodos y soluciones más adaptados al contexto actual, relativo a los nuevos materiales, y con el objetivo de encontrar diseños más fiables a la par que económicos, se marca el objetivo inicial de lograr una sinergia con tecnologías propias de la Geomática; concretamente la correlación digital de imágenes. Esta técnica proporcionará un mejor conocimiento del material en su conjunto, a mayores de otras ventajas de índole económica.

Inicialmente el trabajo se centra en comparar y aplicar la citada técnica geomática para mejorar la caracterización de materiales compuestos aptos para soluciones presurizadas (recipientes, tuberías, etc). Además, los datos obtenidos permiten caracterizar el comportamiento variable del material, a través de un enfoque de tipo probabilístico. Por otro lado, se adaptan los procesos de cálculo numérico al nuevo enfoque, a la par que se aplican técnicas de análisis sensible en la búsqueda de obtener los parámetros críticos del diseño. También, se avanza en el tratamiento de los resultados; lo que constituye el siguiente escalón evolutivo de la ingeniería. Esto es, pasar de enfoques determinísticos a enfoques probabilísticos, apoyándose en lo que se conoce como Ingeniería Robusta asistida por métodos subrogados para lograr definir procedimientos viables de cara a ser transferidos al ámbito industrial.

Abstract

Science and Technology are indispensable tools in modern Society. Nowadays we are immersed in a dynamic world of Science and Technology that aims to find solutions to daily problems, to continuously advance knowledge, meet new challenges, find new solutions and to improve Society's Technological level. This philosophy is the base to the present Ph.D.

Years ago, people thought that some Fields were reaching their 'technological ceilings' but when this happened in Engineering, there was a new revolution thanks to the creation of composites. Although nowadays, it is true that engineering is supported by great tools and techniques, we still tend to apply traditional methods and acquired knowledge to new situations. In the current work, such traditional methods do not always give reliable results, given the complex behaviour of, and the lack of experience in using these new materials.

This work aims to progress by looking for methods and solutions which are better adapted to the current context in Engineering, concerning to composites. The first objective is to achieve a synergy with Geomatic technologies; specifically Digital Image Correlation. This technique will give a better understanding of materials as a whole, as well as other economical advantages.

Initially, this work focuses on comparing and applying the cited geomatic technique to improve the characterization of composites appropriate for pressurised solutions (containers, piping, etc). Also the data obtained allows for characterising of the variable behaviour of the material through a probabilistic technique. The numerical calculus processes are adapted to this new technique and at the same time are combined with sensitive analysis techniques to obtain design critical parameters. Also there is an advance in the analysis of the results, that constitutes the next evolutionary step in engineering; that is, to move from a deterministic focus to a probabilistic one. This is supported by what is known as Robust Engineering, assisted by surrogate methods to enable viable procedures to be applied to the industrial environment.

Índice

Introducción.....	1
Objetivos.	17
Capítulo I: Smartfire, Intelligent platform for monitoring fire extinguishers and their building environment.....	19
Capítulo II: Combining digital image correlation and probabilistic approaches for the reliability analysis of composite pressure vessels.....	41
Capítulo III: Digital image correlation and reliability-based methods for the design and repair of pressure pipes through composite solutions.....	57
Conclusiones y trabajos futuros.....	75
Bibliografia.	79
Anexo I: Indexación y factor de impacto de las publicaciones científicas.....	85

Introducción

Los recipientes a presión se hayan presentes en todas las instalaciones industriales modernas, desde pequeños depósitos de aire comprimido a recipientes de mayor envergadura como pueden ser los reactores de las centrales químicas y energéticas (J.Massa & J.Giro, 2015). Si se acota a un entorno más cercano, se pueden encontrar aplicaciones que van desde el almacenamiento de gases medicinales o combustibles domésticos – propano o butano entre otros- hasta pequeñas latas de bebidas, haciendo que el rango de aplicación de los recipientes a presión, o vasijas a presión como son conocidas de la traducción del término anglosajón “*pressure vessels*”, sea muy amplio. Esta flexibilidad de aplicaciones hace que los recipientes a presión copen gran parte de la actividad económica de un país, obteniéndose volúmenes de facturación que se expresan en billones de dólares dentro de un mercado que se halla en clara expansión (Fig.1).

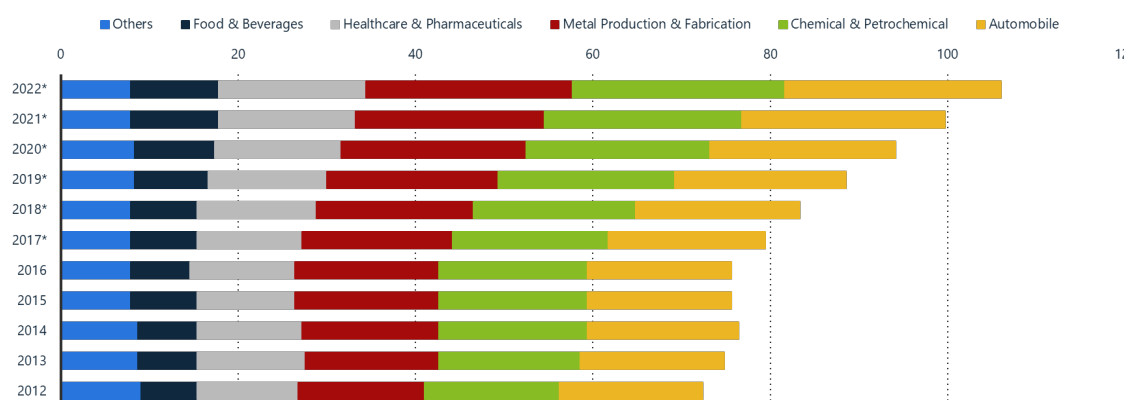


Fig.1 Tamaño global del mercado de los gases industriales por aplicación 2012-2022 expresado en billones de dólares USA. Fuente: Statista estimates; TechSci Research; [ID 919755](#)

Se entiende como recipiente a presión a aquella vasija cerrada capaz de almacenar un fluido a presión manométrica, ya sea mediante presión interna o vacío, independientemente de su forma y dimensiones. Dentro de esta definición se pueden englobar no sólo a aquellos elementos destinados al almacenamiento, sino también a aquellas aplicaciones relativas al transporte de fluidos que presentan un gradiente de presión entre el interior y el exterior del contenedor; desde pequeños circuitos hidráulicos (maquinaria industrial, vehículos) a canalizaciones a grandes distancias como las empleadas en el transporte de gas y petróleo; donde nuevamente las cifras hacen patente la importancia de estas aplicaciones. Actualmente existen miles de kilómetros de tuberías instaladas alrededor del mundo y las previsiones a nivel mundial es que el número de

tuberías a presión siga aumentando en los próximos años (*The world factbook field listing: pipelines*, 2013). Un ejemplo claro de este fenómeno se puede encontrar en España, donde el número de kilómetros de tubería instalada se vio incrementado a finales del siglo XX debido a la introducción del gas natural en los hogares, y se halla en expansión permanente tal que en la actualidad en España se cuenta con una red de distribución de más de 87.700 km (*Informe anual SEDIGAS*, 2018).

En lo concerniente al fluido confinado, éste puede estar sujeto a cambios de estados como sucede en los reactores químicos, calderas de vapor o extintores de CO₂, donde el efecto de la temperatura afecta seriamente a los valores de presión interna (Chung, Li, Lee, & Starling, 1985). Esto puede desembocar en situaciones peligrosas, de ahí que sea vital el garantizar que el recipiente sea a prueba de fugas y lo suficientemente resistente para ser capaz de soportar las condiciones de operación (Arunkumar, Eshwara Moorthy, & Karthik, 2020). Todo ello ocasiona que los recipientes a presión sean diseñados, fabricados y operados bajo regulaciones y normas ingenieriles exigentes. Por esas razones, el diseño y certificación de un recipiente diseñado para contener presión varía de país a país, y requiere definir parámetros tales como la presión y temperatura máxima admisible (*ASME BPVC-VIII. Boiler and Pressure Vessel Code*, 2019; *ISO 15649 Industrias de petróleo y gas natural - Tuberías*, 2001; *UNE-EN 764 Equipos a presión*, 2015)

Los grandes depósitos a presión empezaron a ser diseñados y construidos durante la revolución industrial, en particular en Gran Bretaña como calderas para máquinas de vapor, pudiéndose encontrar, en la actualidad, en gran variedad de aplicaciones y formas. Las partes básicas de todo depósito a presión son la evolvente, las terminaciones (cabeza y extremo), la tobera o boquilla de salida y el soporte (Chattopadhyaya, 2004) (Fig.2). La evolvente o cuerpo del recipiente suele ser cilíndrico o esférico, aunque se pueden encontrar formas toroidales (Enoma & Zingoni, 2020). En cuanto a los del contenedor o terminaciones estas pueden adoptar diferentes formas -planas, hemisféricas, toriesféricas entre otras- predominando la forma elíptica tal que maximizan el volumen y peso frente a otras geometrías (Nicolich, 1993).

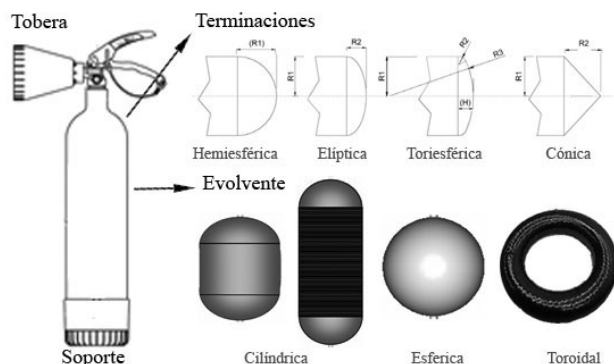


Fig.2 Recipiente a presión, componentes básicos.

1. Materiales

En lo relativo a la composición, tradicionalmente las vasijas a presión se constituyen con materiales metálicos, predominando claramente el acero y sus aleaciones (Takeuchi et al., 2014) (en el caso de los diseños más exigentes). El acero es un material bien conocido, resistente y barato, pero que posee ciertas desventajas inherentes a los materiales ferrosos (CC Technologies, 2002) de ahí que se hayan buscado alternativas como el aluminio (Hackworth & Henshaw, 2000) o los cada vez más presentes materiales compuestos.

Los materiales compuestos o composites (AEMAC, 2005) se presentan como una buena alternativa a los materiales metálicos debido fundamentalmente a sus elevados índices de rendimiento o PI (*Performance Index*), tanto a nivel estructural (M. F. Ashby, 2011) donde presentan grandes niveles de resistencia mecánica (Fig. 3a), resistencia a fatiga (Ochola, Marcus, Nurick, & Franz, 2004) y de absorción de energía, así como nivel químico (Gibson, 2010) con elevadas resistencias frente a los agentes medioambientales y ante atmósferas corrosivas (Shamsuddoha, Islam, Aravinthan, Manalo, & Lau, 2013), todo ello con elevados ratios frente al peso (Fig. 3b).

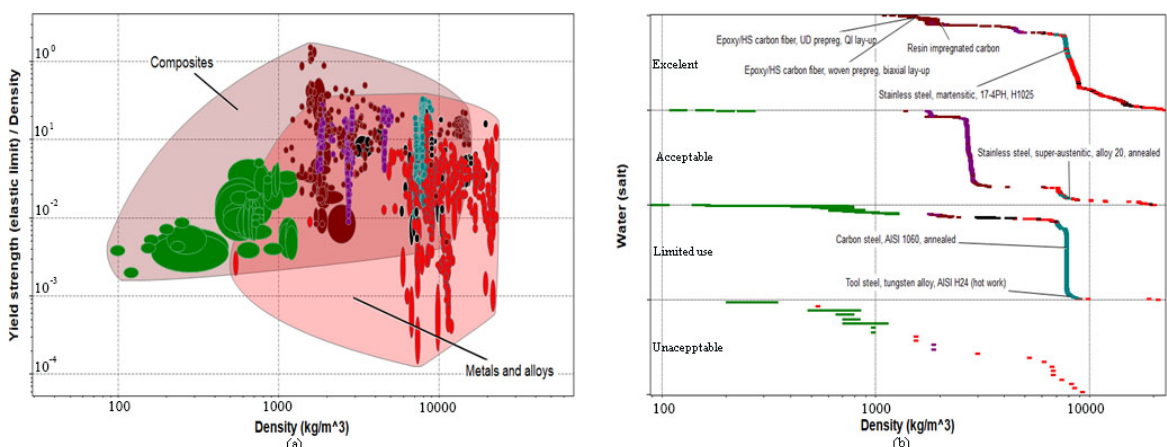


Fig. 3. Índices de rendimiento de los materiales metálicos frente a los materiales compuestos a) criterio resistencia mecánica vs peso para elementos sometidos a presión interna. b) criterio resistencia a ambientes salinos vs peso.

Conviene reseñar que el empleo y desarrollo de los materiales compuestos proviene de sectores muy concretos, especialmente aquellos más tecnológicos o relacionados con grandes industrias como la automotriz (Delogu, Zanchi, Dattilo, & Pierini, 2017) o la aeroespacial (Zhu, Sun, Li, Cheng, & Li, 2018).

Los materiales compuestos surgen de la unión de dos o más materiales para conseguir una combinación de propiedades que no es posible obtener de los materiales originales.

Estos se clasifican en función de la geometría del refuerzo (Askeland, 2001)(Fig. 4). A nivel macroscópico, se pueden diferenciar dos fases: i) un refuerzo consistente bien en partículas o en fibras, tanto largas como cortas orientadas aleatoriamente o con un orden determinado, cuya misión es aportar altas propiedades mecánicas y; ii) una matriz en la cual va embebido el refuerzo, encargada de distribuir los esfuerzos y proteger al refuerzo entre otras funciones. Estos constituyentes, matriz y refuerzo, pueden pertenecer tanto a la misma como a diferentes familias de materiales (Miravete, 2011).

De entre las configuraciones posibles (Fig. 4), la que mejor se adapta a la necesidad planteada en esta Tesis Doctoral son los materiales compuestos de fibra continua multidireccionales de matriz polimérica y refuerzo cerámico (Kendall, 2007), conocidos como polímeros reforzados con fibra (FPR s- *Fiber Polymer Reinforced*), concretamente los GFPR (*Glass Fiber Polymer Reinforced*) y los CFPR (*Carbon Fiber Polymer Reinforced*), siendo estos tal vez los más conocidos ya que están muy extendidos en el mundo de deporte (Miyamoto & Minamiguchi, 1995) o del automóvil (Delogu et al., 2017).

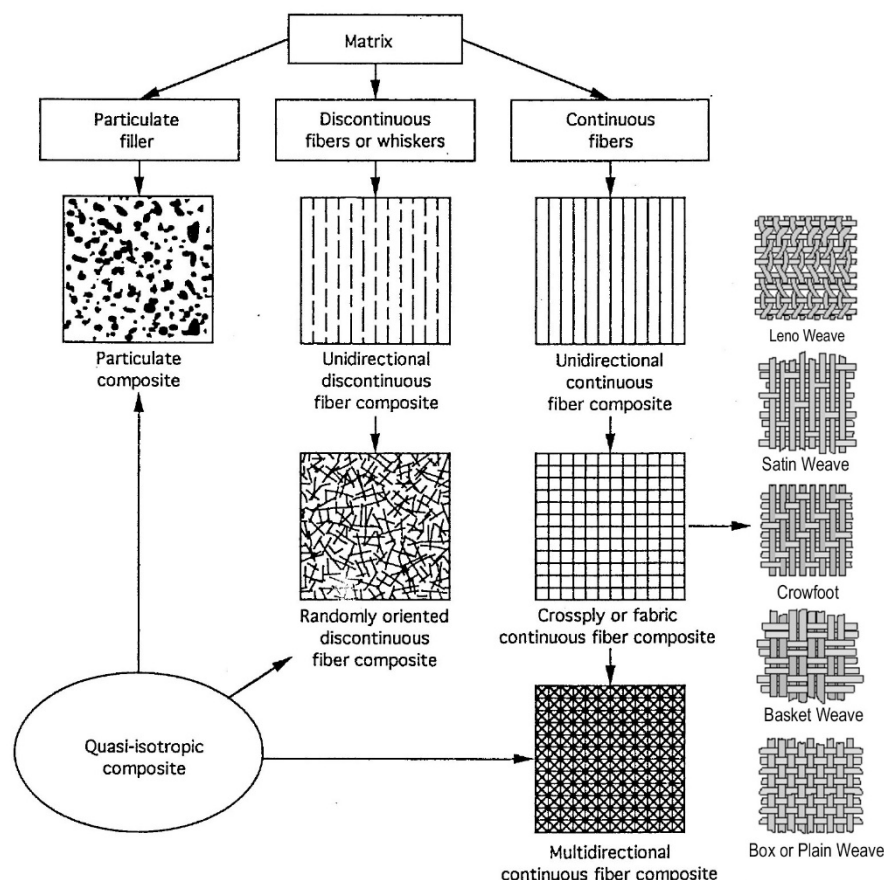


Fig. 4. Clasificación de los materiales compuestos en función del tipo de refuerzo. Fuente: New Engineering Mechanics of Composite Materials-DANIEL & ISHAID. Oxford University Press, 1994

1.1. Procesos de fabricación

El material compuesto se puede presentar en varios formatos, bien el refuerzo y la matriz por separado, los cuales se van combinando a medida que se van arrollando sobre el molde, o bien se emplea el formato conocido como *prepeg* que son fibras pre-impregnadas con la matriz, habitualmente de tipo termoplástica o resina epoxídica sin polimerizar (Shamsuddoha et al., 2013). En ambos casos resulta necesario aplicar una técnica de fabricación que dé lugar al material final, el composite. Para el caso de los recipientes a presión elaborados con materiales compuestos o COPVs (*Composite Overwrapped Pressure Vessels*), dos son las técnicas fundamentales de fabricación: i) *Roll Wrapping* y ii) *Filament Winding* (FW), técnica de molde perdido. En ambos casos el proceso consiste en enrollar el composite alrededor de un mandril o una preforma (molde).

Roll Wrapping es una técnica indicada tanto para la fabricación de tuberías como para su reparación (Mazurkiewicz et al., 2017). Esta consiste en enrollar un *fabric* o un *prepeg*, sobre un mandril cilíndrico en el caso de tubería nueva. En el caso de reparaciones, se arrolla la lámina alrededor de la zona afectada por la reparación, tal que la tubería a reparar actúa como molde o mandril, en estos casos la superficie a reparar requiere ser preparada, de modo que quede limpia (óxido, suciedad) y previo a la aplicación del composite se nivela la superficie afectada con un relleno (*putty*) normalmente de naturaleza epoxídica (Duell, Wilson, & Kessler, 2008).

En el caso de tuberías o recipientes más exigentes en cuanto a presiones de servicio, la técnica más empleada es el *Filament Winding* (FW) (Ger, Hwang, Chen, & Hsu, 1988). Como se ha indicado el FW es una técnica de molde perdido, donde el proceso de fabricación consiste en bobinar sobre una preforma o mandril conocido como *Liner*, una fibra continua habitualmente de vidrio, carbono o aramida (Cui, Liu, Sun, & Li, 2020; Fleischer et al., 2018), la cual actuará como refuerzo del composite final. Estas fibras se suelen impregnar en un baño de resina epoxi o vinil-éster (Rafiee, 2016), material que constituye la matriz, antes de ser bobinadas en un proceso conocido como *Wet Filament Winding*. Otra alternativa consiste en utilizar *prepregs* (Venkateshwar Reddy, Ramesh Babu, Ramnarayanan, & Das, 2017).

En ambos procesos de fabricación, y en especial en el segundo de ellos, la obtención de las propiedades del compuesto, a partir de las de sus componentes dista de ser trivial dado que el comportamiento no se ajusta a la teoría de láminas (Reddy, 2003) y entran en juego gran número de variables, las cuales son relativas a los componentes (propiedades mecánicas de la resina y fibra), al diseño (número de capas, espesor y orientación de las mismas, secuencia de apilamiento, tipo de capa: circular o helicoidal), proceso de fabricación y equipo empleado (tensión sobre el hilo, tiempos y velocidades de fabricación, etc) las cuales afectan notablemente al comportamiento final del producto terminado; en el caso del *Wet FW* se han llegado a detectar hasta 50 variables que influyen notablemente en el resultado final, no sólo a la calidad del recipiente sino que también sobre la resistencia a

tensión del COPV (Cohen, 1997). En la tabla 1 se muestran una clasificación de las que mayor influencia ejercen expresado este valor en tanto por ciento.

Posición	Variable	%
1	Tensión del hilo	71
2	Variabilidad de la resistencia de la fibra	62
3	Secuencia de apilamiento	62
4	Etapa-B de la Resina (curado latente)	57
5	Daño en la fibra durante el bobinado	57
6	Impregnado de la fibra	57
7	Gradiente de tensión en el bobinado	48
8	Contenido en resina	43
9	Tiempo total de bobinado	43
10	Tiempos de arrollamiento entre capas	43
11	Espesor de capas circulares	43
12	Capas helicoidales cortadas vs no cortadas	38

Tabla 1: Ranking de las 12 variables de mayor influencia (expresada en %) en la resistencia a presión interna en COVPs elaborados mediante la técnica de FW.

Todo lo anterior hace que el material compuesto sea en un material complejo desde el punto de vista mecánico, con un comportamiento ortotrópico o totalmente anisótropo (Vasiliev & Morozov, 2001) en contraposición de la isotropía y homogeneidad mostrada por el acero.

2. Análisis numérico avanzado

La complejidad inherente en este tipo de nuevos materiales, los composites, exige ir más allá del planteamiento analítico propio de Resistencia de Materiales (en especial la teoría de láminas) e introducirse en enfoques numéricos avanzados como son los propios del Método de los Elementos Finitos (MEF). Dicho tipo de simulación numérica, basada en la discretización del medio continuo, permite obtener los outputs necesarios, en forma de desplazamientos, tensiones y deformaciones unitarias, requeridos para el análisis de soluciones industriales en composite (Canal et al., 2019; Velosa, Nunes, Antunes, Silva, & Marques, 2009).

Estos outputs que se consiguen a través del empleo de técnicas específicas de modelado; que van desde el nivel de los constituyentes (micro-escala), a nivel de las capas en composites (meso-escala) hasta el nivel del componente (macro-escala) (Sasikumar, Suresh, Vijayaghosh, & Gupta, 2015), y modelos constitutivos de material (Wang & Duong, 2016) desde los más sencillos empleados en materiales isótropos lineales como Von Misses que quedan definidos por 4 parámetros, hasta aquellos como Tsai -Hill o Tsai-Wu (Vanegas Useche & Arias Maya, 2004) aptos para composites en cuyo caso el número de parámetros se puede disparar hasta 13 (Padaui & Enrique, 2013) y esto sólo en lo relativo al factor material.

Si bien el MEF muestra un conjunto de ventajas que lo sitúan como una de las estrategias numéricas predilectas en el análisis de soluciones industriales, están deben ser alimentadas convenientemente con un conjunto de inputs como por ejemplo el Módulo de Young o la Resistencia a Compresión entre otros, que hacen indispensable llevar a cabo campañas experimentales para su caracterización.

3. Caracterización de inputs

Como bien se señaló con anterioridad, el MEF es sin duda el enfoque numérico de mayor proyección en el análisis mecánico de soluciones en materiales compuestos. Enfoque que demanda un conjunto de inputs que han de extraerse de campañas experimentales, procesos en donde se extraen propiedades mecánicas específicas del material al someterse este a diferentes tipos de solicitud (e.j compresión, tensión o flexión).

El enfoque más habitual a día de hoy, y el que quizás más tradición lleve a sus espaldas, es el empleo de técnicas de contacto a través del uso de dispositivos como los LVDTs (*Linear Variable differential transformers*), los extensómetros y las galgas extensiometrías (Orell et al., 2018; Tekieli, De Santis, de Felice, Kwiecień, & Roscini, 2017). Enfoque que basa su éxito en la instalación de sensores sobre la probeta a ensayar, permitiendo obtener así la respuesta del material (en forma de deformaciones y/o desplazamientos incrementales) en puntos locales del mismo. Algunos de estos sensores se hallan integrados en la propia máquina de ensayo, como los extensómetros, cuya medida pueden verse afectada por las deformaciones de los componentes del equipo.

Las citadas técnicas se ven fuertemente influenciadas por el factor temperatura lo que precisa de la aplicación de factores de corrección. Otro rasgo común de las técnicas de contacto es que suelen requerir de un complejo proceso para la implementación de los sensores como sucede con galgas extensiometrías (Hoffmann, 1974), siendo esta una de las técnicas más habituales, donde a pesar de ser de uso común no deja de ser un método plagado de inconvenientes. La medida de estas galgas se ven muy influenciada por el estado de las superficies (grietas, picaduras, etc) lo que requiere de una preparación de la zona de contacto.

Por otro lado, también se requiere de cierta destreza a la hora de manipular e implementar las galgas, por ejemplo una mala alineación de los ejes de la galga respecto del espécimen, dañar la galga al manipularla, el exceso de temperatura, etc, lo que implica de la necesidad de detallados protocolos de manipulación y montaje (uso de adhesivos, soldadura, etc).

Estas técnicas de contacto también exigen de un conexionado, habitualmente bastante sofisticado, lo cual aumenta tanto la complejidad del ensayo como los costes de este, al mismo tiempo que se asocian a precisos a la par que onerosos equipos de medida, lo que sumado al coste de la propia galga, la cual queda inservible después del ensayo, hacen que esta sea una técnica costosa.

Finalmente, las citadas técnicas son capaces de dar valores de medidas en zonas puntuales, con lo que resultan poco representativas en casos en los que se requiere conocer la respuesta global del sistema (materiales compuestos). A mayores el carácter invasivo de los sensores empleados puede modificar el comportamiento del material.

La alternativa a estas soluciones de contacto se encuentra, como es obvio, en las soluciones de no contacto o remotas. Dentro de dicho abanico de posibilidades, cinco son las técnicas más sobresalientes (Tabla 2): i) la interferometría de Moiré (Seif, Khashaba, & Rojas-Oviedo, 2007); ii) el sistema de velocimetría por análisis de imágenes de partículas PIV (*Particle Image Velocimetry*) (Callaway, Gilbert, & Smith, 2012); iii) la fotoelasticidad (Sampson, 1970); iv) el *multi-camera tracking* (Gabriel, Verly, Piater, & Genon, 2003) y; v) la correlación digital de imágenes DIC (*Digital Image Correlation*) (Hild & Roux, 2006). En la tabla 2 se muestran las ventajas e inconvenientes de cada una de estas tecnologías.

De entre ese abanico de posibilidades, el método DIC es sin lugar a dudas el más extendido en el análisis de materiales (Biscaia, Franco, & Chastre, 2018; Orell et al., 2018; Tekieli et al., 2017), siendo capaz de obtener desplazamientos y deformaciones de cualquier punto del espécimen ensayado con altos niveles de precisión, pudiéndose mejorar aún más esta precisión (nivel de subpíxel) con la implementación de métodos de interpolación (Luu, Wang, Vo, Hoang, & Ma, 2011).

El principio fundamental de la técnica del DIC consiste en encontrar los parámetros de deformación (traslaciones y sesgos) de áreas concretas de la probeta antes y después de su deformación. Problema que pivota en los principios de correlación de la imagen digital y para lo cual es altamente recomendable (y en algunos casos hasta necesario) un patrón Speckle (Hua et al., 2011). El patrón Speckle proporciona un conjunto de referencias (niveles de grises) sobre la superficie del elemento a ensayar, bien empleando la propia textura del material (Speckle natural) o generándolo de manera artificial (Dong & Pan, 2017), siendo un parámetro crucial a la hora de determinar la precisión de la medida.

Básicamente la técnica DIC consiste en adquirir imágenes de alta resolución del elemento ensayado a diferentes niveles de carga del caso de estudio. Para ello se requiere de un sistema de captación de imágenes, iluminación y control adaptado al método empleado. Las imágenes obtenidas se procesarán posteriormente mediante correlación en base a algoritmos y enfoques de diferenciación numérica (M. A. Sutton, Wolters, Peters, Ranson, & McNeill, 1983). Esta técnica se puede encontrar en sus dos variantes, 2D y 3D (H. S.-J. O. A. Sutton, 2009). La primera de ellas empleada para superficies planas, de manera que con una única cámara se pueden obtener mediciones con gran precisión y, la segunda, se emplea cuando se trabaja con superficies que no son planas. El DIC 3D se basa en el principio de la estereovisión binocular (Viguié et al., 2011). Esta variante requiere del uso de dos cámaras las cuales han de estar sincronizadas. Al igual que en DIC 2D se pueden obtener medidas de precisión fuera del plano y en superficies curvas como las que presentan las tuberías, depósitos, etc.

Método	Ventajas	Inconvenientes
<i>Interferometría Moiré</i>	<ul style="list-style-type: none"> - Sencillez de procesado de datos. - Reducido coste. 	<ul style="list-style-type: none"> - En Moiré geométrico puede ser complejo al requerir de una rejilla. - En Proyección de Franjas, el Moiré necesita una calibración y un desenvolvimiento de fase. - Resultados muy sensibles a la calidad de las imágenes.
<i>Fotoelasticidad</i>	<ul style="list-style-type: none"> - Equipo relativamente económico. - Fácil implementación. - En reflexión: aplicable a modelos opacos. - En transmisión: aplicable a modelos transparentes. 	<ul style="list-style-type: none"> - Necesidad de polaríscopio. - Necesidad de desenvolvimiento de fase (<i>unwrapping</i>).
<i>Multi-camera tracking</i>	<ul style="list-style-type: none"> - Permite resolver problemas de oclusión cuando un objetivo (<i>target</i>) no es visible en una cámara, pero en otra sí. - Permite cubrir un área amplia que con una sola cámara. - Resultados de seguimiento más precisos mediante el uso de múltiples vistas para una identificación mejor del objetivo (<i>target</i>). 	<ul style="list-style-type: none"> - Necesidad de resolver el problema de datos asociados cuando se determina la correspondencia entre objetivos (<i>targets</i>) en cámaras diferentes. - Coste elevado del sistema de multicámaras con respecto a una sola cámara debido al uso extra de sensores. - Necesidad de situar <i>targets</i>, con formas determinadas, a lo largo del espécimen.
<i>Sistema de velocimetría por análisis de imágenes de partículas (PIV)</i>	<ul style="list-style-type: none"> - Método no intrusivo. - Evita el uso de tubos de Pitot, anemómetros de alambre caliente u otras sondas para mediciones de flujo. - Los marcadores agregados (si se eligen correctamente) apenas causan distorsión del flujo del fluido. - Es capaz de medir secciones transversales bidimensionales completas del campo de flujo simultáneamente. - Los valores de desplazamiento de subpixeles permiten un alto grado de precisión. 	<ul style="list-style-type: none"> - En casos de mayor densidad las partículas no siguen perfectamente el movimiento del fluido. - Imposibilidad de medir componentes a lo largo del eje z (hacia o desde la cámara). - Uso de láseres de clase IV y cámaras con alta resolución y velocidad, restringiendo el coste y la seguridad.
<i>Correlación digital de imágenes (DIC)</i>	<ul style="list-style-type: none"> - Fácil preparación de los modelos de estudio. - Rapidez en la obtención de los resultados. - Obtención directa del campo de desplazamientos y deformaciones. 	<ul style="list-style-type: none"> - Necesidad de tener una distribución buena de niveles de grises (patrón Speckle). - Necesidad de calibración del sistema estereoscópico para obtener medidas 3D. - Resultados dependientes de la calidad de las imágenes.

Tabla 2: Ventajas e inconvenientes de las técnicas de no contacto existentes en la actualidad.

4. Nuevas perspectivas en el análisis: el enfoque probabilista y el diseño óptimo basado en fiabilidad

Una acción necesaria e importante respecto a la estrategia de toma de datos en el composite, es que debido a la citada heterogeneidad (Tabla 1) se necesita tomar medidas en diversos puntos del material a fin de determinar correctamente su comportamiento global, tal que cuanto mayor sea el número de muestras mayor será la precisión del proceso. Este hecho afecta tanto al método escogido para la obtención de datos, como al tratamiento posterior de estos que requerirán de herramientas estadísticas para su tratamiento, debiendo dar el salto hacia enfoques probabilistas en contraposición de aquellos deterministas usados tradicionalmente en materiales metálicos (das Neves Carneiro & Conceição António, 2019) que no ofrecen resultados satisfactorios para composites (Rafiee, 2017; Rafiee, Reshadi, & Eidi, 2015; Rafiee & Torabi, 2018).

Si bien es cierto que en lo relativo al cálculo con el MEF tradicionalmente se adoptan estrategias o enfoques determinísticos, tal como se ha citado anteriormente no son capaces de proporcionar coeficientes de seguridad del diseño lo suficientemente adecuados cuando se trata de materiales compuestos como en el caso de estudio, donde intervienen un gran número de variables y fundamentalmente de carácter aleatorio, por lo que una estrategia probabilística o estocástica es el enfoque más adecuado, tanto cuando se trabaja con variables discretas, las cuales vendrán definidas por su función de distribución de probabilidad, como con variables continuas (en intervalos), en cuyo caso se requerirá determinar la función de densidad de probabilidad (PDF) de cada variable en juego, y es en este punto donde la técnica de medida cobra especial importancia, tal que una técnica que sea capaz de captar información de múltiples puntos nos permitirá conformar las PDFs, donde se perseguirá encontrar el mejor ajuste dentro de las PDFs más habituales (Normal, Normal - Logarítmica, Weibull y Gamma) (Cordero Martínez, 2017). La calidad del ajuste se lleva a cabo mediante la aplicación de los conocidos como test de bondad del ajuste (Koziol, 1987).

Se ha destacado la importancia de las PDFs, encargadas de caracterizar las variables aleatorias, las cuales pueden estar o no correlacionadas, donde a su vez pueden presentar una relación espacial en lo que se denomina como campo estocástico, donde destaca la técnica de *Random Fields* empleada en optimización topológica (Chen, Chen, & Lee, 2010), concretamente *robust shape and topology optimization* (RSTO).

En el sector de los recipientes a presión, la exigencia en lo concerniente a los requisitos de seguridad es muy elevada, habitualmente sujeta a una normativa muy restrictiva en lo relativo a coeficientes de seguridad, por lo que la determinación de la probabilidad de fallo es un parámetro de suma importancia.

4.1 Probabilidad de fallo de un sistema

La determinación de la probabilidad de fallo de un sistema (P_{fk}) sometida a una serie de restricciones (G_k) puede ser obtenida a través de la evaluación de la integral de la ecuación [1], donde $f_X(X)$ es la PDF del vector aleatorio $X \in R^m$ y el vector de diseño $d \in R^n$ (p.e. configuración de la estructura y dimensiones) (Lopez & Beck, 2012). En la práctica, y por diversos motivos, es imposible encontrar la solución a esta integral, de ahí que se empleen métodos para aproximar el valor de la misma: i) métodos de simulación; ii) métodos de expansión; iii) métodos basados en el punto más probable; iv) métodos basados en metamodelos y; v) métodos de integración aproximada (Cordero Martínez, 2017).

$$P_{fk} = \int_{G_k(d,X) < 0} f_X(X) dX \quad [1]$$

De los citados métodos para la estimación de la probabilidad de fallo destacan los métodos basados en el punto más probable: métodos FORM / SORM (*First / Second Order Reliability*) así como el método de Montecarlo (*Monte Carlo Sampling*) (Lopez & Beck, 2012). El primero de los enfoques permite obtener probabilidades del fallo del sistema de una forma rápida y directa pero muchas veces poco precisa, habiendo de optar por el segundo de ellos, el MCS, si lo que se desea son resultados altamente fiables. Dicho enfoque estadístico, el cual se basa en producir situaciones equiprobables de un sistema, demanda altos costes computacionales y muchas veces prohibitivos, requiriéndose del orden de 10^5 simulaciones (Bautista-De Castro et al, 2019).

Para superar este inconveniente habitualmente se suelen aplicar técnicas de reducción de varianza, así como la implementación de metamodelos (Tabla 3) o modelos subrogados (Barton & Meckesheimer, 2006). Los metamodelos permiten generar un modelo matemático equivalente con apenas coste computacional, que replica la respuesta del sistema permitiendo realizar un gran número de simulaciones con gran precisión, en tiempos razonables (Marelli & Sudret, 2019).

Kriging Models	KM	Modelos Kriging
Radial Basis Function	RBF	Funciones De Base Radial
Neural Networks	NN	Redes Neuronales
Surface Response Method	SRM	Método de la Superficie de Respuesta

Tabla 3: Métodos basados en metamodelos

Por otro lado la literatura muestra que la combinación de métodos resulta ser más eficiente que su empleo por separado, como por ejemplo ocurre con el modelo subrogado *Polynomial-Chaos-Kriging* (PC- Kriging o PCK) (Marelli & Sudret, 2019). Este algoritmo representa una de las opciones más empleadas (Bautista-De Castro et al., 2019), basado en la combinación de un método de expansión, *Polynomial Chaos Expansión* (PCE) y un método basado en metamodelos, *Kriging*. Su expresión (Eq. 2) se compone de dos términos, el primero correspondiente al método PCE que se encarga de evaluar el comportamiento global de la respuesta del modelo computacional $Y = M(X), X \in R^m$,

mientras que el segundo término correspondiente al metamodelo Kriging, interpola las variaciones locales de Y .

$$Y \approx M^{PCK}(X) = \sum_{\alpha \in A} y_\alpha \Psi_\alpha(X) + \sigma^2 Z(X, w) \quad [2]$$

Siendo los términos relativos a PCE, $\Psi_\alpha(X)$ que representa los polinomios multivariable ortonormales respecto a la PDF ($f_X(X)$), $\alpha \in A \in N^m$ representan los multi-índices e y_α son los coeficientes correspondientes. En cuanto a los términos concernientes a Kriging, σ^2 y $Z(X, w)$ son la varianza y la medida del valor cero del proceso Gausiano estacionario, respectivamente.

4.2 El método RBDO

A mayores de la posibilidad de estimar la probabilidad de fallo, la tendencia actual en el campo del diseño en ingeniería busca obtener diseños óptimos que implican el menor consumo de material (y por tanto coste de fabricación) para el cual la probabilidad de fallo es aceptable (D., D., & Masoud, 2006). Dentro de este contexto se pueden encontrar dos tipos de formulaciones: i) el Diseño Óptimo Basado en Fiabilidad (Lee & Jeong, 2020; Yang, Zhang, & Han, 2020) o RBDO (*Reliability-Based Design Optimization*) donde el efecto de las incertidumbres es cuantitativamente expresado mediante probabilidades de fallo y; ii) el Diseño Óptimo Robusto (Schuëller & Jensen, 2008) o RDO (*Robust Design Optimization*). Cada una de estas estrategias persigue un fin diferente, aunque ambos métodos incorporan la incertidumbre dentro del proceso de diseño (Tabla 3) (Cordero Martínez, 2017). El RDO se centra en disminuir la variabilidad de la respuesta debida a la aleatoriedad de las variables. Este método se determina mediante criterios que evalúan la variabilidad de la respuesta en torno a su valor medio, empleando habitualmente como medida la desviación estándar. Mientras el RBDO está vinculado a las probabilidades de fallo, buscando consigo aquel diseño para el cual la probabilidad de fallo es inferior a un determinado valor. Este último método el que mayor proyección y aplicación presenta dentro del campo de los composites (D. et al., 2006; Díaz, Cid Montoya, & Hernández, 2016).

	Diseño Óptimo Robusto	Diseño Óptimo basado en Fiabilidad
Descripción de la incertidumbre	Media y desviación estándar	Función de distribución de probabilidad
Objetivo de diseño	Reducir variabilidad	Min. bajo restricciones probabilísticas
Tipo de análisis	Análisis variacional (dispersión)	Análisis fiable (probabilidades de fallo)
Estrategia	Reducir variación respuesta	Mover media respuesta

Tabla 4: Comparación entre RDO y RBDO.

Como bien se ha indicado con anterioridad, el método RBDO tiene como principal objetivo obtener una solución para la cual el sistema físico es seguro con un cierto grado de probabilidad y además emplea el menor material posible. Para llegar a dicho fin es necesario plantear un problema de optimización numérica en el cual se trate de disminuir no solo una función de coste preestablecida (e.j. espesor de las capas del composite) sino también satisfacer una probabilidad de fallo, tal que este problema se puede plantear (Eq. 3):

$$\text{minimizar } J(d, X) \text{ sujeto a } \begin{cases} f_j(d) \leq 0, \{j = 1, \dots, s\} \\ G_k(d, X) \leq 0 \leq P_{f_k}^{\text{adm}}, \{k = 1, \dots, n\} \end{cases} \quad [3]$$

Esta es una formulación general para el caso que tanto d como X pueden ser variables. La función de coste J es minimizada frente a las variables de diseño, sometida a las denominadas restricciones blandas (f_j) relativas al espacio de diseño, en contraste frente a las restricciones fuertes (G_k), que varían desde 1 al número de restricciones definidas (n). G_k representa las funciones que describen el comportamiento del sistema (Schöbi, Marelli, & Sudret, 2017), donde se considera que el fallo se producirá para la condición $G_k(d, X) \leq 0$. En el caso del RDBO se requiere que la probabilidad de fallo (Eq.1) sea menor que un valor límite ($P_{f_k}^{\text{adm}}$).

La solución a dicho problema puede ser abordada de tres formas diferentes: i) con enfoques de un solo nivel (*mono-level*); ii) con enfoques de dos niveles (*two-level*) o; iii) a través de las denominadas aproximaciones desacopladas (*decoupled*) (Dan M. Frangopoulis, 2008), siendo el más empleado el enfoque *two-level* (Moustapha & Sudret, 2019), enfoque que resuelve el problema a través de diversas iteraciones que buscan el mínimo de la función de coste y que además cumplen una determinada probabilidad de fallo expresada a través de los métodos citados con anterioridad (e.j. métodos FORM/SORM o Monte Carlo).

5. Estructura de la Tesis Doctoral

Tomando en consideración lo anteriormente reseñado, la presente Tesis Doctoral se desarrolla por compendio de tres artículos científicos de impacto, de acuerdo con el procedimiento de 15 de febrero de 2012 de la Comisión de Doctorado de la Universidad de Salamanca. Todos los artículos han sido publicados en revistas internacionales de alto impacto y estos suponen un salto en el estado del arte del análisis y simulación de materiales compuestos y su aplicación en aplicaciones reales de la industria 4.0.

La estructura presentada en esta tesis se adapta al orden lógico de los objetivos iniciales de la misma y a la secuencia en la que se desarrolló la investigación que aquí se presenta:

- Introducción.
- Objetivos.
- Capítulo I: *Smartfire, Intelligent platform for monitoring fire extinguishers and their building environment.*
- Capítulo II: *Combining digital image correlation and probabilistic approaches for the reliability analysis of composite pressure vessels.*
- Capítulo III: *Digital image correlation and reliability-based methods for the design and repair of pressure pipes through composite solutions.*
- Conclusiones y trabajos futuros.
- Anexos.

A continuación se proporciona una visión general de los apartados de esta tesis y como se relacionan entre ellos.

Introducción: Este trabajo combina diferentes técnicas y métodos para lograr el objetivo general planteado, *avanzar en la integración de las técnicas de correlación de imágenes y métodos probabilísticos, para el desarrollo de recipientes a presión elaborados con materiales compuestos*, de tal manera que esta introducción describe el estado del arte de las diferentes técnicas y herramientas evaluadas, así como la importancia del tema planteado.

Se hace un recorrido de la evolución de los recipientes presurizados, se introducen las herramientas y técnicas a emplear: técnicas de no contacto, método de los elementos finitos, herramientas estadísticas destacando el método RDBO y la metamodelización, mostrando como se han de adaptar estas técnicas al problema planteado.

Objetivos: Se plantea el objetivo principal del trabajo, así como los objetivos específicos en los que se desglosó este, los cuales representan el camino natural seguido para alcanzar la meta final.

Capítulo I: Este capítulo recoge los primeros pasos de la investigación en los que se diseña y evalúa un sistema de medida de bajo coste, capaz de integrar una técnica de no contacto apta para materiales compuestos.

Capítulo II: Representa la continuación del primer capítulo donde el sistema de medida diseñado se haya plenamente integrado con la técnica de no contacto DIC2D, siendo esta verificada. Posteriormente, los resultados del DIC2D son empleados para caracterizar el composite seleccionado desde un punto de vista probabilístico, a través de la definición de las PDFs. Para la generación de las PDFs se emplea un enfoque más convencional, proviniendo los datos de una serie de extensómetros virtuales sitos en sobre la superficie del composite. A su vez en este capítulo recoge la evolución de modelos determinísticos a estocásticos, donde los parámetros críticos del diseño fueron determinados a través de un estudio de análisis sensible para posteriormente conformar el diseño RBDO implementando métodos subrogados de cara a mejorar los tiempos de cálculo.

En este capítulo se alcanzan gran parte de los objetivos de esta tesis, de ahí que sea uno de los capítulos que mayores recursos consumió y cuyos resultados tuvieron un mayor impacto.

Capítulo III: En este punto se presenta la evolución del modelo probabilístico, donde se aumenta la escala de medida pasando a nivel meso, lo que exige de una modelización de mayor calidad a la par que complejidad, dado el orden de magnitud del número de referencias a tratar.

El número de referencias obtenidas vía DIC cambia el orden de magnitud, tal que en esta ocasión se descarta la medición en puntos concretos (uso de extensómetros virtuales) pasando a trabajar con el campo completo de deformaciones. Esto se realiza implementando la técnica de *Ramdon Variable* lo que supone una evolución respecto al capítulo anterior. Se conforma de nuevo un estudio de fiabilidad RBDO, consolidando la integración de la técnica de campo completo empleada en geomática DIC2D, la cual pasa a integrarse en lo que hoy representa la punta de lanza del diseño en ingeniería moderna que es la ingeniería robusta, en este caso vía RBDO. A su vez en este capítulo se fortalece el análisis sensible, como una herramienta para la selección de las variables de diseño de composites, así como la metamodelización como una técnica imprescindible para mejorar los costes computacionales. Esto último permite implementar métodos más aptos para el diseño de composites, lo cual representa otro avance respecto al trabajo previo.

Conclusiones y trabajos futuros: Se exponen las conclusiones generales del trabajo, así como las perspectivas futuras, que permitirán afianzar y explotar el conocimiento generado lo que se plasmará en futuros avances.

Anexos: El Anexo I aporta información sobre la métrica de las revistas en las cuales los artículos han sido publicados.

Objetivos

El objetivo general perseguido en la presente Tesis Doctoral no será otro que el de ***avanzar en la integración de las técnicas de correlación de imágenes y métodos probabilísticos, para el desarrollo de recipientes a presión elaborados con materiales compuestos.***

Cumplir con dicho objetivo general llevará consigo la necesidad de acometer los siguientes objetivos específicos:

- *Definir un sistema de medida de bajo coste.*
- *Implementar una técnica de no contacto para la caracterización de materiales compuestos*
- *Explotar los datos ofrecidos por el método DIC para la extracción de las funciones de distribución de las variables mecánicas de composites.*
- *Integrar la metodología del Análisis Sensible para la determinación de parámetros críticos.*
- *Generar modelos FEM alimentados mediante DIC y adaptados a procesos de cálculo de tipo estocástico.*
- *Evaluar la aplicabilidad de métodos de subrogación o metamodelos para la reducción del coste computacional en simulaciones probabilísticas*
- *Implementar técnicas de Ingeniería robusta basada en modelos de fiabilidad en el diseño de elementos presurizados*

Capítulo I

SMARTFIRE: INTELLIGENT PLATFORM FOR MONITORING FIRE EXTINGUISHERS AND
THEIR BUILDING ENVIRONMENT

RESUMEN

En el primer trabajo publicado se propone la introducción de nuevas técnicas de medida para la caracterización de materiales compuestos, a partir de la medida de las deformaciones.

El **objetivo** perseguido es seleccionar una técnica de no contacto válida para la caracterización de materiales compuestos que proporcione información de campo completo y, a su vez, definir un sistema de medida de bajo coste que sea capaz de implementar la técnica de medida seleccionada. Una vez seleccionada la técnica y definido el sistema de medida (hardware y protocolo de actuación), se procede a la verificación del mismo. La **metodología** empleada es la fabricación de un **patrón calibrado** sobre el que se realizarán medidas para verificar la nueva técnica de medida con técnicas ya contrastadas como la extensiometría. Se procede de igual forma para la validación del prototipo, empleando un sistema de adquisición de datos (DAS) calibrado HBM Quantum MX840A.

Por el volumen de información generada, este artículo se centra sólo en la definición del sistema de medida de bajo coste denominado *Smartfire*, donde se desarrolla una plataforma basada en un microcontrolador de la serie Arduino, asistido por un API (Autómata Programable Industrial) capaz de realizar medidas (*Smartfire* vs DAS) con una precisión en el rango de trabajo del 0.3% en lo relativo a la adquisición de medidas de carácter mecánico. Al mismo tiempo a la plataforma desarrollada se le pueden incorporar sensores de otra naturaleza (temperatura, humedad, etc.). La comparación de los resultados teóricos vs DAS, proporcionan una precisión aceptable, siendo los errores inferiores al 4%. Estos resultados se emplearán posteriormente para la verificación del DIC.

La **conclusión** es que el patrón definido es apto para usarse para labores de calibración y que el sistema de medida diseñado cumple con los requisitos exigidos.

Otra consecuencia importante es que se encuentra una aplicación industrial para el resultado de este trabajo, por lo que las posibilidades de transferir el conocimiento a corto plazo son elevadas, debido a que el *Smartfire* puede ser empleado para la supervisión de recipientes a presión.

Aprovechando la sinergia con otros grupos de investigación, se diseña un software para la monitorización de extintores que implementa técnicas de inteligencia artificial (*Soft Agents*), donde se combinan las medidas puramente mecánicas con parámetros ambientales, de tal forma que se puede determinar el estado de un extintor e incluso emplear la información generada para predecir incendios.

Article

SmartFire: Intelligent Platform for Monitoring Fire Extinguishers and Their Building Environment

Roberto Garcia-Martin ¹, Alfonso González-Briones ^{2,3,*} and Juan M. Corchado ^{2,3,4,5}

¹ Mechanical Engineering Department, University of Salamanca, 49022 Zamora, Spain; toles@usal.es

² BISITE Research Group, University of Salamanca, Edificio I+D+i, Calle Espejo 2, 37007 Salamanca, Spain; corchado@usal.es

³ Air Institute, IoT Digital Innovation Hub (Spain), Carbajosa de la Sagrada, 37188 Salamanca, Spain

⁴ Department of Electronics, Information and Communication, Faculty of Engineering, Osaka Institute of Technology, Osaka 535-8585, Japan

⁵ Pusat Komputeran dan Informatik, Universiti Malaysia Kelantan, Karung Berkunci 36, Pengkaan Chepa, Kota Bharu 16100, Kelantan, Malaysia

* Correspondence: alfonsogb@usal.es; Tel.: +34-923-294-400 (ext. 5479)

Received: 12 April 2019; Accepted: 23 May 2019; Published: 25 May 2019

Abstract: Due to fire protection regulations, a minimum number of fire extinguishers must be available depending on the surface area of each building, industrial establishment or workplace. There is also a set of rules that establish where the fire extinguisher should be placed: always close to the points that are most likely to be affected by a fire and where they are visible and accessible for use. Fire extinguishers are pressure devices, which means that they require maintenance operations that ensure they will function properly in the case of a fire. The purpose of manual and periodic fire extinguisher checks is to verify that their labeling, installation and condition comply with the standards. Security seals, inscriptions, hose and other seals are thoroughly checked. The state of charge (weight and pressure) of the extinguisher, the bottle of propellant gas (if available), and the state of all mechanical parts (nozzle, valves, hose, etc.) are also checked. To ensure greater safety and reduce the economic costs associated with maintaining fire extinguishers, it is necessary to develop a system that allows monitoring of their status. One of the advantages of monitoring fire extinguishers is that it will be possible to understand what external factors affect them (for example, temperature or humidity) and how they do so. For this reason, this article presents a system of soft agents that monitors the state of the extinguishers, collects a history of the state of the extinguisher and environmental factors and sends notifications if any parameter is not within the range of normal values. The results rendered by the SmartFire prototype indicate that its accuracy in calculating pressure changes is equivalent to that of a specific data acquisition system (DAS). The comparative study of the two curves (SmartFire and DAS) shows that the average error between the two curves is negligible: 8% in low pressure measurements (up to 3 bar) and 0.3% in high pressure (above 3 bar).

Keywords: fire extinguishers; monitoring; SmartFire; soft agents systems

1. Introduction

One of the most crucial safety aspects of any building is ensuring that all the necessary fire safety measures are in place. The building must have a clearly marked emergency exit route that will safely guide people out of the building [1]. However, within the possibilities of the building, other measures must also be in place to try, as far as possible, to extinguish or contain fire. Fire extinguishers are one such measure, which are used to extinguish or control small fires in emergency situations. However, they are not designed for use in uncontrolled fires that endanger the user (i.e., no exit route, smoke, explosion hazard, etc.), or that requires the expertise of a fire department.

Typically, a fire extinguisher consists of a cylindrical pressure vessel containing an agent that can be discharged to extinguish fire. There are also fire extinguishers made from non-cylindrical pressure vessels but they are less common [2,3]. There are two main types of fire extinguishers: stored-pressure and cartridge-operated. In stored pressure units, the expellant is stored in the same chamber as the firefighting agent itself. Different extinguishers are used depending on the fuel that has caused the fire; these are classified by letters, which refer to the type of fire the extinguisher is designed for. The types of fire are:

- Class A: Fires that involve solid fuels such as wood, cardboard, plastic, etc.
- Class B: Fires that involve liquid fuels such as oil, gasoline or paint.
- Class C: Fires that involve gas fuels such as butane, propane or city gas.
- Class D: Fires of this type are the rarest, the fuel is a metal, and the burning metals are magnesium, sodium or aluminium powder.

Taking this categorization into account, we can better understand the types of available fire extinguishers and the fire extinguishing agents they contain. The most common extinguishing agents include:

- Water: Suitable for Type A fires always in places where there is no electricity. Water is not suitable for fires involving liquid fuels such as gasoline or oil because it is denser than those liquids; as a result, the fuel would remain on top of the water and it would not be possible to extinguish the fire.
- Water spray: Ideal for extinguishing Type A fires and suitable for Type B fires. They should never be used in the presence of electric current as water could cause electrocution. This type of fire extinguisher is good outside of homes where there is no electrical risk, such as gardens, barbecues, etc.
- Foam: Ideal for Type A and B fires; we have all seen firefighters spray foam at emergency drills. As with the previous one, it is dangerous in the presence of electricity.
- Dust: It is the most common type and is used in any building. It is suitable for fires of Types A, B and C. It is powdery so it can be used in the presence of electricity. It is the most recommended extinguisher for houses, offices or any other type of building.
- CO₂ extinguishers: CO₂ is a gas and thus cannot conduct electricity. This type of fire extinguisher is suitable for fires of Types A, B and C. It is usually used in the presence of delicate elements where other types of extinguishers would damage the objects. If we use a standard fire extinguisher in a laboratory, for example, the foam or powder could damage expensive machines and equipment. Thus, CO₂ extinguishers are ideal for this type of environments. Although they are the most versatile of all available extinguishers, they are also the most sensitive ones; changes in temperature can affect them considerably. Given that they do not have a manometer, it is impossible to know their pressure in real time, thus manual inspection is necessary.

Since fire extinguishers are pressure appliances, they require maintenance operations to ensure they function properly in the case of a fire. For this reason, the condition of fire extinguishers is checked periodically, including their security seals, inscriptions, hoses, etc. This mainly includes checking the state of charge of the extinguisher (weight and pressure), the bottle of propellant gas (if available), and the state of all mechanical parts (nozzle, valves, hose, etc.). All this is done to make sure they are safe and that they will be effective in extinguishing a fire. Moreover, it is necessary to ensure that they are located in a visible place that is easy to access [4].

Currently, the inspection of the fire extinguishers must be performed by a specialized operator. These checks are carried out manually every three months, one year or five years, depending on the type of the fire extinguisher. All fire extinguishers cannot exceed twenty years of useful life. Thus, the investigation of automated inspection methods would be of great benefit as it would allow

one to control the condition of the fire extinguishers in real time. As a result, the company responsible for inspecting the fire extinguishers would be notified immediately after an abnormal condition (in terms of weight or pressure) is detected by the automated system. Hence, an automated system is going to provide the confidence that all the fire extinguishers are in their optimal condition in the case of a fire. Moreover, this would contribute to economic saving since it would no longer be necessary for operators to go for periodic inspections. The automated system would review the state of all the fire extinguishers simultaneously. At the time of inspection, both mechanical components and pressure are checked. It is unusual to detect faults in the state of the mechanical components, although it is possible to detect faults in the state of the pressure of the extinguisher. The reason for inspecting both aspects of the fire extinguishers at the same time is more for economic reasons rather than functional reasons. However, reviews are also carried out in the event of detection of a mechanical defect (lack of any component, damaged elements, etc.) or variation in pressure (small and inaccurate manometers or lack thereof, e.g., in CO₂ extinguishers).

To be able to monitor the state of the extinguishers in real time and perform autonomous control, it is necessary to place sensors on them, including pressure, temperature, humidity and smoke sensors [5,6]. Devices with high levels of pressure such as CO₂ units require sensors that are more expensive than the extinguisher itself, and thus the proposed system provides a much more economical solution.

In this way, it is possible to analyze the impact of the incidence of factors such as humidity or temperature on the condition of the fire extinguisher. However, there are even greater possibilities if a position sensor is deployed. If the set of sensors includes a position sensor, it would be possible to find out (when the temperature began to rise in the building) when each fire extinguisher was used; how the fire spread through the building; and the order in which the fire extinguishers were used (when it was removed from its support). The platform will therefore provide mechanisms that will allow one to understand how people behave in the event of a fire. This, in turn, would allow one to assess the security measures deployed in the building and adapt them to the behavior of people in emergency situations [7,8].

This information is very useful as it enables us to understand how people act in the event of a fire. Human behavior during the initial phase of a fire is, therefore, an important factor in terms of survival [9,10]. This would enable the development or optimization of exit routes within buildings or dwellings.

The goal of the work presented in this article was to provide a novel system of soft agents for the detection of pressure changes in fire extinguishers, as well as to record changes in the parameters that affect them, such as temperature, humidity, etc. If the information indicates any incidence or if any value is outside its normal range of values, an alert will be sent [11]. There is a similar system called en-Gauge Fire Extinguisher (<http://www.engaugeinc.net/fire-extinguisher-monitoring>) to the one presented in this article but it is a commercial product adapted to a concrete fire extinguisher model, which warns when the pressure level has fallen below an operable level, and also requires the installation of a plate on the wall. Our prototype can be used in any fire extinguisher, does not require work on the wall and thanks to the web platform can visualize the pressure at any time, which will allow in the future including machine learning techniques to perform predictive maintenance processes.

The main contributions of this paper include: the use of sensors to acquire information on the state of fire extinguishers and the detection of anomalies in the pressure of the extinguisher without the need for human intervention. The platform will could even provide knowledge on the behavior of people during a fire and on their use of the fire extinguishers. This is because one will know the area where the fire originally occurred by knowing which extinguisher was used first. To complement the data acquired from the fire extinguisher, the developed platform obtains data from the building environment [12]. The developed system uses a combination of information from the fire extinguishers and the building environment, providing knowledge of variables that influence the state of fire extinguishers, making real-time inspection possible without the need for operators.

The rest of the article is structured as follows: Section 2 reviews related state-of-the-art projects and most commonly used technologies. Section 3 describes the SmartFire platform. Section 4 outlines the case studies that were performed to evaluate the proposed platform. Section 5 outlines the results. Finally, Section 6 draws conclusions from this proposal and discusses future lines of research.

2. Related Work

This section presents a thorough review of state-of-the-art literature in the field of fire extinguishers. We analyzed the variables that affect the pressure under which the internal composition of fire extinguishers is stored and also performed an in-depth study of how to correctly measure the pressure of a fire extinguisher from its outside. Moreover, we looked into different technologies used in the literature, examining their advantages and disadvantages for the development of our platform.

We must point out, however, that the current literature does not present any type of platform that would be capable of analyzing the parameters that affect the pressure in fire extinguishers. This makes evident the contribution of our platform, which collects data autonomously and controls whether the parameters of all fire extinguishers are similar, detecting and notifying possible incidents.

The measurement of pressure is related to the measurement of deformation and in the case of small deformations the technology most used for this purpose is the use of strain gauges. These are used fundamentally for the determination of tensions, such that in our case it is sought to relate these with the pressure [13,14].

Another of the conditioning factors/limitations of this work consisted in finding a low-cost monitoring platform that would not make the final price of the extinguisher more expensive, capable of taking measurements (temperature, humidity, etc.) inside buildings with wireless communication and low consumption [15].

2.1. Proposals with SmartFire Sub-Objectives

There are no systems that realize in a single prototype the objectives proposed in this article. Here are some works that have proposed some solutions for partial objectives covered by the SmartFire prototype. Park et al. proposed the measurement of pressure gauge using color segmentation for the safety management of fire extinguisher [16]. The main idea is that pressure gauge includes a green color indicating the normal pressure. In the work done by Jia-ming Jin, the release characteristics of the gas extinguishing agent from fire extinguisher vessel at different filling conditions was studied [17,18]. The results show that the outlet pressures of the fire extinguisher vessel have the same trend basically at different initial temperature: all of them decline rapidly with the jetting time and then tend to be gentle. Park et al. [18] proposed again a fire extinguisher maintenance system using smart NFC communication as well as real-time pressure measurement. The proposed system consists of three steps in the flow of information. The first step is to identify the fire extinguisher through NFC tagging in the fire extinguisher module using the smart device. The fire extinguisher appearance check and the real-time pressure measurement is performed in the second step, and the last step sends the check status information to the management server. In particular, the actual pressure value is calculated based on the angle of the green area and the indicating needle. However, the use of NFC severely limits these systems in large multi-story office buildings. Other work is based on measuring pressure drops such as the work presented by [19]. They developed an application of the portable fire extinguishing equipment in fire prevention of power transmission line results and showed that massive wildfires can be extinguished quickly. By using the equipment, electric power company's ability of resisting wildfires has gained remarkable improvement.

2.2. Algorithm for Calculating the Pressure of a Fire Extinguisher

In mechanical design, to be able to calculate the stress of an element, it is necessary to know what material it is made of, its geometry and the conditions it is subjected to. In terms of the development of behavioral theories (the development presented in this paper), they are based on two principles:

(i) equilibrium, i.e., both external forces (in this case pressure) and internal forces (the reaction of the material) counteract each other; and (ii) compatibility of deformations, i.e., the deformations in different elements are contiguous with each other.

With regard to pressurized vessels, there are two theories [20], depending on the relationship between the radius of the element and its thickness.

If the thickness (t) is at least one order of magnitude smaller than the inner radius, it will be considered as a thin-walled case; there are also some other upper limits for these criteria given in the literature such as $r_i/t > 20$ where r_i is the inner radius, which means that, when $r_i/t < 20$, the thickness is more relevant than the radius [21]. Thus, a different formulation must be used in each case.

A pressure vessel can be spherical or cylindrical with hemispheric or ellipsoidal endings. We took measurements of the cylindrical part since it is a well-defined area, in which the following stresses appear (Figure 1):

- σ_θ , the tangential tension, goes in the tangent direction to the circumference. It is the highest of all and increases the perimeter of the cylinder, as a result of the level of deformations, the wall of the cylinder separates along its generator.
- σ_r , the radial stress goes in the direction of the radius at the deformation level, making the radius increase in length. It is the smallest of them all.
- σ_z , the stress in the direction z makes the cylinder increase in length, at the deformation level it is as if the cylinder were pulled at the ends and stretched.

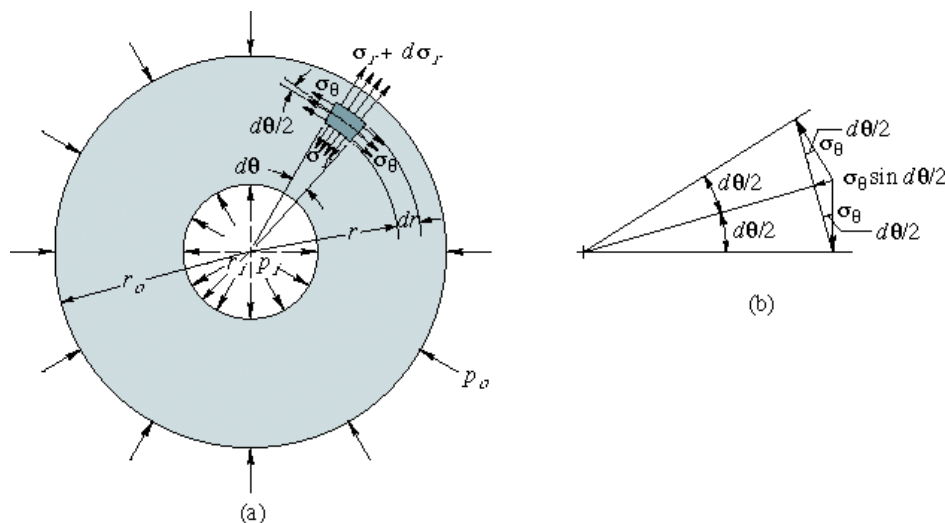


Figure 1. Stress diagram: thick-walled case.

In mechanical engineering, depending on the case, i.e., thin or thick wall, different formulations are available, the latter being the most complex.

1. Thin wall, $r_i/t > 20$. In this case, the effect of the thickness is not considered, hence the radial stress (σ_r) is not taken into account, since it is assumed that the tangential stress (σ_θ) is much larger than the radial stress, which is therefore ignored; the expressions for these stresses [20] are:

Tangential stress:

$$\sigma_\theta = Pr/t \quad (1)$$

Axial stress:

$$\sigma_z = Pr/2t \quad (2)$$

Radial stress:

$$\sigma_r = 0 \quad (3)$$

These expressions relate internal pressure (P), radius (r) and thickness (t). For the case of the radius, we assume (since thickness is not considered) that both internal and external radii are equal ($r_i = r_o$). Some authors use the mean radius (r_m), which is more accurate.

In our case, what we can measure are deformations and not stresses, but through Hooke's Law [22], which relates tensions and deformations (Equations (5) and (6)) within the linear elastic regime, it is possible to relate the deformation caused by the internal pressure of the gauge because our extinguisher works in this regime.

$$\sigma_{ij} = E\varepsilon_{ij} \quad (4)$$

The linear modulus of elasticity (E) is a known characteristic of the material, and ε_{ij} is the deformation measured with the gauge, where the subscripts ij indicate the direction in which the deformation occurs.

In radial systems, the spatial directions x,y,z are replaced by the radial direction (r), tangential (θ) and z is maintained.

The objective of this work was to relate the deformation (ε) with the pressure (P) that it produces; we can relate the values of P with ε since we know the stress values as functions of the pressure (Equations (1) and (2)) and the value of the deformation (ε) is obtained directly from the gauge. Depending on how the gauge is positioned on the container, it is measured. If the gauge is positioned in the axial direction, the value of ε_z is measured and if it is placed tangentially, ε_θ is obtained.

$$\sigma_{r,\theta,z} = E\varepsilon_{r,\theta,z} \quad (5)$$

Then the value of the tangential stress (Equation (1)) is introduced in Equation (5); thus, via algebra, we can obtain the internal pressure of the vessel (Equation (6)) since it presents the relation P vs. ε_θ according to known geometrical parameters and material properties, in this case, the Young's modulus (E), and the Poisson's ratio (ν), which is a parameter of the material and is provided by the manufacturer or obtained through mechanical test. We operate in the same way to obtain the relationship between P and ε_z (Equation (7)). In thin wall cases, the radial direction deformation value is ignored, and the gauge cannot be placed in this direction.

A large diameter fire extinguisher with a common pressurization (13 bar) is a thin-walled type of fire extinguisher (wheeled extinguisher and extinguishing tanks). In Equation (5), the values measured by the gauge in tangential direction together with Equation (1) are replaced by Equation (6). Similarly, we operate in the z (axial) direction, providing Equation (7), which is the expression to be used in metal containers, since in the radial direction the deformation value is ignored and the gauge cannot be placed.

Measurement of the deformation in tangential direction:

$$P = \varepsilon_\theta E \frac{t}{r_m} \quad (6)$$

Measurement of axial deformation:

$$P = \varepsilon_z E \frac{2t}{r_m} \quad (7)$$

Most of the portable devices are pressurized to 13 bar and their diameters are larger than the thickness (especially in wheeled extinguisher and extinguishing tanks) with the aim of optimizing the volume, thus thin wall is the most common situation, except the CO₂ devices due to the high pressure.

2. Thick wall, $r_i/t < 20$ In this case, the idea is the same, but the formulation is more complex because it is not possible to apply the simplification of negligible thickness in the equations, as it does have an influence here. In Figure 1, we see that the internal pressure generates a series of stresses that will deform the material, as shown in Figure 2. In Figure 2, we can see an undeformed and a deformed element, where the value of the deformation can be calculated by applying finite differences in such a way that we can obtain the value of the deformation according to the displacements.

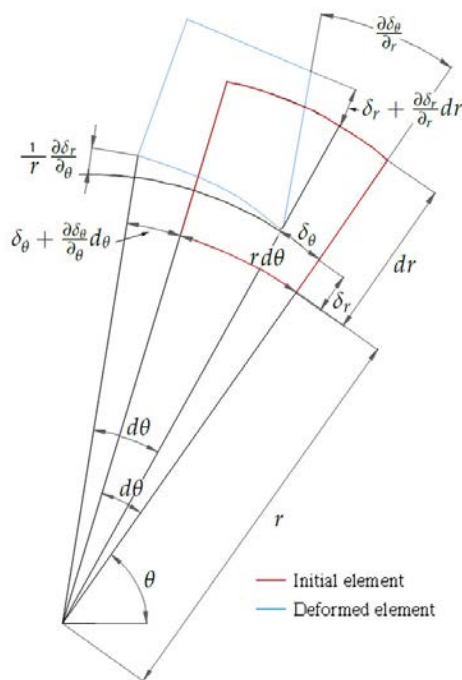


Figure 2. Deformation scheme: thick-walled case.

Equations (8) and (9) allow relating deformations to stress, and are fundamental equations exposed in the Fundamentals of Machine Elements deformation theory [23]. These equations are used in the following steps for the calculation of pressure.

$$\varepsilon_r = \frac{\delta_r + \frac{\partial \delta_r}{\partial r} dr - \delta_r}{dr} = \frac{\partial \delta_r}{\partial r} \quad (8)$$

$$\varepsilon_\theta = \frac{(r + \delta_r)d\theta - rd\theta}{rd\theta} = \frac{\delta_r}{r} \quad (9)$$

Here, again, our goal is to calculate pressure as a function of deformation. We know that pressure generates stresses that in turn generate deformations. Now, we reverse this logic and obtain the stresses from the deformations. This is achieved by applying Hooke's law (Equation (4)) where the expressions of both radial (Equation (10)) and tangential (Equation (11)) deformations are functions of both radial and tangential stresses.

$$\varepsilon_r = \frac{1}{E}(\sigma_{r-\theta}\sigma_\theta) \quad (10)$$

$$\varepsilon_\theta = \frac{1}{E} (\sigma_{\theta-\vartheta} \sigma_r) \quad (11)$$

By equating Equations (8) and (10), we obtain Equation (12), and, by equating Equations (9) and (11), we obtain Equation (13).

$$\frac{\partial \delta_r}{\partial r} = \frac{1}{E} (\sigma_{r-\vartheta} \sigma_\theta) \quad (12)$$

$$\frac{\delta_r}{r} = \frac{1}{E} (\sigma_{\theta-\vartheta} \sigma_r) \quad (13)$$

Equations (12) and (13) form a system of two equations and three unknowns, where, if we apply the criterion of equilibrium to the system of forces that generate the tensions (Figure 1), we obtain Equation (14), such that this equation complements the previous system and it can be solved as a compatible and determined system.

$$\begin{aligned} (\sigma_r + d\sigma_r)(r + dr)d\theta dz - \sigma_r r\theta dz - 2\sigma_\theta \sin \frac{d\theta}{2} dr dz &= 0 \\ \sin(\frac{d\theta}{2}) &= \frac{d\theta}{2} \rightarrow \sigma_\theta = r \frac{d\sigma_r}{dr} + \sigma_r \end{aligned} \quad (14)$$

By substituting Equation (14) into Equation (13) and deriving it from r , we get Equation (15)

$$\begin{aligned} \frac{\delta_r}{r} &= \frac{1}{E} (r \frac{d\sigma_r}{dr} + \sigma_{r-\vartheta} \sigma_r) \rightarrow \delta_r = \frac{r}{E} (r \frac{d\sigma_r}{dr} + \sigma_{r-\vartheta} \sigma_r) \\ \frac{\partial \delta_r}{\partial r} &= \frac{2r}{E} \frac{\partial \sigma_r}{\partial r} + \frac{r^2}{E} \frac{\partial^2 \sigma_r}{\partial r^2} + \frac{\sigma_r}{E} + \frac{r}{E} \frac{\partial \sigma_r}{\partial r} - \frac{\vartheta \sigma_r}{E} - \frac{r\vartheta}{E} \frac{\partial \sigma_r}{\partial r} \end{aligned} \quad (15)$$

If we now substitute Equation (14) into Equation (12) and equate it to Equation (15), by substituting and operating, we obtain the relationship in Equation (16), which can also be expressed as Equation (17).

$$0 = 3 \frac{\partial \sigma_r}{\partial r} + r \frac{\partial^2 \sigma_r}{\partial r^2} \quad (16)$$

$$0 = 2 \frac{\partial \sigma_r}{\partial r} + \frac{\partial}{\partial r} (r \frac{\partial \sigma_r}{\partial r}) \quad (17)$$

Integrating once:

$$0 = 2\sigma_r + r \frac{\partial \sigma_r}{\partial r} + C_1 \quad (18)$$

Re-integrating and simplifying:

$$0 = \frac{\partial}{\partial r} (r^2 \sigma_r) + C_1 r \quad (19)$$

Integrating once again:

$$\sigma_r = \frac{-C_1}{2} - \frac{-C_2}{r^2} \quad (20)$$

Applying the boundary conditions to Equation (20), for a general pressurization case where we would have to:

$$\sigma_r|_{r=r_i} = P_i \rightarrow P_i = \frac{-C_1}{2} - \frac{-C_2}{r_i^2} \quad (21)$$

$$\sigma_r|_{r=r_0} = P_o \rightarrow P_o = \frac{-C_1}{2} - \frac{-C_2}{r_o^2} \quad (22)$$

By operating, we obtain the value of the constants:

$$c_2 = \left(\frac{P_o - P_i}{r_o - r_i} \right) \left(\frac{r_o^2 - r_i^2}{r_i^2 r_i^2} \right) \quad (23)$$

$$c_1 = -2 \left[\frac{1}{r_o^2} (P_o - P_i) \left(\frac{r_o^2 - r_i^2}{r_i^2 r_i^2} \right) + P_o \right] \quad (24)$$

such that, by substituting the value of the constants in Equation (20) and simplifying, we obtain:

$$\sigma_r = \frac{P_i r_i^2 - P_o r_o^2 + (P_o - P_i) \left(\frac{r_o r_i}{r} \right)^2}{r_o^2 - r_i^2} \quad (25)$$

The tangential stress is provided by Equation (14), where by substituting the value of the radial stress (Equation (25)) and the value of its derivative with respect to r (Equation (26))

$$\frac{\partial \sigma_r}{\partial r} = \frac{-2(P_o - P_i)(r_o r_i)^2}{r^3(r_o^2 - r_i^2)} \quad (26)$$

$$\sigma_\theta = r \frac{-2(P_o - P_i)(r_o r_i)^2}{r^3(r_o^2 - r_i^2)} + \frac{P_i r_i^2 - P_o r_o^2 + (P_o - P_i) \left(\frac{r_o r_i}{r} \right)^2}{r_o^2 - r_i^2} = \frac{P_i r_i^2 - P_o r_o^2 - (P_o - P_i) \left(\frac{r_o r_i}{r} \right)^2}{r_o^2 - r_i^2} \quad (27)$$

For this particular case, where $P_o \ll P_i$, it is assumed that $P_o = 0$, substituting in Equations (25) and (27) would give particular stress values.

$$\begin{aligned} \sigma_r &= \frac{P_i r_i^2 \left(1 - \left(\frac{r_o^2}{r^2} \right)^2 \right)}{r_o^2 - r_i^2} \\ \sigma_\theta &= \frac{P_i r_i^2 \left(1 + \left(\frac{r_o}{r} \right)^2 \right)}{r_o^2 - r_i^2} \end{aligned} \quad (28)$$

Finally, to return to Equation (11), we can relate the deformation with the pressure

$$\varepsilon_\theta = \frac{1}{E} (\sigma_\theta - \vartheta \sigma_r) = \frac{1}{E} \left(\frac{P_i r_i^2 \left(1 + \left(\frac{r_o}{r} \right)^2 \right)}{r_o^2 - r_i^2} - \vartheta \frac{P_i r_i^2 \left(1 - \left(\frac{r_o^2}{r^2} \right)^2 \right)}{r_o^2 - r_i^2} \right) \quad (29)$$

Since the strain gauge is placed on the outside radius, the expression is reduced to:

$$\varepsilon_\theta = \frac{1}{E} \left(\frac{P_i r_i^2 \left(1 + \frac{r_o^2}{r^2} \right)}{r_o^2 - r_i^2} - \vartheta \frac{P_i r_i^2 \left(1 - \frac{r_o^2}{r^2} \right)}{r_o^2 - r_i^2} \right) = \frac{1}{E} \frac{2P_i r_i^2}{r_o^2 - r_i^2} \rightarrow P_i = \varepsilon_\theta E \frac{r_o^2 - r_i^2}{2r_i^2} \quad (30)$$

Since both the material and the geometry are known, by placing a gauge on the outside of the fire extinguisher in the tangential (circumferential) direction, we can determine the value of the internal pressure in the vessel (fire extinguisher).

2.3. Agent Based Monitoring Platform

Nowadays, the evolution of the electronics field has allowed us to greatly reduce the size of sensors, thus we are able to collect values for very different parameters through the placement of small devices. The field of communications has also evolved enormously through the development of communication protocols that allow us to send long distance data with little power consumption. For this reason, the developed device is going to allow us to measure the pressure of the extinguishers

autonomously and send the measurements to an external platform that manages those measurements and detects anomalies.

There is no device for measuring pressure changes in fire extinguishers with the size and accuracy characteristics required for this task, nor is there a platform to monitor a set of fire extinguishers and send notifications to the personnel responsible for their maintenance. There are some similar works but their focus is not the same as that of this work. One of these works is the one proposed by Chow, who presented a fire safety classification system (EB-FSRS) to evaluate the fire safety provisions in the existing high rise non-residential buildings in Hong Kong. The aim is to investigate to what extent the fire safety provisions of existing buildings deviate from the expectations of the new codes [24]. Other work has focused on the development of computer vision techniques to be used by drones to detect fires in open spaces, such as those developed by Chamoso et al. [25] and Verstock et al. [26].

Rashid et al. developed a multi-sensor-based fire-extinguishing robot and demonstrated its implementation with a brief discussion on its construction and operation [27]. As can be seen from these works, the great majority are focused on extinguishing or detecting fires but not on ensuring that the security measures are in optimum condition.

In this respect, the system of soft agents allows one to implement one agent in each SmartFire prototype in a building in a way that allows them to communicate, coordinate and cooperate when monitoring the set of extinguishers in the building. This agent methodology has been widely applied in the monitoring work in various areas [28,29].

Thanks to the monitoring of the environmental conditions of an extinguisher, the use of this methodology in the future is going to make it possible to analyze the origin of a fire, the conditions in which it occurred and the behavior of people in this situation. With the environmental values of each extinguisher, new soft agents can be deployed for the application of big data techniques based on preventing possible sources of fires.

3. SmartFire Platform

This section details the SmartFire architecture, the description of the prototype and the software architecture that allows us to apply the algorithm for calculating the pressure of a fire extinguisher.

3.1. Prototype Overview

At the Mechanical Engineering Department laboratory, University of Salamanca, Zamora, we have HBM equipment, a Quantum MX840A (Figure 3c), which is used specifically for data acquisition and is particularly accurate when measuring with strain gauges. The Quantum system is used exclusively to calibrate the SmartFire prototype.

The proposed architecture (Figure 4) requires both a signal capture system (input) and wireless communications (output) all managed by a control system. The management system uses a microcontroller of the Arduino series, specifically the wemos WiFi and bluetooth Battery, which allows for wireless communications. This is of vital importance because the system should be coupled with the extinguisher and be an isolated component. In other words, the system does not need to be connected to a power supply network or to a fixed data network, as it has an autonomous power supply system (it can even be connected to a solar panel). The prototype includes a DH22 sensor on the outside of the housing to also obtain temperature and humidity data.

The features are: WiFi module (ESP-WROOM-02) with digital and analog 10-bit I/O, hence the use of the amplifier (HX711 Load Cell Amplifier Module), which provides 12 bits. The amplifier is the same as that used when weighing systems, which in the end uses a strain gauge that relates the deformation of the weighing systems with the applied load. The latter is connected to a wheatstone bridge for gauging.

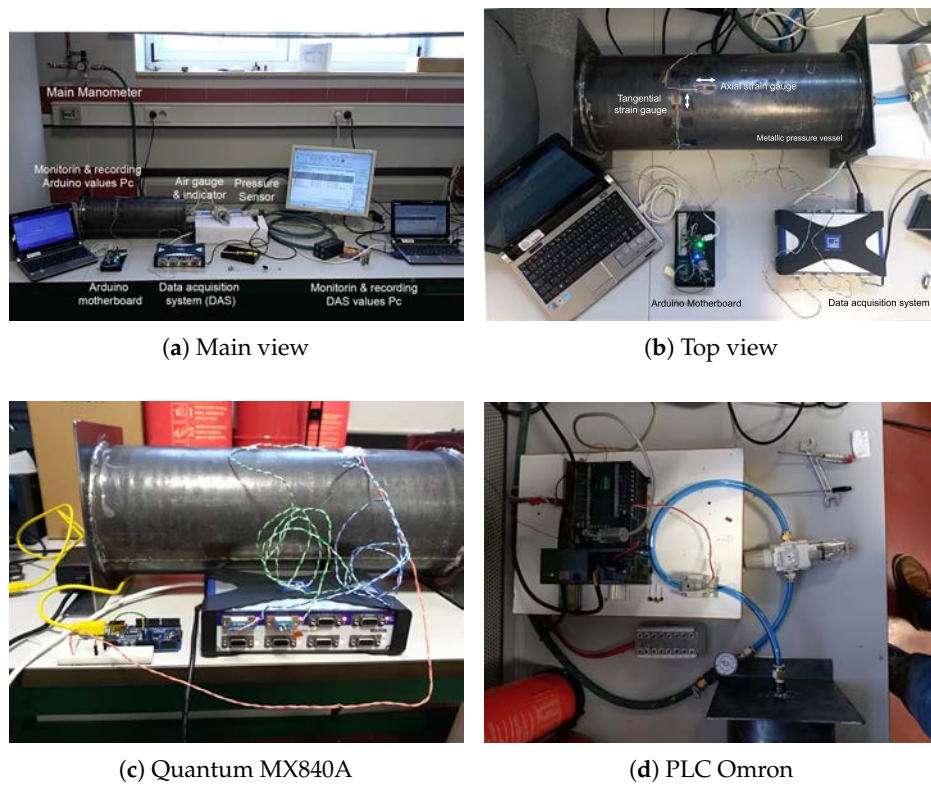


Figure 3. Overview of the pressure measurement equipment.

A Programmable Logic Control (PLC) of the Omron CP1H-XA brand is used (the A indicates that it has an analog I/O card; Figure 3d). This element is used to control all the generated test equipment (general prototype). The PLC manages the entire power system of the installation, controls the valves of the circuit that provide the pressure to the test specimen (pressure vessel). In addition, the pressure sensor is connected to the analog board of the PLC, which works in trigger mode, sending the order to both, the prototype and the Quantum to record the pressure values obtained in steps of 0.5 bar (50 kPa).

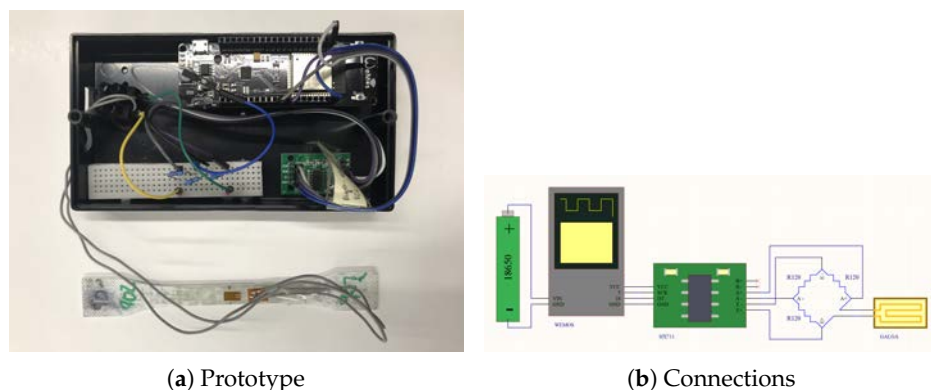


Figure 4. SmartFire prototype.

Pneumatic elements: The laboratory of Mechanical Engineering of the EPSZ has diverse pneumatic material with which the tests were performed, from the compressor, ducts, and electrovalves to instruments for measuring pressure, both basic (manometers) and high precision (head pressure sensor rotary 0–10 mpa Panasonic), as well as pressure regulators. The manometers are used as redundant instruments (a total of two are used) to verify that the measurement offered by the PLC of the pressure

sensor is within the proper range (the accuracy of the pressure gauge is ± 0.1 bar and that of the sensor is ± 0.01 bar. This is done as a control method, to avoid configuration failures in the PLC).

3.2. Soft Agent Platform

The autonomy of soft agent systems allows them to interact with each other without human intervention. Their ability to perceive and react to changes in the environment makes this methodology an ideal approach for obtaining environmental data and responding to those changes with appropriate actions. Characteristics such as extensibility and flexibility make it possible to add new functionalities or include other algorithms and sensors. These advantages have led to numerous monitoring proposals that employ agent systems [30,31].

Agent systems are often applied in the field of process automation due to their ability to deal with more complex systems. Various agent systems have been developed for the management of energy optimization processes [29]. However, there is no record of any state-of-the-art developments that would use a soft agent platform to monitor the state of fire extinguishers in a building. This soft agent platform allows us to communicate with the SmartFire prototype for the reception of pressure values in real time for each of the monitored fire extinguishers.

The platform was developed using the JADE framework which facilitates the development of communication processes between agents by making use of the FIPA-ACL communication standard (Figure 5). This platform based on an architecture of lightweight agents communicates with the SmartFire prototype for the reception of pressure values in real time for each fire extinguisher monitored. The platform makes it possible to visualize this data through a website, as shown in Figure 6, and to send notifications to the people responsible for the maintenance of the extinguishers in the event that a fire extinguisher is out of the threshold of normal pressure values. Figure 7 shows the diagram of the functional concept of architecture, which shows how the agent-based system allows to carry out part of the reception of the measurements of the deployed prototypes to make notifications, statistics or visualization of data among others.

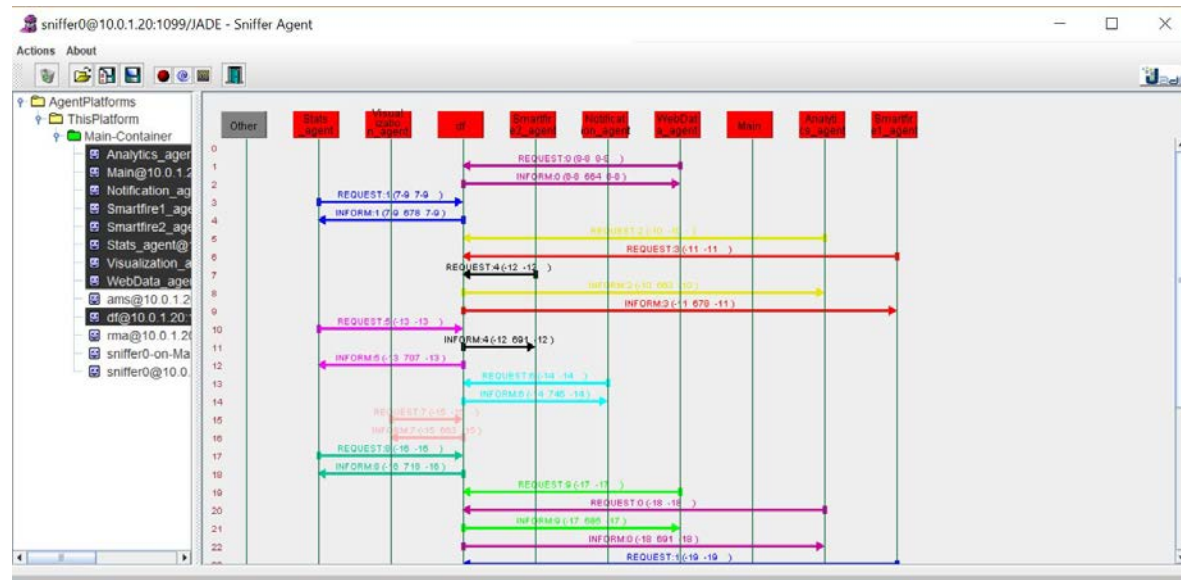


Figure 5. Visualization of agent communications on the SmartFire agent platform (JADE sniffer).



Figure 6. Visualization of the pressure values of the different extinguishers deployed in the building via the SmartFire web system.

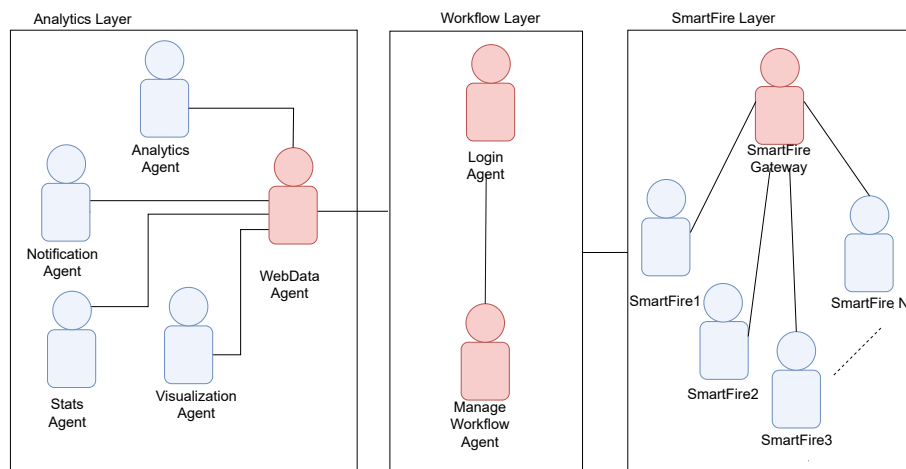


Figure 7. SmartFire platform diagram of the functional concept of the architecture.

4. Case Study: Laboratory Validation

This section details all the components that were involved in the case study (Figure 8) and how the case study was conducted.

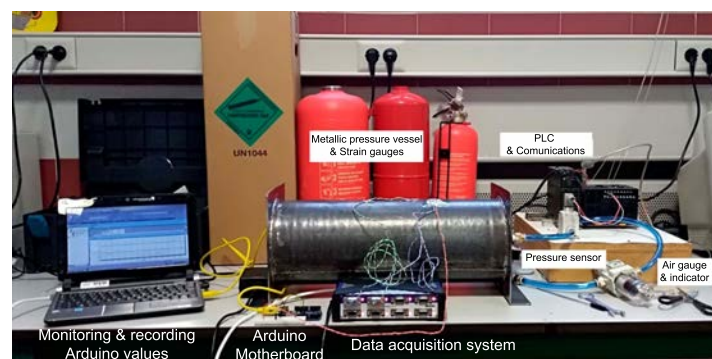


Figure 8. Laboratory validation of pressure measurement equipment.

The main idea was to take redundant measures and make sure that all of their values were the same, so that some methods would work for others. Step 1: Make a thin wall pressure vessel. Since the theory of cylinders has been sufficiently tested and its use for metallic materials has been proven, a calibrated specimen made of metal was constructed.

In our case, a controlled pattern pressure vessel (Figures 3 and 8) was manufactured with the following dimensions: inner diameter, $d_i = 170$ mm; length, 450 mm; and thickness, $t = 1.5$ mm. The vessel was made of steel of controlled properties (Table 1).

Table 1. Characteristics of steel St 37-2 according to standard EN 10025-2: 2004, grade S235JR.

Property	Value	Unit
Mechanical		
Ultimate Strength	425	MPa
Yield Strength	333	MPa
Young's modulus	205	GPa
Poisson's ratio	0.29	—
Thermal		
Thermal expansion coefficient	11.5	$\mu\text{strain}/^\circ\text{C}$

The dimensions of this test specimen (pressure vessel) were mainly determined by the pressure limitations of the test laboratory; although it was possible to access higher pressure levels, this was not necessary since the results were perfectly extrapolated.

A series of strain gauges (Figure 9) were placed on the extinguisher, arranged in both radial and axial directions, the purpose of which was to capture measurements in different directions, since redundant measurements increase precision.



Figure 9. Strain gauges.

These gauges were connected to both of HBM's commercial data acquisition system (DAS), Quantum (Figure 3c, blue and green cables), and the microcontroller (Figure 3, orange cable). The data acquired by the Quantum were displayed on the notebook (Figure 8) through the commercial Catman Easy software version 3.1.3.22.

Step 2: Calibrate pressure sensor. By means of the pressure regulator (Figure 3a), which includes a manometer, fixed pressure values were administered to the container. The values were verified with the different manometers inserted in the circuit and compared with the reading provided by the pressure sensor (Figure 3a). The pressure sensor was placed in a series with the rest of the manometers in the circuit. The reading of the pressure sensor was performed by the PLC, to which the pressure

sensor was initially connected. This reading was displayed on the computer through its control software (CX-one), which provided measurements in real time. It was observed that the readings of all the pressure gauges, as one of the pressure sensors, coincided with what the calibration of the PLC considered good. The function of the PLC was to detect the pressure level to obtain the pressure values. Once the pressure set point was reached, it allowed 10 s to elapse. During this period, the value stabilized and was then recorded.

Step 3: Check the gauge dimension. Once the validity of the pressure measurement system was checked, the strain gauge measurement was checked and the formulation was applied (Section 2.2). The specimen parameters (material and geometry) and pressure were entered into the computer and the theoretical deformation measurement of the vessel was obtained in both tangential and axial directions. The theoretical results were then compared with the measurements provided by the Quantum. The obtained results confirmed the measures.

Step 4: Check the SmartFire system measurement Figure 10. Pressure was applied progressively, where the PLC, at prescribed pressure steps, ordered both the Quantum and the SmartFire prototypes to register the deformation values, such that pressure–deformation measurements were obtained from both systems.



Figure 10. A SmartFire prototype situated in a fire extinguisher in the building of the case study.

5. Results

Once the case study was validated, it was necessary to compare the results obtained by both the PLC system and the SmartFire prototype to validate whether the prototype was as precise in calculating the changes in pressure as the professional machine. To find out if the small prototype had the same precision, the curves obtained in Step 4 of the case study were compared (Figure 11).

This comparison showed that the error between the two curves occurred in low pressure measurements (up to 3 bars) was an average of 8%. At high pressure (from 3 bar up to 8 bar, maximum value used in the test), there was an average error of 0.3%, a negligible value. These values were used to verify the measurement capabilities of SmartFire.

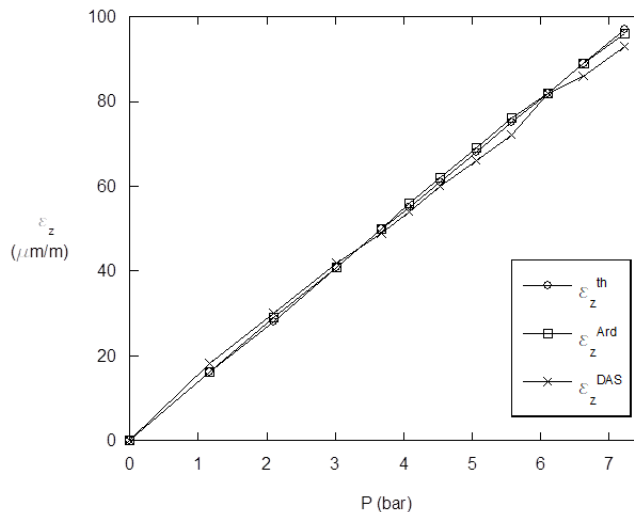


Figure 11. Comparison chart of the measurements obtained: $\varepsilon_z^{\text{th}}$, theoretical values; $\varepsilon_z^{\text{Ard}}$, SmartFire; $\varepsilon_z^{\text{DAS}}$, data Acquisition system. All values correspond to the longitudinal deformations (ε_z) included in Table 2, and are expressed in microns. Notice that the longitudinal axis is used as reference for the deformations, whereas the transversal axis is used for validating the DAS measurements.

Taking into account that the input data (geometry, material and pressure) are known, the theoretical value of deformation was calculated and then compared with the ones obtained experimentally (Table 2). According to the obtained results, the deviation between the data obtained by the prototype vs. theoretical values was always lower than 2%, whereas the values obtained by DAS vs. theoretical ones were lower than 4%. From these results, it can be concluded that the errors were higher in low pressure values in the testing program. This was predictable since the deformation was too low and the temperature affected the gauges.

Table 2. Longitudinal deformation measurement (in microns) by different techniques vs. Pressure. $\varepsilon_z^{\text{th}}$, theoretical values; $\varepsilon_z^{\text{Ard}}$, SmartFire; $\varepsilon_z^{\text{DAS}}$, data Acquisition system.

Pressure (Bar)	$\varepsilon_z^{\text{th}}$	$\varepsilon_z^{\text{Ard}}$	$\varepsilon_z^{\text{DAS}}$
0	0	0	0
1.17	16	16	18
2.097	28	29	30
3.02	41	41	42
3.677	50	50	49
4.072	55	56	54
4.532	61	62	60
5.056	68	69	66
5.575	75	76	72
6.105	82	82	82
6.63	89	89	86
7.226	97	96	93

6. Conclusions and Future Work

In this work, a novel platform has been presented for monitoring fire extinguishers in a building. The platform consists of a prototype that makes it possible to detect changes in pressure in real time and record the environmental conditions in which they have occurred (temperature, humidity, etc.). The use of soft agents has allowed for communication between the SmartFire prototype and the platform. Moreover, it has made it possible to read the pressure values of each extinguisher at all times. The architecture on which the platform is based allows us to integrate new agents by monitoring new factors, including agents that implement big data techniques to predict when a fire extinguisher will

fail before it is produced. Experimental validation in the laboratory has allowed us to certify that the SmartFire prototype rigorously complies with the precision requirements of safety monitoring devices. In addition, the SmartFire prototype allows, in a very economical way, to carry out a review of the extinguishers of a building versus the traditional method, as it is not necessary to send anybody to check the device physically, because one can know instantaneously when the extinguisher ceases to be in optimal conditions.

As future lines of work, we intend to design a case study in an office building for real-time monitoring of fire extinguishers. This will allow us to find out when a fire extinguisher is not suitable for use immediately after an anomaly occurs. Moreover, it will be possible to calculate the average time that the extinguisher would continue to be in an anomalous state if only traditional inspections existed. This case study would show the average time that elapses from the time an anomaly has occurred in the fire extinguisher, to the moment it gets its periodic check, which can be up to three months, a period by which many extinguishers may have failed. Carrying out this experiment will further validate this proposal, eliminating high-risk situations in which there is a fire in a building whose fire extinguishers are not operational. Furthermore, The case of CO₂ extinguishers will be studied in more detail, so much so that in this study it has become clear that it is a different and more complex case that requires a more in-depth study.

Author Contributions: R.G.-M. conceived and designed the SmartFire prototype; A.G.-B. has developed the software system. R.G.-M. performed the experiments; R.G.-M., A.G.-B. and J.M.C. formalize the problem, designed the appropriate method, reviewed the state of the art and reviewed the work. All the authors contributed in the redaction of the paper.

Funding: This work was financed by ERDF funds through the V Sudoe Interreg program within the framework of the COMPRESSer project, Ref. SOE2/P1/E0643.

Conflicts of Interest: The authors declare no conflict of interest.

References

1. Rubadiri, L.; Ndumu, D.T.; Roberts, J.P. Predicting the evacuation capability of mobility-impaired occupants. *Fire Technol.* **1997**, *33*, 32–53. [[CrossRef](#)]
2. Xing, E.; Jin, J.; Zhang, Z.; Pan, R.; Li, Q.; Zheng, J. Simulation on flow rate characteristics of gas fire extinguishing agent with expansion nozzle based on AMESim. In Proceedings of the CSAA/IET International Conference on Aircraft Utility Systems (AUS 2018), Guiyang, China, 19–22 June 2018.
3. Wu, Y.; Zhuang, H.; Yu, P. Numerical Simulation of Gas-Solid Two-Phase Jet in a Non-pressure-accumulated and Handheld Fire Extinguisher. In Proceedings of the 2018 3rd International Conference on Modelling, Simulation and Applied Mathematics (MSAM 2018), Shanghai, China, 22–23 July 2018.
4. Schroll, R.C. *Industrial Fire Protection Handbook*; CRC Press: Boca Raton, FL, USA, 2016.
5. Cournoyer, M.E.; Waked, R.R.; Granzow, H.N.; Gubernatis, D.C. Verification study of an emerging fire suppression system. *J. Chem. Health Saf.* **2016**, *23*, 26–32. [[CrossRef](#)]
6. Lim, Y.S.; Lim, S.; Choi, J.; Cho, S.; Kim, C.K.; Hu, Y.W.L.H.; Zhang, H.; Hu, H.; Xu, B.; Li, J.; et al. A fire detection and rescue support framework with wireless sensor networks. In Proceedings of the 2007 International Conference on Convergence Information Technology (ICCIT 2007), Gyeongju, Korea, 21–23 November 2007; pp. 135–138.
7. JiJi, R.D.; Hammond, M.H.; Williams, F.W.; Rose-Pehrsson, S.L. Multivariate statistical process control for continuous monitoring of networked early warning fire detection (EWFD) systems. *Sens. Actuators B Chem.* **2003**, *93*, 107–116. [[CrossRef](#)]
8. Guan, Y.X.; Fang, Z.; Wang, T.R. Fire Risk Assessment and Daily Maintenance Management of Cultural Relic Buildings Based on ZigBee Technology. *Procedia Eng.* **2018**, *211*, 192–198. [[CrossRef](#)]
9. Purser, D.A.; Bensilum, M. Quantification of behaviour for engineering design standards and escape time calculations. *Saf. Sci.* **2001**, *38*, 157–182. [[CrossRef](#)]
10. Pires, T.T. An approach for modeling human cognitive behavior in evacuation models. *Fire Saf. J.* **2005**, *40*, 177–189. [[CrossRef](#)]

11. Hu, H.; Wang, G.; Zhang, Q.; Wang, J.; Fang, J.; Zhang, Y. Design wireless multi-sensor fire detection and alarm system based on ARM. In Proceedings of the 2009 9th International Conference on Electronic Measurement & Instruments, Beijing, China, 16–19 August 2009; pp. 3–285.
12. Lee, K.C.; Lee, H.H. Network-based fire-detection system via controller area network for smart home automation. *IEEE Trans. Consum. Electron.* **2004**, *50*, 1093–1100.
13. Zick, L.; Carlson, C. Strain gage technique employed in studying propane tank stressesunder service conditions. *Steel* **1948**, *86*, 88.
14. Choi, Y.; Ahn, J.; You, H.; Jo, C.; Cho, Y.; Noh, Y.; Chang, D.; Chung, H.; Bergan, P.G. Numerical and experimental study of a plate-stiffened prismatic pressure vessel. *Ocean Eng.* **2018**, *164*, 367–376. [[CrossRef](#)]
15. Diego, F.J.; Esteban, B.; Merello, P. Design of a hybrid (wired/wireless) acquisition data system for monitoring of cultural heritage physical parameters in smart cities. *Sensors* **2015**, *15*, 7246–7266. [[CrossRef](#)] [[PubMed](#)]
16. Park, K.H.; Lee, Y.S.; Kim, S.J.; Kim, Y.H.; Park, B.C. Computer Vision-based Pressure Gauge Measurement for Fire Extinguisher Inspection. In Proceedings of the 2017 International Conference on Platform Technology and Service (PlatCon), Busan, Korea, 13–15 February 2017; pp. 1–4.
17. Jin, J.M.; An, F.L.; Shou, Y.; Pan, R.M.; Xuan, Y.; Li, Q.W. Simulation on Release Characteristics of the Gas Extinguishing Agent in Fire Extinguisher Vessel with Different Filling Conditions Based on AMESim. *Procedia Eng.* **2018**, *211*, 315–324. [[CrossRef](#)]
18. Park, K.; Park, B. Fire Extinguisher Maintenance System using Smart NFC Communication and Real-Time Pressure Measurement. *J. Digit. Contents Soc.* **2017**, *18*, 403–410. [[CrossRef](#)]
19. Lu, J.; Zhou, T.; Li, B.; Wu, C.; Liu, Y. The Pressure Loss Calculation Method and Application of Portable Fire Extinguishing Equipment for Power System. In Proceedings of the 2015 International Conference on Electrical, Automation and Mechanical Engineering, Phuket, Thailand, 26–27 July 2015.
20. Sinclair, G.; Helms, J. A review of simple formulae for elastic hoop stresses in cylindrical and spherical pressure vessels: What can be used when. *Int. J. Press. Vessel. Pip.* **2015**, *128*, 1–7. [[CrossRef](#)]
21. Richard, G.B. *Advanced Strength and Applied Stress Analysis*; McGraw Hill Publishing Companies Inc.: New York, NY, USA, 1999.
22. Timoshenko, S.; Lessells, J. *Applied Elasticity*; Westinghouse Technology: Monroeville, PA, USA, 1925.
23. Schmid, S.R.; Hamrock, B.J.; Jacobson, B.O. *Fundamentals of Machine Elements*; CRC Press: Boca Raton, FL, USA, 2013.
24. Chow, W. Proposed fire safety ranking system EB-FSRS for existing high-rise nonresidential buildings in Hong Kong. *J. Archit. Eng.* **2002**, *8*, 116–124. [[CrossRef](#)]
25. Chamoso, P.; González-Briones, A.; De La Prieta, F.; Corchado, J.M. Computer vision system for fire detection and report using UAVs. In Proceedings of the Robust Solutions for Fire Fighting (RSFF’18), L’Aquila, Italy, 19–20 July 2018.
26. Verstockt, S.; Vanooosthuyse, A.; Van Hoecke, S.; Lambert, P.; Van de Walle, R. Multi-sensor fire detection by fusing visual and non-visual flame features. In Proceedings of the International Conference on Image and Signal Processing, Trois-Rivières, QC, Canada, 30 June–2 July 2010; pp. 333–341.
27. Rashid, H.; Ahmed, I.U.; Ullah, A.; Newaz, M.F.; Robin, M.S.R.; Reza, S.T. Multiple sensors based fire extinguisher robot based on DTMF, bluetooth and GSM technology with multiple mode of operation. In Proceedings of the 2016 International Workshop on Computational Intelligence (IWCI), Dhaka, Bangladesh, 12–13 December 2016; pp. 41–46.
28. González-Briones, A.; Chamoso, P.; Yoe, H.; Corchado, J.M. GreenVMAS: Virtual Organization Based Platform for Heating Greenhouses Using Waste Energy from Power Plants. *Sensors* **2018**, *18*, 861. [[CrossRef](#)] [[PubMed](#)]
29. González-Briones, A.; De La Prieta, F.; Mohamad, M.; Omatu, S.; Corchado, J. Multi-agent systems applications in energy optimization problems: A state-of-the-art review. *Energies* **2018**, *11*, 1928. [[CrossRef](#)]

30. Garijo, F.; Pavón, J. The ICARO Goal Driven Agent Pattern. In *Ibero-American Conference on Artificial Intelligence*; Springer: Berlin, Germany, 2016; pp. 51–62.
31. González-Briones, A.; Prieto, J.; De La Prieta, F.; Herrera-Viedma, E.; Corchado, J. Energy optimization using a case-based reasoning strategy. *Sensors* **2018**, *18*, 865. [CrossRef] [PubMed]



© 2019 by the authors. Licensee MDPI, Basel, Switzerland. This article is an open access article distributed under the terms and conditions of the Creative Commons Attribution (CC BY) license (<http://creativecommons.org/licenses/by/4.0/>).

Capítulo II

DIGITAL IMAGE CORRELATION AND RELIABILITY-BASED METHODS FOR THE DESIGN AND
REPAIR OF PRESSURE PIPES THROUGH COMPOSITE SOLUTIONS

RESUMEN

En el segundo trabajo publicado se va un paso más allá del trabajo anterior, incorporando el DIC a los métodos de diseño más avanzados en el campo del diseño dentro de la ingeniería, lo que se conoce como Ingeniería Robusta.

Actualmente se distinguen dos tipos de formulaciones estocásticas dependiendo de las funciones que se ven afectadas por la incertidumbre, el Diseño Óptimo Robusto (RDO) y el Diseño Óptimo Basado en Fiabilidad (RBDO) siendo la implementación de este último método el **objetivo** de este trabajo. A su vez y con el objetivo de reducir el coste computacional de estas técnicas, es también una meta de este trabajo evaluar la aplicación de métodos de subrogación o metamodelos.

La **metodología** seguida consiste en implementar aproximaciones RBDO, donde la probabilidad de fallo se estimada mediante el método de simulación de Monte Carlo (MC) para el diseño y reparación de tuberías empleando la técnica de *Roll Wrapping*. Este trabajo se sirvió del prototipo *Smartfire* para la calibración del DIC2D y la posterior adquisición de datos.

El método MC requiere alto número de simulaciones, las cuales son implementadas a través de la técnica de elementos finitos (FEM) mediante el software AbaqusTM, haciendo uso también del lenguaje de programación integrado *Python* para automatizar las múltiples simulaciones. El proceso descrito implica un coste computacional muy elevado; se ha de tener en cuenta que parte de las variables que alimentan el modelo FEM son de tipo aleatorio, variables definidas por sus PDFs siendo estas generadas con los datos proporcionados por la técnica DIC, en este caso a través de la generación de extensómetros virtuales (EV).

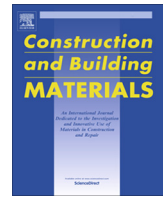
Los inputs que alimentan el modelo FEM son previamente seleccionadas a través de un análisis sensible, el cual se conforma mediante el Método de Sobol. Con objeto de reducir el coste computacional tanto del RBDO como del análisis sensible se recurre a los métodos subrogados, concretamente al método de expansión en caos polinomial, PCE (*Polynomial Chaos Expansion*).

Finalmente se optimiza la solución a través de un algoritmo genético, que impone la restricción de mínimo coste.

Los **resultados** muestran la variable que más influyen en el diseño es la tensión máxima seguido del Módulo de Young. Para ello se realizan 204 mediciones de las constantes elásticas gracias a los EV. Para el análisis de fiabilidad se emplean 500 simulaciones evaluadas vía meta modelización con un polinomio de grado 5, donde se alcanza la solución con una probabilidad de fallo inferior a 0.0015 con un índice de fiabilidad de 3 para un número de capas del composite de 15. El resultado más sobresaliente es la reducción del coste computacional pasando de tiempos de 29 días a sólo 2 horas

La **conclusión** es que el DIC es una técnica apta para la medida de deformaciones de un material compuesto con altos niveles de precisión. A su vez se ha logrado integrar con éxito técnicas de diseño robusto fusionadas con cálculo FEM para la obtención de diseños óptimos basados en la fiabilidad.

Finalmente, las técnicas de análisis sensible y el empleo de métodos de propagación de incertidumbres se integran con éxito, consiguiendo mejorar notablemente los tiempos de cálculo concluyendo que la incorporación de la ingeniería robusta se presenta como la mejor opción para el diseño y optimización de costes de composites, siempre que se mantenga el equilibrio frente al coste computacional, equilibrio que se demuestra factible gracias a la integración de los métodos subrogados.



Digital image correlation and reliability-based methods for the design and repair of pressure pipes through composite solutions



Roberto García-Martin ^a, Jorge López-Rebollo ^{b,*}, Luis Javier Sánchez-Aparicio ^c, José G. Fueyo ^a, Javier Pisonero ^b, Diego González-Aguilera ^b

^a Department of Mechanical Engineering, University of Salamanca, Higher Polytechnic School of Zamora, Campus Viriato, Avenida Requejo, 33, 49022 Zamora, Spain

^b Department of Cartographic and Land Engineering, University of Salamanca, Higher Polytechnic School of Ávila, Hornos Caleros, 50, 05003 Ávila, Spain

^c Department of Construction and Technology in Architecture (DCTA), Polytechnic University of Madrid, Av. Juan de Herrera 4, 28040 Madrid, Spain

HIGHLIGHTS

- The DIC methodology allowed to extract the PDF of the main mechanical properties.
- The use of an adaptative space PCE metamodel has allowed the reduction of the computational time.
- The use of Sobol indices have allowed the evaluation of the input variables in the output response.

ARTICLE INFO

Article history:

Received 13 December 2019

Received in revised form 28 January 2020

Accepted 28 February 2020

Available online 6 March 2020

Keywords:

Digital Image Correlation

Reliability-based methods

Polynomial Chaos Expansion

Carbon fiber

Pressure Pipes

ABSTRACT

This work aims to develop an approach for the reliability-based analysis for the design and repair of pressurized pipes by means of composite solutions. To this end, the approach uses a simulation method to estimate the failure probability of the solution based on the Monte Carlo approach and a Polynomial Chaos Expansion surrogate metamodeling strategy. This combination allows us to reduce the computational time required for evaluating the system's probability of failure as well as extracting the Sobol' indices during the sensitivity analysis stage. The uncertainties related with the composite solution were obtained by means of the Digital Image Correlation approach, allowing us to extract the Probabilistic Distribution Functions (PDF) of its main mechanical parameters. This methodology is validated through the design and repair of a pressurized pipe using a carbon fiber solution and roll wrapping technology. The results show the strong potential of the proposed methodology for the safety evaluation of pressurized composite pipes.

© 2020 Elsevier Ltd. All rights reserved.

1. Introduction

There are many applications of pressurization based on liquid storing and gas and oil transportation, e.g. underground steel pipelines are one of the most effective and safest systems for oil and gas transportation over a long distance [1,2]. Due to their exposure to environmental agents, metal pipes can corrode, considerably affecting their useful life and thus the economy of the countries [3]. The behaviour of metal pipes is well known, in terms of both mechanical design and lifecycle problems. Furthermore, most of these applications are subject to different regulations

and standards, and are frequently revised in the knowledge progress [4].

Step by step, new material solutions have been replacing the traditional steel applications towards composite materials [5]. This is due to their combination of properties providing a high performance index [6–8], and a good long-term performance [9–11]. Therefore, these new materials represent a very interesting solution for high corrosion and mechanical loaded environments, e.g. chemical industry piping. Within this context, the most common material solution is the fiber-reinforced polymer (FRP), mainly by carbon (CFPR) or glass (GFPR) fiber into an epoxy resin matrix [5,8,12–14]. Several techniques could be used for manufacturing FRP pipes, [1,5,9,12,14,15]. Among them, roll wrapping technology is interesting, since it opens up a new field of application: the reparation of steel pipes [5,16–18]. The use of this approach for

* Corresponding author.

E-mail addresses: toles@usal.es (R. García-Martin), jorge_lopez@usal.es (J. López-Rebollo), l.j.sanchez@upm.es (L.J. Sánchez-Aparicio), fueyo@usal.es (J.G. Fueyo), j_pisonero@usal.es (J. Pisonero), daguilera@usal.es (D. González-Aguilera).

Nomenclature

DoE	Design of Experiments	P_f	Probability of failure
E	Young's Modulus	TSFD	Tensile Strength Fiber Direction
MIG	Mean Intensity Gradient of the speckle pattern	β	Reliability index
PDF	Probabilistic Distribution Functions	ν	Poisson's ratio

repairing pipes could overcome the main problems of the traditional methods, as well as offering better resistance and performance [16].

However, these new composite solutions entail difficulties to determine accurately its properties due to the presence of heterogeneous properties [19] and their highly directional behaviour [20,21]. Within this context, the contact techniques are not capable of properly capturing the mechanical behaviour of these solutions [22–24]. To overcome this drawback, several full-field optical methods have been developed [25–27]. Among them, Digital Image Correlation (DIC) has become as one of the most promising tools. This method allows us to obtain a full-field of displacements and strains through the use of correlation-based matching procedures and numerical differentiation algorithms [28]. Thanks to this major advantage, DIC has been widely used for the experimental testing of composite solutions under different loading configurations [22,29–34]. Data obtained by this method is commonly used for the evaluation of strain distribution, damage analysis and microstructure observation [22,29,34,35] and, to a lesser extent, as input for probabilistic analysis [36]. This approach, probabilistic analysis, is considered to be the most reliable strategy for numerical simulation of composite solutions [37–39]. In contrast to deterministic methods, the main goal of these approaches is to determine the probability of failure of a mechanical system under the influence of different uncertainties, such as loads or material properties among others [38]. Studies carried out by Rafiee and Ali Torabi [38] and Rafiee et al. [40–39], highlights the relevance of considering these manufacturing uncertainties since it is highly likely that composite prototypes experience failures below the deterministic value. As stated Sriramula and Chryssanthopoulos [21], these uncertainties might be considered at a constituent, ply or component level. The estimation of this probability of failure could be carried out by means of approximation methods such as the First (FORM) and Second Order Reliability (SORM) methods or even by means of simulation strategies such as the Monte Carlo Sampling (MCS) method [41]. MCS highlights for its simple and direct implementation [38,39]. However, the cost of this approach increases rapidly when a low probability of failure is required [37], requiring a huge number of simulations and a large computational time [38]. To cope with this lamination, variance reduction techniques and metamodels are commonly used [37,42]. As a result of these techniques, it is possible to construct an equivalent and computationally inexpensive mathematical replica of the system, allowing the carrying out of huge numbers simulations with great accuracy.

As a consequence, this paper therefore aims to progress the effective integration of the DIC approach with the latest advances in probabilistic analysis of engineering solutions. To this end, this approach integrates a surrogate modelling strategy and a reliability analysis with the aim of obtaining the failure probability of a composite solution used for the design and repair of pressurized pipes. In the Methods (Section 2) we describe the composite materials used as well as the experimental and numerical strategies adopted. In Section 3, we show the experimental results obtained by the combination of DIC and the reliability approach in the design and repair of pressurized pipes. Finally, in the Conclusion (Section 4) we summarise the findings and discuss future studies.

2. Materials and methods

2.1. Composite solution evaluated

Compared to other materials or other composites solutions such as GFPR, carbon fiber capabilities exceed those of its competitors. It should be noted that the surface of the carbon fiber is a microcrystalline graphite structure, which entails that the distribution of stresses and the generation and propagation of fissures can be adjustable [43]. In addition, its resistance to high temperatures and corrosion must be considered. All this makes carbon fiber the most suitable material for high-performance pipes [44].

Hence, the material used for testing was a carbon fiber polymer reinforcement CC 200 T-120® with a thickness of 0.32 mm (Table 1), an epoxy resin matrix CR82® and a hardener Biresin CH80-10®. Technical characteristics of epoxy resin and hardener are the same as used by García-Martin et al. [36]. The material has been made from a 200 g Plain where 9 plates of 21 × 29 cm have been obtained. The mix ratio, for a specific amount of 200 g, was 158 g of resin plus 42 g of hardener.

The first layer of reinforcement was placed with proper orientation, then it was impregnated by the resin and catalyst mixture. This process was repeated a total of nine times giving as a result a composite solution made up by nine layers: [±90]9. Each time a layer was added, a light pressure was exerted in order to remove the resin surplus. To obtain the desired thickness of 2 mm [45], the mold was machined with the proper measure. The block was cured in a drying oven for 50 min, at a temperature of 50 °C. Once the material was prepared, the specimens were machined with the proper dimensions (Fig. 1). During this process, computer numerical controlled cutting was used, and programmed according to current regulations specifications [45].

2.2. Mechanical characterization of the composite solution: the 2D digital image correlation method

The composite solution was evaluated by means of tensile tests according to guideline ISO 527 [45]. The electromechanical tensile machine Servosis ME-405/50/5 technical specifications are shown in Table 2.

To capture the displacement and strains suffered by the composite solution during the tensile tests a 2D-DIC approach was used. The acquisition of these images was carried out by means of the DIC prototype developed by García-Martin et al. [36]. This

Table 1
Technical characteristics of fibers CC 200 T-120®.

Mechanical properties	Values
Thickness (mm)	0.32
Density (warp × weft) (end/cm)	1.76
Tex (warp × weft)	500 × 500
Width (cm)	120 ± 1
Weight (g/m ²)	200 ± 5
Weight per roll (kg)	110
Tensile strength (MPa)	3530
Elongation at maximum tensile strength (%)	1.5

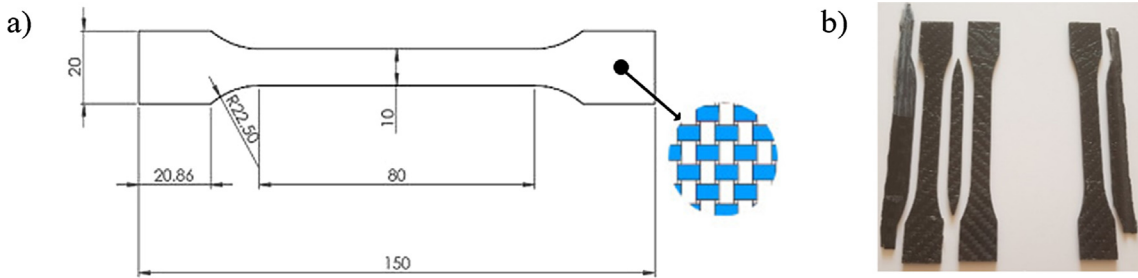


Fig. 1. Manufacturing process: a) dimensions of the tested specimens in mm and; b) image of the specimens.

prototype is composed of a high resolution camera Canon EOS 700D with a 60 mm prime macro-lens and a PLC connected with the load cell.

Once the images were acquired, a standard DIC protocol was applied in order to obtain the full field of displacements and strains. During this stage, the Region Of Interest (ROI) of each image was split into subsets [46] which allow the images to be tracked through the Zero mean Normalized Cross-Correlation (ZNCC) index due to its robustness [47]. During this tracking stage, it was assumed that each subset could suffer a deformation result of the linear combination of six degrees of freedom (translation, elongation and shear deformation in the x and y axis) (Fig. 2) (Eqs. (1) and (2)) for which the basic form of displacement of a subset is $(u, v, \frac{\delta u}{\delta x}, \frac{\delta u}{\delta y}, \frac{\delta v}{\delta x}, \frac{\delta v}{\delta y})^T$.

$$x' = u + \frac{\delta u}{\delta x} \Delta x + \frac{\delta u}{\delta y} \Delta y \quad (1)$$

$$y' = v + \frac{\delta v}{\delta x} \Delta x + \frac{\delta v}{\delta y} \Delta y \quad (2)$$

where x' and y' are the final displacements of the subset; u and v are the displacements components of the subset center P ; Δx and Δy are the distance between the initial center's subset and the final position and; $\frac{\delta u}{\delta x}$, $\frac{\delta u}{\delta y}$, $\frac{\delta v}{\delta x}$, $\frac{\delta v}{\delta y}$ are the displacement gradients of the subset.

Complementary to the ZNCC index, and with the aim of obtaining sub-pixel accuracy, a refinement stage was carried out by means of the following strategies: i) a bi-quantic b-spline interpolation scheme to pass from the discrete values of the images (0–255) to a continuum space and; ii) the Inverse Composition Gauss-Newton method for the minimization of the cost function that match the reference subset with the deformed one. For more details about the algorithms used the reader is referred to [47].

The procedure previously shown was reproduced in all the image's subsets allowing us to obtain a full-field of displacements. The strains of the specimens were calculated by means of the Green-Lagrangian strain tensor using the gradients obtained during the evaluation of the displacements [36]. In order to obtain the full field strain, this procedure was applied throughout ROI.

The success of the tracking carried out during the DIC approach strongly depends on the random intensity distribution of the ROI, which must present the following features: distinct, unique, non-periodic and stable grayscale [48]. Due to the absence of a proper gray variation on the specimen's surface, it was necessary to apply

an artificial Speckle pattern using the approach defined by Garcia-Martin et al. [36]. This strategy allows us to obtain a suitable Speckle pattern through the perturbation of a regular circular grid, which was printed and applied with the help of an elastic prime over the specimen surface.

Apart from the considerations previously shown, the images captured by the sensor suffer from lens distortion that could be considered as another source of error [47]. The minimization of this error requires the removal of these radial and tangential distortions. Therefore, the present case applied the calibration procedure proposed by Vo et al. [49].

In order to guarantee the accuracy and quality of the data obtained with the DIC approach, it is mandatory that all previously determined steps are carried out by skilled technicians. First, the prototype must be properly configured to synchronize all data. A bad Speckle pattern with insufficient contrast could cause the subsets not to be detected correctly and the correlation was not performed. In addition, all parameters have to be defined according to the test configuration for the correlation algorithm runs properly. Finally, the calibration process has to be carefully carried out in order to obtain a high accuracy in the results, since a bad calibration could cause incoherent displacements and strains.

2.3. Numerical strategy for the reliability analysis

As stated in the Introduction, the main goal of the reliability analysis is to find the probability function of a mechanical system under the influence of different uncertainties. These uncertainties could be considered at material (random variables and random field) or ply level (layer-wise random variable). For the present study, we considered the mechanical uncertainties of the composite solution at ply level. These uncertainties were extracted by means of the DIC approach previously described. The evaluation of the probability function was carried out through the Monte Carlo (MC) approach following the next formulation (Eq. (3)). The input data required for the MC simulation was obtained combining a finite element modelling simulation with a surrogate modeling strategy, allowing reduction of computational costs as well as the estimation of the Sobol' indices for the sensitivity analysis of the mechanical solution. The proposed workflow was carried out with different number of plies until the probability of failure of the model was less than the minimum threshold of probability of failure (optimal solution) (Fig. 3). This failure threshold corresponds to the reliability target (β) which guarantees the safety of the model.

$$P_f = Prob[G(Y) \leq 0] = \int_{G(Y) \leq 0} p_y(Y) dY \quad (3)$$

where P_f is the probability of failure; G is the performance function; Y is the variable's vector and p_y is the joint probability density function.

Table 2
Servosis ME-405/50/5 technical specifications.

Maximum Load	500 kN
Load Cell	REP Transducer Type TC4 50 kN
Grip	MTS Model XSA304A

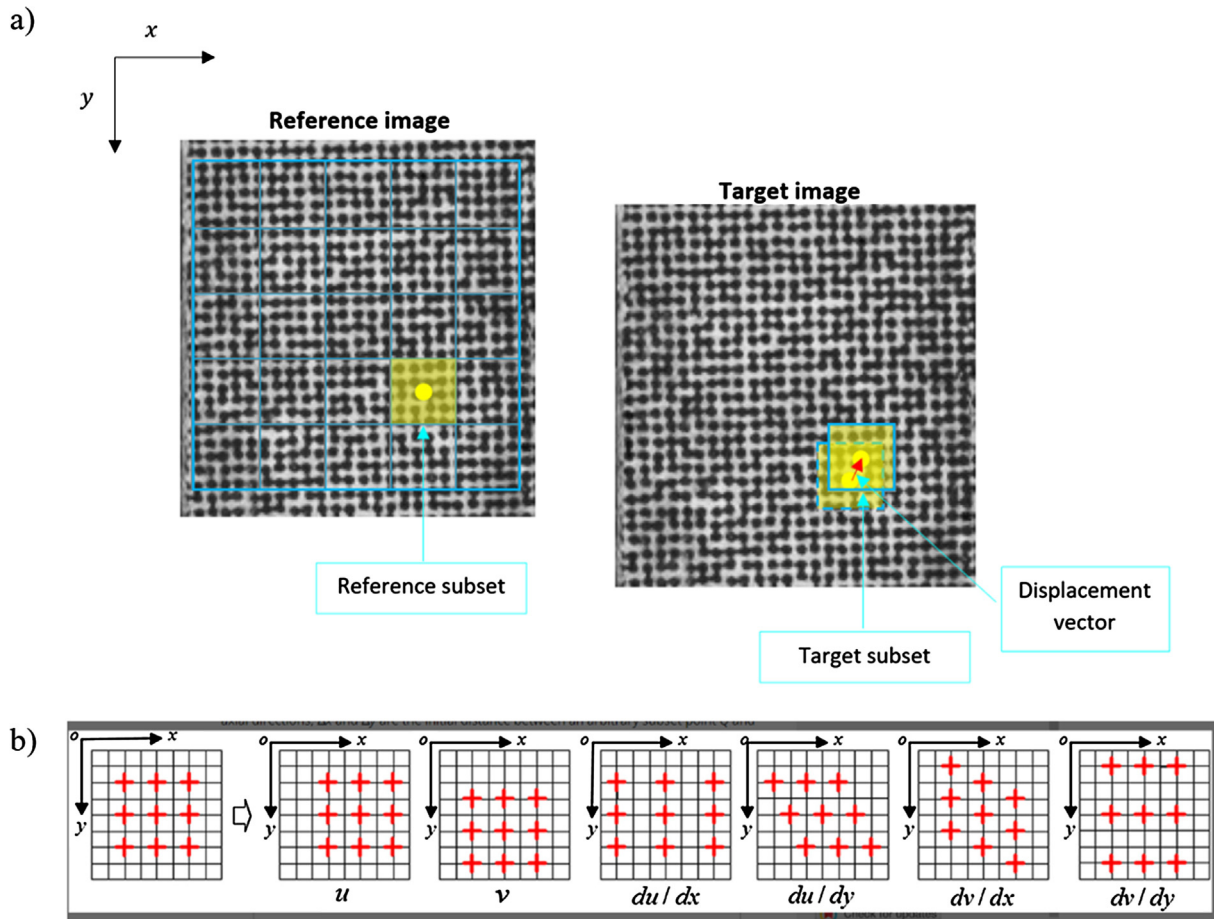


Fig. 2. Graphical representation of the DIC approach: (a) evaluation of the displacement suffered by a subset and (b) degrees of freedom considered during the displacement analysis.

2.3.1. Definition of the performance function for the reliability analysis: the Tsai-Wu failure criterion

Among the different methods able to simulate the failure of composite solutions, the Tsai-Wu failure criterion is one of the most used in the literature [7,12,14,50]. This criterion assumes that the failure of a composite solution takes place when the Failure Index (FI) (Eq. (4)) is higher than 1 [51].

$$FI = F_1\sigma_1 + F_2\sigma_2 + F_3\sigma_3 + F_{11}\sigma_1^2 + F_{22}\sigma_2^2 + F_{33}\sigma_3^2 + 2F_{12}\sigma_1\sigma_2 + 2F_{23}\sigma_2\sigma_3 + 2F_{31}\sigma_3\sigma_1 + F_{44}\sigma_4^2 + F_{55}\sigma_5^2 + F_{66}\sigma_6^2 \leq 1 \quad (4)$$

where:

$$\begin{aligned} F_1 &= \frac{1}{X_T - X_C} & F_2 &= \frac{1}{Y_T - Y_C} & F_3 &= \frac{1}{Z_T - Z_C} \\ F_{11} &= \frac{1}{X_T X_C} & F_{22} &= \frac{1}{Y_T Y_C} & F_{33} &= \frac{1}{Z_T Z_C} \\ F_{44} &= \frac{1}{S_{yz}^2} & F_{55} &= \frac{1}{S_{zx}^2} & F_{66} &= \frac{1}{S_{xy}^2} \\ F_{12} &= (-\frac{1}{2})\sqrt{F_{11}F_{22}} & F_{23} &= (-\frac{1}{2})\sqrt{F_{22}F_{33}} & F_{31} &= (-\frac{1}{2})\sqrt{F_{33}F_{11}} \end{aligned}$$

$X_T \equiv$ Tensile strength

$X_C \equiv$ Compressive strength

$Y_T \equiv$ Tensile strength in the transversal isotropic surface

$Z_T \equiv$ Tensile strength in the transversal isotropic surface

$Y_C \equiv$ Compressive strength in the transversal isotropic surface

$Z_C \equiv$ Compressive strength in the transversal isotropic surface

$S_{xy}; S_{yz}; S_{zx} \equiv$ Shear strength in the transversal isotropic surface

According to the formulation previously exposed, the performance function of a composite solution in terms of Tsai-Wu failure

criterion could be expressed as (Eq. (5)). Taking this into consideration, the composite solution is operating in the safety range if $G > 0$ and in the failure state if $G < 0$, and the surface $G = 0$ is the limit state of the solution.

$$G = 1 - FI \quad (5)$$

where G is the performance function and FI is the failure index obtained from the Tsai-Wu criterion.

2.3.2. Metamodelling strategy

The proposed methodology considers the use of the MC sampling method for solving the probability of failure of the system (Eq. (3)). To achieve reliable results, thousands of simulations are required for solving the problem. The computational cost of this task is unacceptable most of the times, so it is necessary to establish an alternative that offers reliable results with a lower computational cost. In this context, the so-called surrogate models or metamodels allow the Input-Output response of a complex system to be approximated with a low number of inputs thanks to its compactness and analytical scalability. Within this context, one of the most robust and used metamodeling strategies is the Polynomial Chaos Expansion (PCE) [52], especially in the propagation of uncertainties in engineering applications [53].

Initially developed by Wiener [54], the PCE is a stochastic metamodeling strategy that approximates the behaviour of a system by means of a spectral representation of random variables in terms of a set of multivariate polynomials. This method assumes that the physical model, in this case the numerical simulation, can be represented as a finite variance model, $f(X)$, whose input x is a random

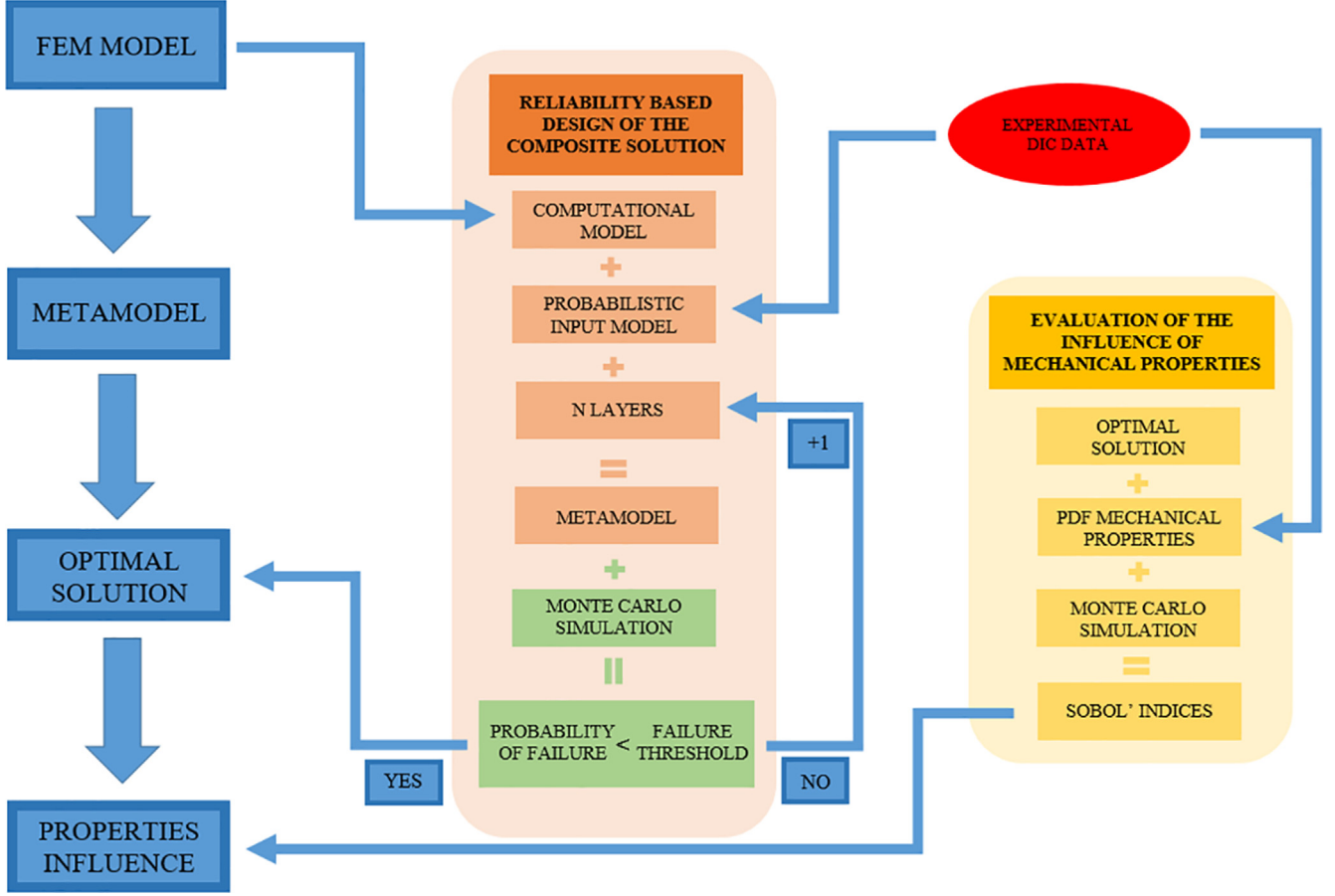


Fig. 3. Workflow adopted for the reliability analysis.

vector of independent and constrained variables $X \in \mathbb{R}^M$. The independence of the input parameters allows us to build these polynomials as a tensorization of univariate polynomials with respect to the marginal PDF's and where the mathematical equation can be summarized as follows (Eq. (6)).

$$Y \approx f(X) = \sum_{\alpha \in A} \gamma_\alpha \varphi_\alpha(X) \quad (6)$$

where $\alpha = \{\alpha_1 \dots \alpha_M\}$ is the multi-index, $A \subset \mathbb{N}^M$ is a set of indices for the multivariate orthonormal polynomials, γ_α are deterministic coefficients to be computed and $\varphi_\alpha(X)$ are multivariate orthonormal polynomials.

The estimation of the coefficients exposed in (Eq. (6)) was carried out by means of a least square minimization problem between the vector of random inputs (X) and the model responses (Y) as follows (Eq. (7)):

$$\varphi_\alpha = \operatorname{argmin} \frac{1}{N} \sum_{i=1}^N \left[\gamma^{(i)} - \sum_{\alpha \in A} \gamma_\alpha \varphi_\alpha(x^{(i)}) \right]^2 \quad (7)$$

In order to overcome a possible over-fitting situation in the presence of high-dimensional inputs, the proposed methodology uses the adaptive sparse PCE based on the least angle regression proposed by Blatman and Sudret [55]. This method applies the

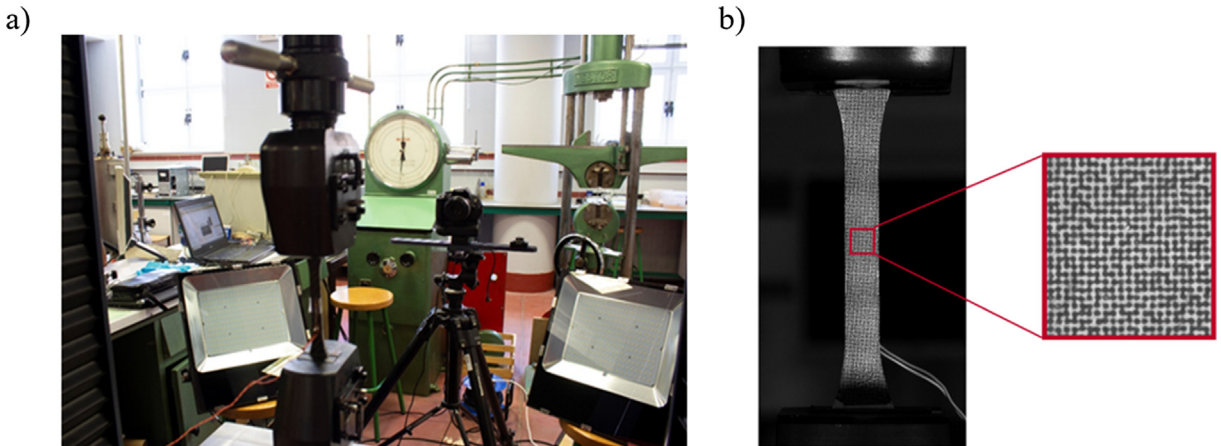


Fig. 4. Digital Image Correlation campaign: a) set-up used and; b) detail of the Speckle pattern applied.

Table 3

Internal parameters obtained during the calibration of the camera. Unit*: pixel.

Parameter	Initial	Refined
Focal length*	$f_u = 1.36286 \times 10^4$	1.5206×10^4
	$f_v = 1.36286 \times 10^4$	1.5208×10^4
Principal point*	$u = 7.2084 \times 10^2$	2.5118×10^3
	$v = 1.3378 \times 10^3$	2.0986×10^3
Radial distortion coefficients	$a_0 = 0$	-8.5316×10^{-2}
	$a_1 = 0$	3.3055×10^{-1}
	$a_2 = 0$	1.0130×10^1
Tangential distortion coefficients	$p_0 = 0$	-3.0724×10^{-3}
	$p_1 = 0$	1.5447×10^{-2}

least angle regression algorithm [56], based on a regularized version of the Eq. (7), to obtain a sparse PCE metamodel. This strategy proves to be very effective in engineering problems with high dimensions [55].

It is worth mentioning that all the metamodels are built from a limited number of inputs coming from the Design of Experiments (DoE). Thus, it is essential to assess the quality of the computed surrogate model. To this end, we propose to use the modified

version of the Leave-one-out error [57] (Eqs. (8) and (9)). This metric of error offers a good compromise between fair error estimation and affordable computational cost.

$$LOO\ error = \frac{1}{N} \sum_{i=1}^N \left(\frac{Y(X^{(i)}) - f^{PCE}(X^{(i)})}{1 - h_i} \right)^2 \quad (8)$$

$$LOO\ error^* = LOO\ error * \left(1 - \frac{\text{card}A}{N} \right)^{-1} \left(1 + \text{tr}(\varphi^T \varphi)^{-1} \right) \quad (9)$$

where $Y(X^{(i)})$ is the computational model; $f^{PCE}(X^{(i)})$ is the surrogate model obtained from a specific DoE with N samples; h_i is the i -th diagonal term of matrix $A(A^T A)^{-1} A^T$; A the experimental matrix; $\text{card } A$ is the number of terms in the truncate series and; $\varphi = \{\varphi_{ij} = \varphi_j(x^{(i)}), \quad i = 1, \dots, N; \quad j = 1, \dots, \text{card}A\}$.

The reduced computational cost of the surrogate metamodeling strategy allows the application of the MCS for different purposes. According to this, it is possible to calculate the influence of each

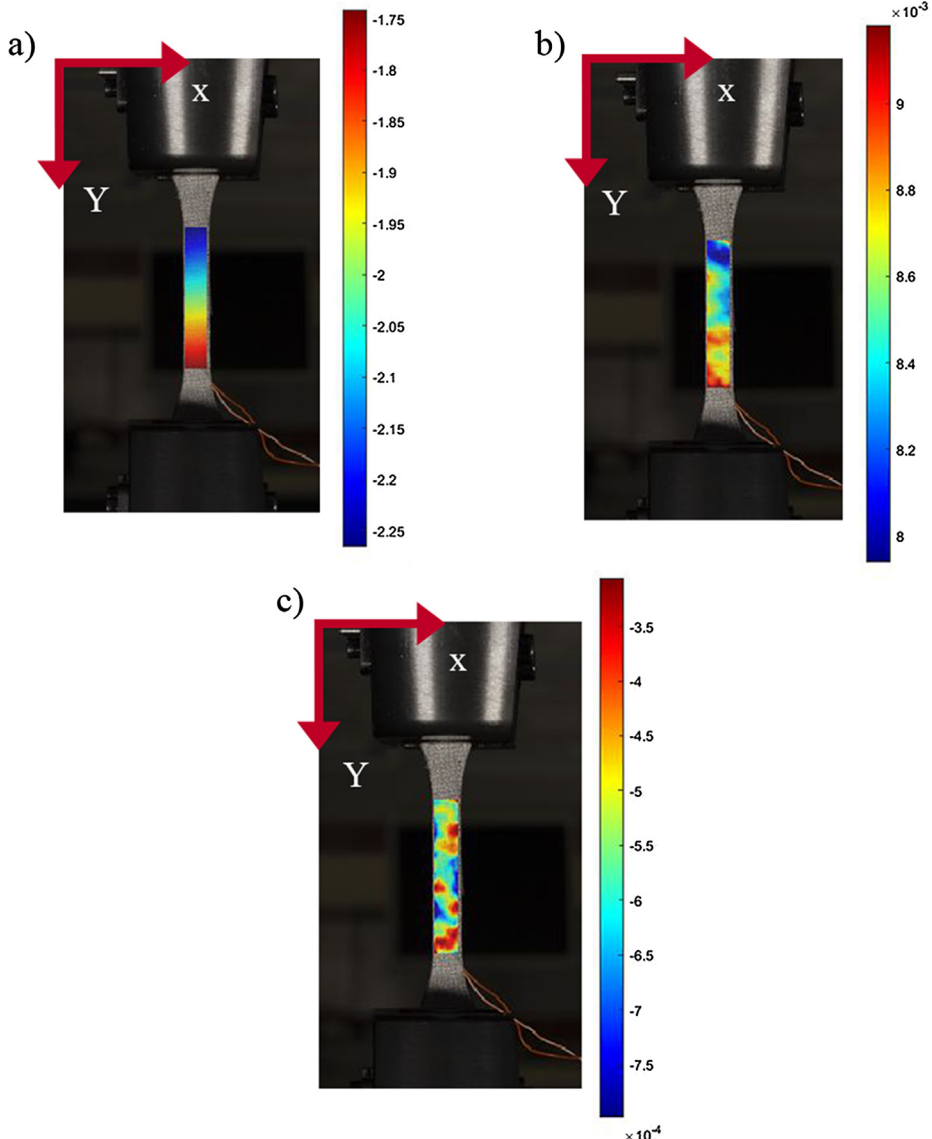


Fig. 5. Displacements and strains obtained by the 2D-DIC approach: a) displacements (Y) in mm; b) strains (Y) in mm/mm and c) strains (X) in mm/mm.

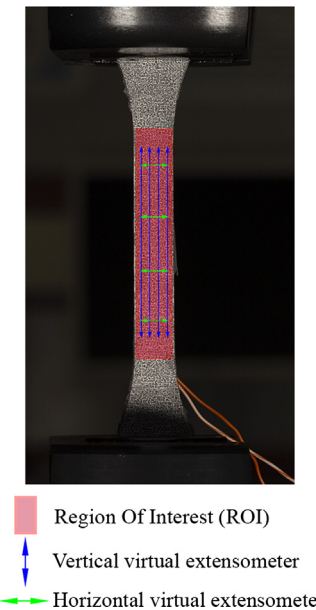


Fig. 6. Extraction of the mechanical parameters: evaluation of the Young's modulus and Poisson's ratio by means of virtual extensometer.

input in the final result of the model. Within this context one of the most used strategies is the estimation of the Sobol' indices. These indices assume that the variance of the model (output) can be described as a sum of the variances of the inputs (Eq. (10)). The normalized version of each variance with respect to the total one allows us to obtain de Sobol' indices with different orders (from 1 to 2^{n-1}) (Eq. (11)). The sum of these indices is the total Sobol' index whose value is equal to 1.

$$V(Y) = \sum_i V_i + \sum_i \sum_{j>i} V_{ij} + \sum_i \sum_{j>i} \sum_{k>j} V_{ijk} + \dots V_{123..N} \quad (10)$$

where $V(Y)$ is the variance of the model; $V_i = V(E(Y|X_i))$ is the first order partial variance; $V_{ij} = V(E(Y|X_i X_j))$ is the second order partial variance, etc.

$$S_i = \frac{V_i}{V(Y)}, \quad S_{ij} = \frac{V_{ij}}{V(Y)}, \text{ etc} \quad (11)$$

where S_i is the first order Sobol' index and S_{ij} is the second-order Sobol' indices.

3. Experimental results

3.1. Analysis of the roll wrapping solution by means of 2D-DIC

3.1.1. Test setup

A total of fifty-one tensile tests were carried out following the BS EN ISO 527-5:2009 guidelines [45]. The images for the DIC analysis were acquired each 400 N of traction force increment, tak-

ing the first image without load in order to obtain the reference image. Previously to the tests, a preparation stage was carried out with the aim of optimizing the results obtained during the tensile tests. This stage comprised the following steps: i) definition of the ground sample distance (GSD) as well as the aperture of the lens; ii) application of the Speckle pattern and; iii) the geometrical calibration of the camera.

The images were acquired with the same camera configuration used by García-Martin et al. [36]. Taking these values into account, a Speckle pattern was designed using the methodology proposed in Section 2.2, using a diameter of 0.324 mm and a step of 0.432 mm and obtaining a covering factor of 44% [58]. Finally, this pattern was printed and applied on the specimen surfaces by means of an elastic prime (Fig. 4). The quality of the pattern was evaluated through the Mean Intensity Gradient (MIG) value [59], obtaining an average value of 50. This value was considered acceptable taking into account the method used [59].

For the camera calibration we used the calibration approach defined in Section 2.2, acquiring a total of 22 images. The following inner parameters were obtained (Table 3).

3.1.2. Displacement and strain results

In order to obtain the displacement and strain on each test specimen, DIC approach defined in Section 2.2 was carried out with the open-source software Ncorr [60]. A subset size of 20×20 pixels and a 35% overlap (step of 7 pixels) were considered to ensure a proper DIC configuration [46], obtaining a full field displacement and strains in all the ROI (Fig. 5).

Taking into consideration the test set-up, the state of stresses along the central area (ROI area) could be considered to be constant. Therefore, if the material is homogeneous, the expected maximum principal strains will be reached at the same time in all the ROI. However, the results of the DIC tests revealed a heterogeneous distribution of the strains in the longitudinal and transverse directions and thus the presence of different mechanical properties along the composite structure. These heterogeneities could be attributed to local variations during the manufacturing process [36].

3.1.3. Extraction of the PDF functions

As stated in Section 2.3, the reliability analysis requires prior knowledge of the probability density functions of the material's variables. The population of each variable evaluated by means of the DIC approach was extracted during the next strategy (Fig. 6) (Table 4): i) creation of several virtual extensometers to evaluate the Young's Modulus and Poisson's ratio and; ii) extraction of maximum principal strain for the evaluation of the ultimate capacity of the material.

With the aim of obtaining a wide population, eight virtual extensometers were placed in each specimen. Four of them were placed vertically (y axis) and other four were placed horizontally (x axis) (Fig. 6). In this way, a total of 204 values were obtained for the Young's Modulus and Poisson's ratio.

This wide population allowed to calculate a significant average value and covariance associated with each of the parameters. In

Table 4
Results obtained from the mechanical characterization of the specimens using DIC approach.

Composite solution evaluated	Parameter	Number of data	Mean	Covariance (%)	Lower bound	Upper bound
E-Young's modulus (GPa)	204	50.7088	4.07	45.0583	57.0596	
v-Poisson's ratio (-)	204	0.0574	41.95	0.0138	0.1462	
T-Maximum principal tensile (MPa)	51	402.5128	8.33	309.5652	461.5762	

Table 5

Goodness of fit (GOF) probability; N-Normal, LN-Lognormal, W-Weibull, G-Gamma; 0-Accept and 1-Reject. Chi-Square (Chi), Kolmogorov-Smirnov (KS) and Anderson-Darling (AD) tests of the Young's Modulus (E), Poisson's ratio (ν) and Maximum principal tensile (T).

PDF	N			LN			W			G			
	GOF	Chi	KS	AD									
E	1	0	0	0	0	0	0	1	1	1	0	0	0
ν	1	0	1	0	0	0	0	1	0	0	0	0	0
T	0	0	0	0	0	0	0	0	0	0	0	0	0

Table 6

Probabilistic distribution functions of the Young's Modulus (E), Poisson's ratio (ν) and Maximum principal tensile (T) of the specimens.

Parameter	Distribution	μ (Log-Normal)/A (Weibull)	σ (Log-Normal)/B (Weibull)
E	Log-Normal	3.9253	0.0405
ν	Log-Normal	-2.9422	0.4176
T	Weibull	417.0948	14.8402

this sense, it is worth mentioning the high value of the covariance associated with the Poisson's ratio. Generally high covariance values of the Poisson's Ratio are obtained in comparison with those of

other parameters [61,36]. These high values are mainly due to the importance of fiber alignment in the manufacturing process as well as the low average value of the Poisson's ratio of the CRFP.

The reliability analysis approach proposed in Section 2.3 allow quantifying the uncertainty of the mechanical properties previously obtained. In order to introduce this uncertainty, it was necessary to adjust these data to a probabilistic distribution.

Along with this test, the goodness-of-fit tests of Chi-Square, Kolmogorov-Smirnov and Anderson-Darling were performed. These techniques allow us to accept or reject the hypothesis that mechanical properties are drawn from populations with a specified distribution [62]. Finally, a curve fit method was performed with the aim of obtaining the PDFs.

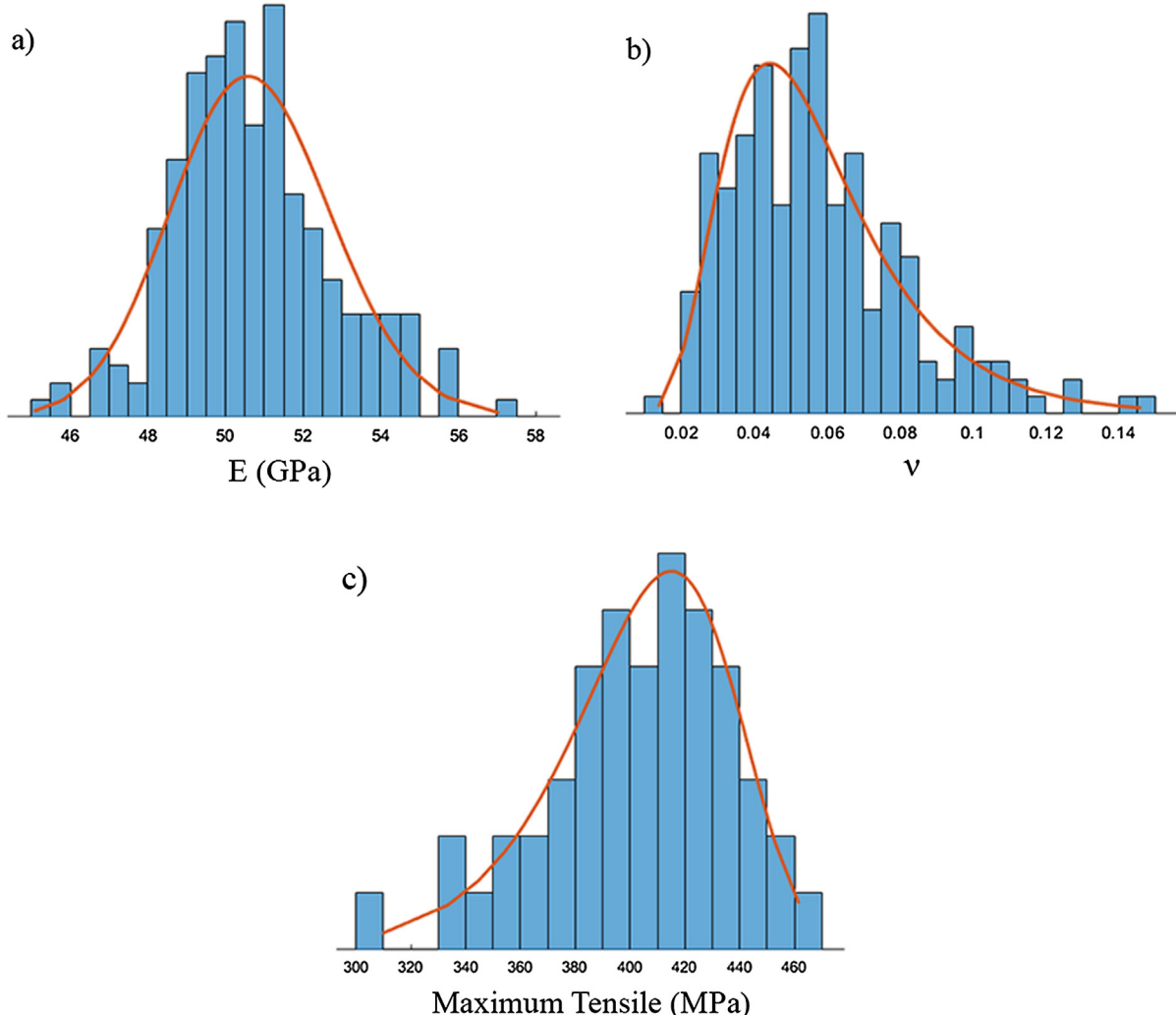


Fig. 7. Graphical representation of the PDFs of each parameter: (a) Log-Normal distribution of the Young's modulus (E); (b) Log-Normal distribution of the Poisson's ratio (ν) and (c) Weibull distribution of the maximum principal tensile (T).

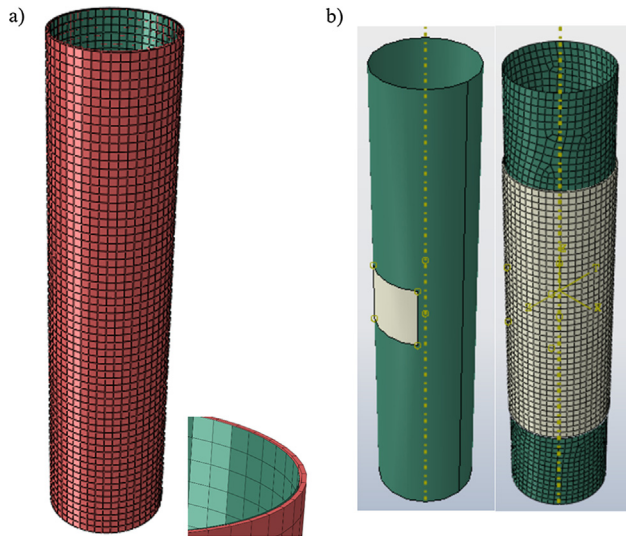


Fig. 8. Numerical meshes used: a) new composite steel pipe and; b) retrofitting of a corroded steel pipe.

Table 7

Results of probability of failure (P_f) and reliability index (β) obtained during the reliability analysis of the composite pipe with 10, 11, 12, 13, 14 and 15 layers.

Number of layers	P_f	β
10	0.5061	0.0154
11	0.1661	0.9696
12	0.0480	1.6645
13	0.0132	2.2200
14	0.00356	2.6912
15	0.00108	3.0645

The candidate PDFs considered were Normal, Log-Normal, Weibull, and Gamma. The acceptance/rejection of distribution is provided in [Table 5](#) where zero indicates acceptance of assumed distribution parameters, and unity indicates rejection. As shown in [Table 5](#), for some parameters there are several candidate PDFs which pass all tests.

Along with these statistical tools, the physical considerations of the parameters were taken into account, obtaining a Log-Normal distribution for the Young's Modulus and Poisson's Ratio and a

Weibull distribution for the maximum principal tensile stress ([Table 6](#) and [Fig. 7](#)). These curves are consistent with those obtained in similar experiments [61].

3.2. Definition of the numerical models

Taking into account the main applications of the roll-wrapping technique, two numerical models were considered for the reliability analysis: i) the design of a new composite pipe and; ii) the repair of a corroded steel pipe ([Fig. 8](#)). Both numerical simulations were carried out in the FEM software ABAQUS 2019®.

On the one hand, the composite pipe was modelled considering the following parts: i) a non-structural polymer liner with 2 mm of thickness; ii) a composite wrap made up of several composite layers with 0.32 mm of thickness. The wrap part was meshed as a continuum shell with reduced integration and eight nodes SC8R elements, while the liner was meshed with in-plane general purpose shell elements with four nodes, S4R. Convergence analyses were done in both models in order to obtain a mesh size which could give good precision results without penalizing enormously the time needed to run the models. This is a paramount aspect to consider because the models had to be repeated 200 times in order to obtain the surrogate models, as it was explained in [Section 2.3.2](#). So, convergence studies were performed using elements between 20 and 1 mm size. It was observed that using elements smaller than 10 mm the results did not improve significantly, but the sizes of the whole models and the time to run them grew exponentially. Finally, a 10 mm size element was considered enough precise for both models. For the loading and boundary conditions, we used an internal pressure on the inside wall of the pipe of 11.2 MPa and plane strain boundary constraints. Under these conditions the principal stresses which works in the pipe were the hoop tensile stresses [63].

On the other hand, we also considered a corroded steel pipe retrofitted with the composite solution exposed in [Section 2.1](#) and by means of roll-wrapping technology. In this sense, the numerical model was made up of the following parts: i) a steel pipe with 4 mm of thickness; ii) a corroded area on which the effective thickness is 2 mm (half of the initial one); iii) a non-structural putty layer and; iv) a roll-wrapping solution made up of different composite layers of 0.32 mm thickness each. It is worth mentioning that the loads and boundary conditions were the same as those previously exposed.

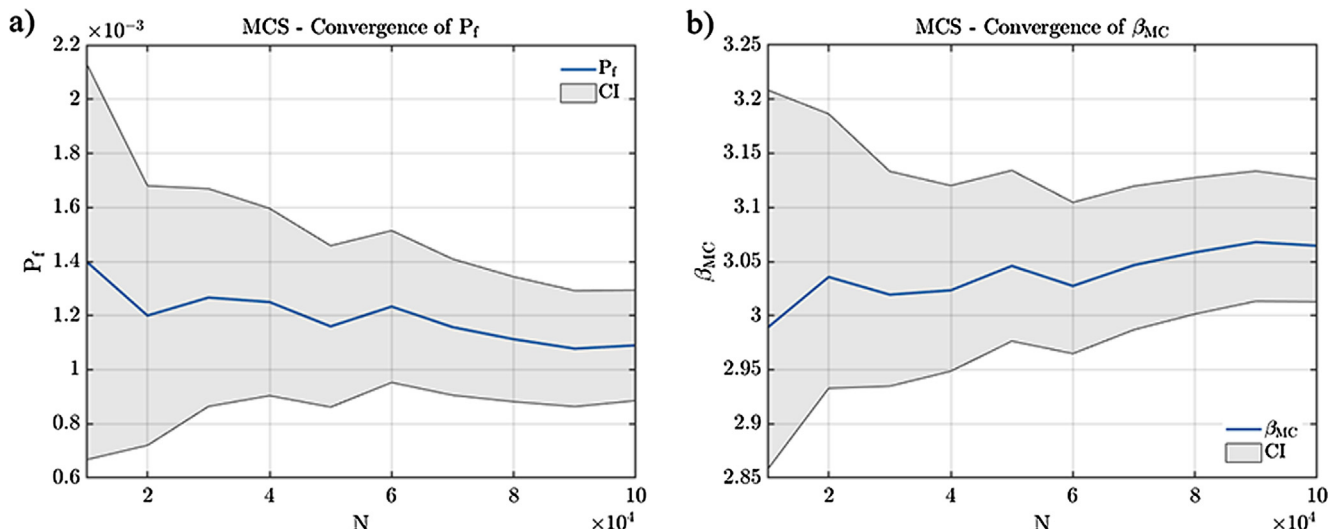


Fig. 9. Convergence of the P_f and β during the Monte Carlo Simulation.

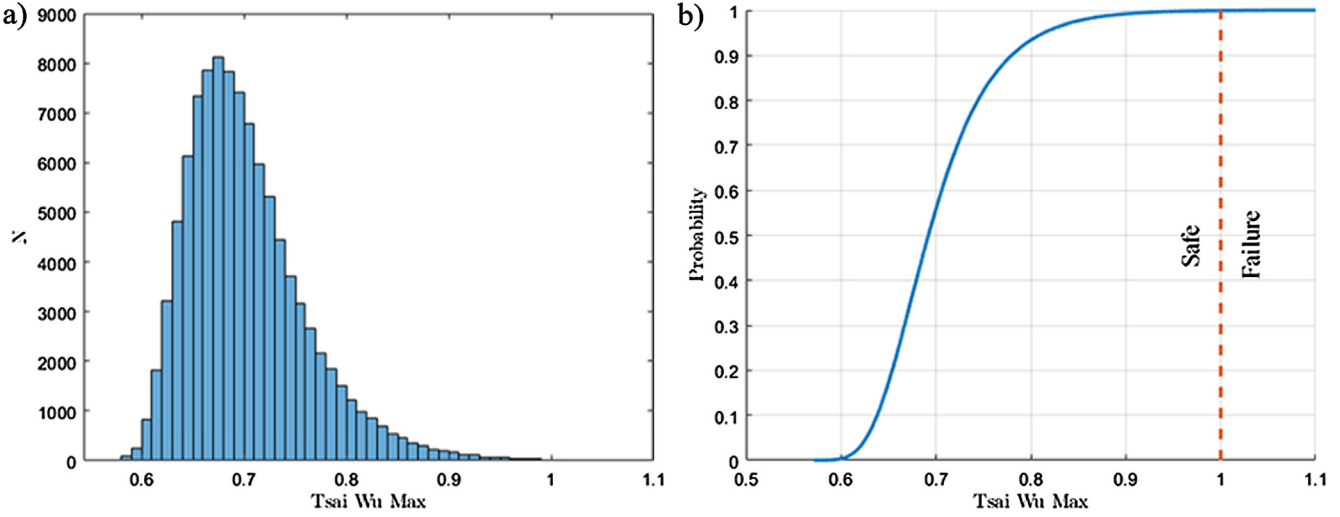


Fig. 10. Reliability analysis of the 15 layer's model: a) PDF function and; b) CDF function.

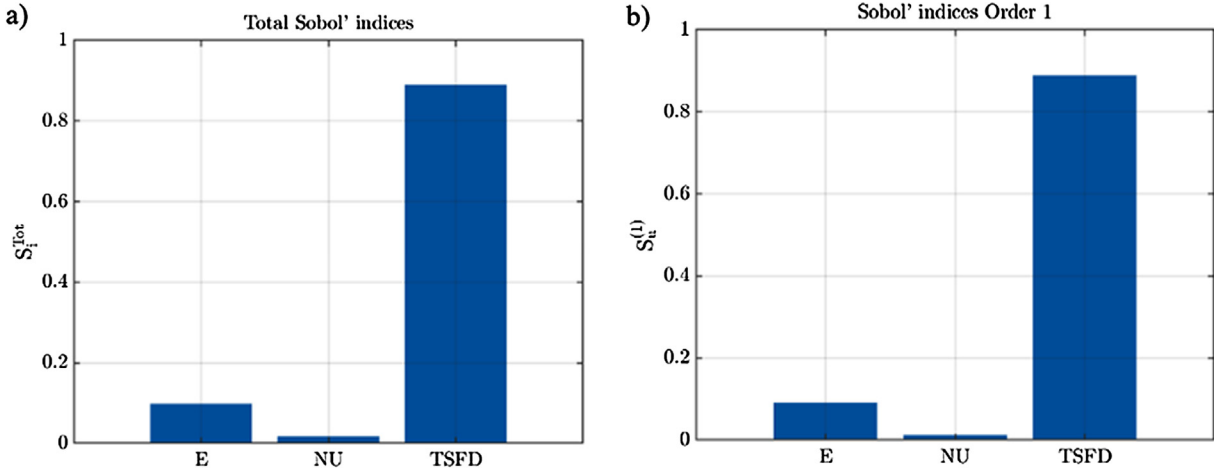


Fig. 11. Results obtained during the sensitivity analysis: a) Total Sobol' indices and; b) First-order Sobol' indices.

The number of layers in each numerical simulation were determined during the reliability analysis. To this end, the iterative approach defined in Section 2.3 was applied, defining a maximum probability of failure of 0.00135 (reliability index of 3.0). This strategy was carried out in the mathematical software MATLAB with the assistance of the open-source library UQLab [64].

3.3. Results obtained during the design of the new composite pipe

With the aim of obtaining the optimal number of layers for the composite pipe previously shown, an iterative reliability analysis proposed in Section 2.3 was carried out. During each iteration a PCE of the model response was built considering as random inputs the mechanical variables of each layer namely: i) Young's Modulus; ii) Poisson's ratio and; iii) tensile strength. The PDFs of these variables were those obtained in the DIC evaluation (Fig. 7). Throughout this process we used the Latin Hypercube Sampling method to create the DoE [65]. This technique is a popular method that allows us to obtain a random DoE ensuring the uniformity of each sample in the domains of the inputs. From the present study case several sizes of the DoE were used to build the metamodel. The accuracy of the metamodel was evaluated by means of the LOO error exposed in (Eqs. (8) and (9)). The metric of this error was comple-

mented by a cross correlation on which we used a different DoE with the same size. The sparsity of the metamodel was carried out by varying the maximum degree of the polynomials from 1 to 20, where the optimal degree was selected according to the smallest LOO error.

After a total of 15 iterations the reliability analysis found a solution which satisfied the failure criteria. In this situation the degree of the polynomials was 5 with an associated LOO error of 0.0047 and a cross-validation error of 0.005.

According to the numerical results obtained, it was necessary to use a total of 15 CFPR layers to satisfy the failure criteria previously defined ($P_f < 0.00135$, $\beta > 3$) (Table 7 and Fig. 9). In this situation, the solution has a probability of failure of 0.00108 and a reliability index of 3.0645 (Fig. 10).

In order to understand which mechanical variables are the most relevant in the safe design of the composite pipe, a Sobol sensitivity analysis was carried out. To this end a new MCS was performed, using in this context a total of 500,000 simulations. During this process it was assumed that all the layers have the same mechanical properties according to the PDF obtained during the DIC analysis (Fig. 7). The figure indicates that the tensile strength of the material is the most relevant mechanical parameter in the safety of the solution followed by the Young's Modulus. This mechanical

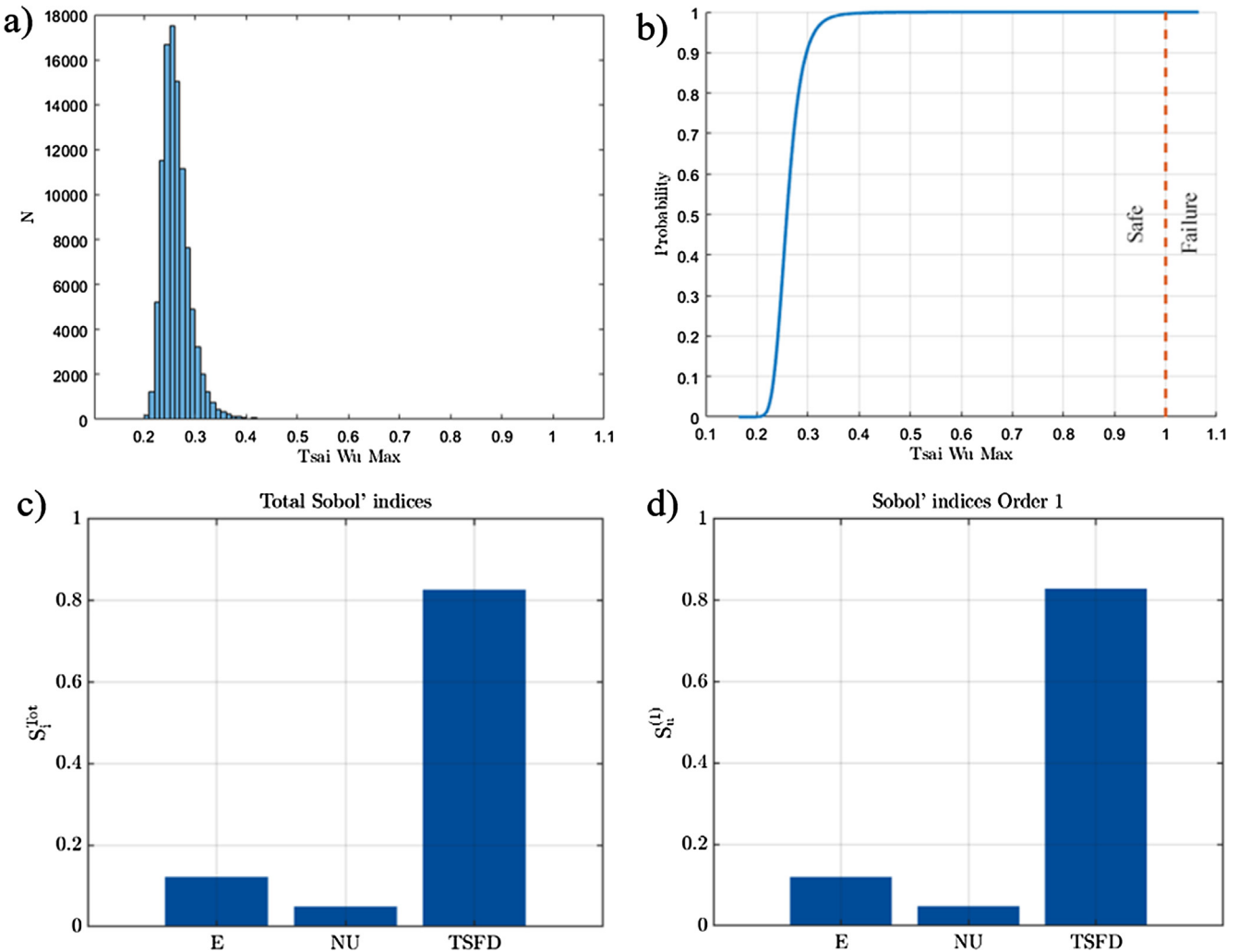


Fig. 12. Results obtained during the reliability analysis of the corroded pipe retrofitted with 4 layers of CFPR: a), b) PDF and CDF functions and; c), d) Sobol' indices.

property explains 89.00% of the total variance (Fig. 11). The great similarity between the first and the total Sobol'-indices highlights the absence of a second-order effect.

3.4. Reliability evaluation of a corroded steel pipe retrofitted with CFPR

Apart from the design of new composite pipes, another relevant application of the method could involve the retrofitting of existing steel pipes. Within this context the most common damage is the corrosion of the pipe which reduces the resistance section of it. According to this, and considering the numerical model of the corroded steel pipe defined in Section 3.2, the proposed iterative reliability analysis was performed. During this analysis we used as inputs the mechanical variables obtained by DIC (Fig. 7) as well as the thickness of the corroded area. The PDF of this input was assumed uniform, varying from 0% (totally corroded) to 100% (no corrosion).

The results of the iterative reliability analysis showed that the minimum number of layers required to fulfil the safety requirements ($P_f < 0.00135$, $\beta > 3$) are 4. With this set-up the probability of failure is 1×10^{-5} and the reliability index is 4.26, using MCS with 10^5 simulation (Fig. 12). These simulations were obtained by means of a PCE metamodel with maximum polynomial degree of 7, a DoE made up by 200 samples and a LOO error of 0.005. This error is similar to the error resulting from the cross-validation estimated in 0.003.

It is worth highlighting that the thickness of the corroded part is a critical parameter in this type of reliability analysis, determining the number of layers required to retrofit the steel pipe. Hence, it is necessary to know the minimum thickness of steel for which the 4 CFPR layers fulfil the safety requirements. To this end, a constrained optimization procedure was carried out using as cost function the thickness of the corroded part and a probability of failure of 0.00135, corresponding to a reliability index of 3. In order to achieve this result, the proposed methodology uses the genetic algorithm described by Goldberg [66]. In this procedure the process starts with an initial population which is repeatedly modified by randomly selecting individuals from the current population and using them as parents to produce the offspring of the next generation. During this process a crossover method creates new individuals on which a mutation strategy ensure that a few genes are modified, exploring a new search space. After several successive generations, the population “evolves” towards an optimal solution [67]. For the present study case the genetic algorithm was based on a population size of 25 individuals with a maximum number of generations equal to 75. For the sequence of creating new populations one individual was chosen to automatically pass to the next generation. The fraction of offspring was established in 75%. In order to obtain the global minimum of the problem, a total of 3 runs were carried out, selecting the run with the best fitness value (Fig. 13). The results of this optimization show that the critical effective thickness is 0.61 mm (15% of the initial section). In this

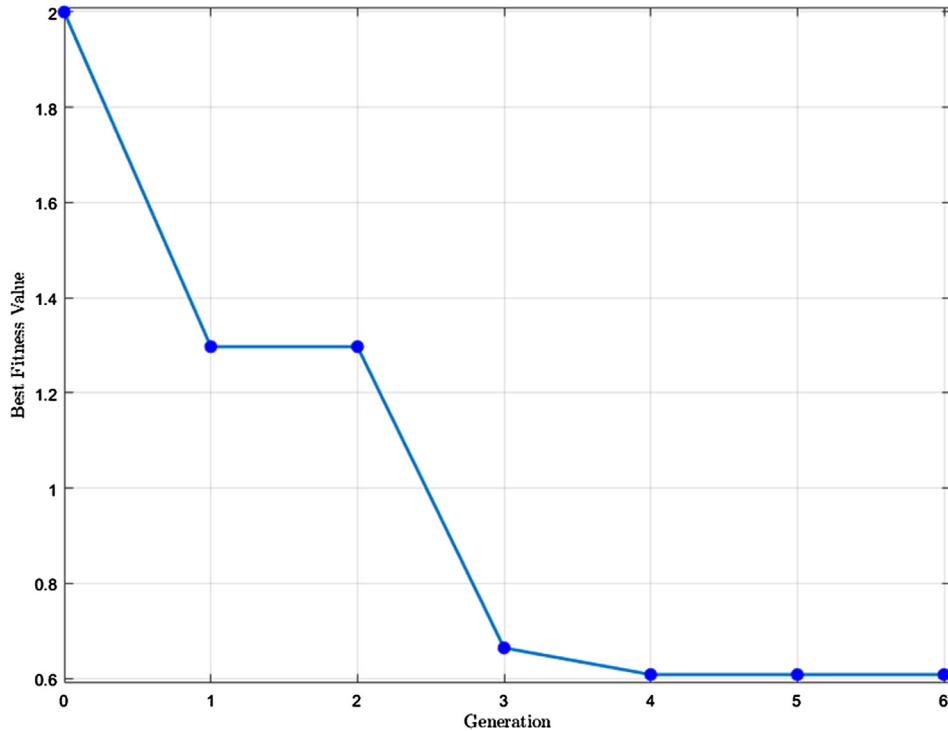


Fig. 13. Convergence plot obtained during the minimization stage.

situation the 4-layer CFPR solution has a reliability index of 3.01 (Figs. 14 and 15).

4. Conclusions

In this paper a new methodology for the reliability analysis of pressurized composite pipes was presented. To this end the method uses the data provided by the digital image correlation approach for the generation of probabilistic distribution function of the different mechanical properties of the composite solution. We subsequently use this data to build a surrogate model of numerical simulation, taking into account the stochastic nature of this type of solution. Therefore, an Adaptive Sparse Polynomial Chaos Expansion was used where the accuracy is evaluated by

means of the Leave one Out error. On the one hand, the Digital Image Correlation approach offers a robust and low-cost alternative to traditional contact measurement techniques such as linear variable differential transformers or electrical resistance strain gauges. This alternative is especially attractive in probabilistic approaches for which a large number of inputs are required. In this situation it is possible to exploit the full-field nature of the data by means of virtual extensometers that allows us to extract the mechanical properties of a sample from different locations. On the other hand, the use of an Adaptive Sparse Polynomial Chaos Expansion allows us to mimic the response of a numerical model with great efficiency, requiring a relative low number of inputs to obtain a good Leave one Out error. For example, the two numerical models considered during the present study requires only 200 samples to build an accurate metamodel with an average Leave

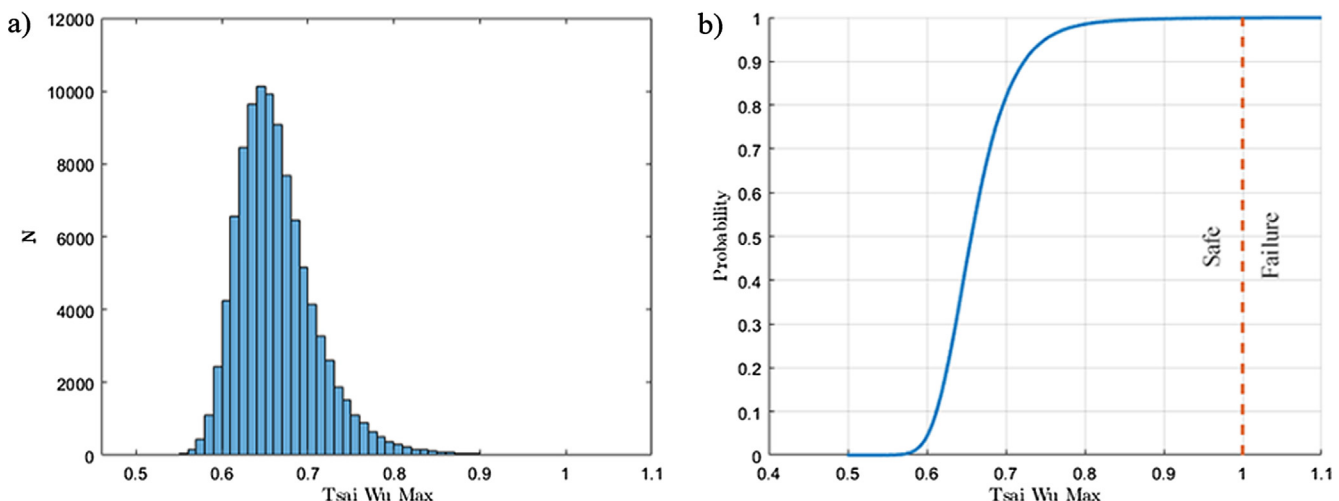


Fig. 14. Results obtained during the reliability analysis of a corroded pipe (15% of the initial section) retrofitted with 4 layers of CFPR: a) PDF and; b) CDF functions.

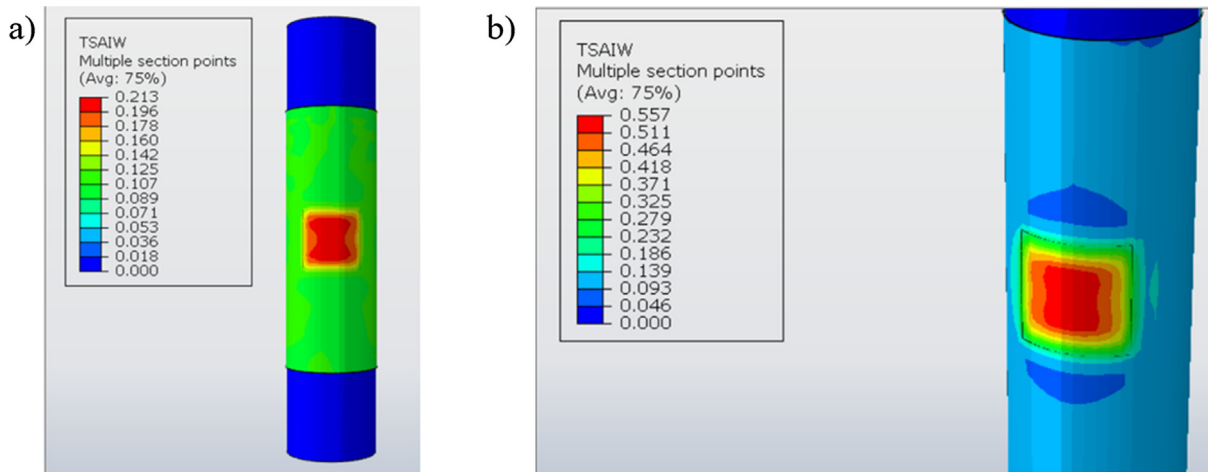


Fig. 15. Distribution of the Tsai-Wu values along the composite solution: a) in a steel pipe with 50% of corrosion and; b) in a steel pipe with 85% of corrosion (maximum value for which the 4-layer CFRP solution is reliable).

one Out Error of 0.005. This metric of error, which is compared with a standard cross validation, is especially efficient since it does not require extra samples to be obtained for the validation. Once the metamodel is obtained, the cost of each evaluation is extremely low, allowing us to carry out a reliability analysis, or even a sensitivity evaluation, by means of the Monte Carlo method. In the context of this study, one numerical evaluation by means of the FEM method requires 25 secs and assumes the investment of 29 days to carry out one Monte Carlo simulation. In contrast, the use of PCE metamodeling requires only 2 h to carry out this simulation (0.3% of the time required to perform this evaluation with FEM simulations alone). Additionally, this surrogate model can be used for optimization purposes (e.g. evaluation of the minimum effective thickness that is able to support a specific composite solution). In this situation the efficient computation cost of the surrogate model allow us to use evolutionary optimization strategies able to find the global optimal of the solution as well as the use of inequalities that introduces uncertainty in the safety evaluation. Within this context the system was able to save 99.7% of the total time required to obtain the optimal solution by means of FEM simulations. All these simulations were carried out in a Intel® XEON E3-1240 v3 processor running at 3.4 GHz with 8 GB RAM DDRII.

Future works will be focused on the use of full-field data provided by the DIC approach to evaluate the uncertainties of the composite solution from a material level by means of Random Field theory. Additionally, the proposed methodology will be used within the context of reliability-based design optimization, integrating minimization algorithms that allow us to estimate the optimal disposition of the composite solution. Also, the proposed method will be applied to other fabrics (plain/satin weave) and materials, where different reinforcements (GFRP) and matrix (especially thermoplastic ones) will be tested.

CRediT authorship contribution statement

Roberto García-Martin: Writing - original draft, Investigation, Funding acquisition. **Jorge López-Rebollo:** Formal analysis, Writing - original draft. **Luis Javier Sánchez-Aparicio:** Conceptualization, Methodology, Writing - review & editing. **José G. Fueyo:** Software, Writing - review & editing. **Javier Pisonero:** Formal analysis, Visualization. **Diego González-Aguilera:** Supervision, Writing - review & editing.

Declaration of Competing Interest

The authors declare that they have no known competing financial interests or personal relationships that could have appeared to influence the work reported in this paper.

Acknowledgements

This work was financed by ERDF funds through the V Sudoe Interreg program within the framework of the COMPRESSer project, Ref. SOE2/P1/E0643. Thanks also to the support provided by the Ministry of Science, Innovation and Universities through the project FaTIMA, Ref. RTI2018-099850-B-I00.

References

- [1] G. Sinclair, J. Helms, A review of simple formulae for elastic hoop stresses in cylindrical and spherical pressure vessels: what can be used when, *Int. J. Press. Vessels Pip.* 128 (2015) 1–7.
- [2] N. Yahaya, N.M. Noor, S.R. Othman, L.K. Sing, M.M. Din, New technique for studying soil-corrosion of underground pipeline, *J. Appl. Sci.* 11 (2011) 1510–1518.
- [3] G.H. Koch, M.P. Brongers, N.G. Thompson, Y.P. Virmani, J.H. Payer, *Corrosion Cost and Preventive Strategies in the United States*, Federal Highway Administration, United States, 2002.
- [4] D.D.N. Veritas, *DNV-OS-C501-Composite Components--Offshore Standard*, 2003.
- [5] M. Mokhtari, A.A. Nia, The application of CFRP to strengthen buried steel pipelines against subsurface explosion, *Soil Dyn. Earthq. Eng.* 87 (2016) 52–62.
- [6] M.F. Ashby, Chapter 5 – Materials Selection. *Materials Selection in Mechanical Design* cop (2011.) 97–124.
- [7] R. Rafiee, On the mechanical performance of glass-fibre-reinforced thermosetting-resin pipes: a review, *Compos. Struct.* 143 (2016) 151–164.
- [8] P. Laney, *Use of Composite Pipe Materials in the Transportation of Natural Gas*, Idaho International Engineering and Environmental Laboratory, Bechtel BWXT Idaho, LLC, 2002.
- [9] R. Rafiee, B. Mazhari, Evaluating long-term performance of Glass Fiber Reinforced Plastic pipes subjected to internal pressure, *Constr. Build. Mater.* 122 (2016) 694–701.
- [10] R. Rafiee, B. Mazhari, Simulation of the long-term hydrostatic tests on glass fiber reinforced plastic pipes, *Compos. Struct.* 136 (2016) 56–63.
- [11] R. Rafiee, F. Elasmi, Theoretical modeling of fatigue phenomenon in composite pipes, *Compos. Struct.* 161 (2017) 256–263.
- [12] J.C. Velosa, J.P. Nunes, P. Antunes, J. Silva, A. Marques, Development of a new generation of filament wound composite pressure cylinders, *Compos. Sci. Technol.* 69 (2009) 1348–1353.
- [13] A. Zaman, S.A. Gutub, M.A. Wafa, A review on FRP composites applications and durability concerns in the construction sector, *J. Reinf. Plast. Compos.* 32 (2013) 1966–1988.
- [14] C. Colombo, L. Vergani, Optimization of filament winding parameters for the design of a composite pipe, *Compos. B Eng.* 148 (2018) 207–216.

- [15] R. Rafiee, M.A. Torabi, S. Maleki, Investigating structural failure of a filament-wound composite tube subjected to internal pressure: experimental and theoretical evaluation, *Polym. Test.* 67 (2018) 322–330.
- [16] K.S. Lim, S. Azraai, N. Noor, N. Yahaya, An overview of corroded pipe repair techniques using composite materials, *Int. J. Mater. Metall. Eng.* 10 (2016) 19–25.
- [17] E. Mahdi, E. Eltai, Development of cost-effective composite repair system for oil/gas pipelines, *Compos. Struct.* 202 (2018) 802–806.
- [18] M. Kara, M. Uyaner, A. Avci, Repairing impact damaged fiber reinforced composite pipes by external wrapping with composite patches, *Compos. Struct.* 123 (2015) 1–8.
- [19] R. Rafiee, M. Fakoor, H. Hesamsadat, The influence of production inconsistencies on the functional failure of GRP pipes, *Steel Compos. Struct.* 19 (2015) 1369–1379.
- [20] J.N. Reddy, Mechanics of Laminated Composite Plates and Shells: Theory and Analysis, CRC Press, 2003.
- [21] S. Sriramula, M.K. Chryssanthopoulos, Quantification of uncertainty modelling in stochastic analysis of FRP composites, *Compos. A Appl. Sci. Manuf.* 40 (2009) 1673–1684.
- [22] O. Orell, J. Vuorinen, J. Jokinen, H. Kettunen, P. Hytönen, J. Turunen, et al., Characterization of elastic constants of anisotropic composites in compression using digital image correlation, *Compos. Struct.* 185 (2018) 176–185.
- [23] S. Sharifi, S. Gohari, M. Sharifitehni, R. Alebrahim, C. Burvill, Y. Yahya, et al., Fracture of laminated woven GFRP composite pressure vessels under combined low-velocity impact and internal pressure, *Arch. Civil Mech. Eng.* 18 (2018) 1715–1728.
- [24] M. Tekieli, S. De Santis, G. de Felice, A. Kwiecień, F. Roscini, Application of Digital Image Correlation to composite reinforcements testing, *Compos. Struct.* 160 (2017) 670–688.
- [25] M.A. Seif, U.A. Khashaba, R. Rojas-Oviedo, Measuring delamination in carbon/epoxy composites using a shadow moiré laser based imaging technique, *Compos. Struct.* 79 (2007) 113–118.
- [26] P. Callaway, M. Gilbert, C.C. Smith, Influence of backfill on the capacity of masonry arch bridges, in: Proceedings of the Institution of Civil Engineers: Bridge Engineering, ICE Publishing, 2012, pp. 147–157.
- [27] L. Sánchez-Aparicio, A. Villarino, J. García-Gago, D. González-Aguilera, Photogrammetric, geometrical, and numerical strategies to evaluate initial and current conditions in historical constructions: a test case in the church of San Lorenzo (Zamora, Spain), *Remote Sens.* 8 (2016) 60.
- [28] B. Pan, Digital image correlation for surface deformation measurement: historical developments, recent advances and future goals, *Meas. Sci. Technol.* 29 (2018) 082001.
- [29] S.M. Daghash, O.E. Ozbulut, Flexural performance evaluation of NSM basalt FRP-strengthened concrete beams using digital image correlation system, *Compos. Struct.* 176 (2017) 748–756.
- [30] C. Unlusoy, G.W. Melenka, Flexural testing of cellulose fiber braided composites using three dimensional digital image correlation, *Compos. Struct.* 230 (2019) 111538.
- [31] T. He, L. Liu, A. Makeev, Uncertainty analysis in composite material properties characterization using digital image correlation and finite element model updating, *Compos. Struct.* 184 (2018) 337–351.
- [32] L. Yu, B. Pan, Experimental study of tensile properties and deformation evolutions of 2D and 2.5 D woven SiO₂/SiO₂ composites using single-camera stereo-digital image correlation, *Compos. Struct.* 200 (2018) 589–598.
- [33] P. Kowalczyk, Identification of mechanical parameters of composites in tensile tests using mixed numerical-experimental method, *Measurement* 135 (2019) 131–137.
- [34] J. Ahn, E. He, L. Chen, J. Dear, Z. Shao, C. Davies, In-situ micro-tensile testing of AA2024-T3 fibre laser welds with digital image correlation as a function of welding speed, *Int. J. Lightweight Mater. Manuf.* 1 (2018) 179–188.
- [35] D. Xu, C. Cerbu, H. Wang, I.C. Rosca, Analysis of the hybrid composite materials reinforced with natural fibers considering digital image correlation (DIC) measurements, *Mech. Mater.* 135 (2019) 46–56.
- [36] R. García-Martin, Á. Bautista-De Castro, L.J. Sánchez-Aparicio, J.G. Fueyo, D. González-Aguilera, Combining digital image correlation and probabilistic approaches for the reliability analysis of composite pressure vessels, *Arch. Civil Mech. Eng.* 19 (2019) 224–239.
- [37] G. das Neves Carneiro, CC. António, Global optimal reliability index of implicit composite laminate structures by evolutionary algorithms, *Struct. Saf.* 79 (2019) 54–65.
- [38] R. Rafiee, M.A. Torabi, Stochastic prediction of burst pressure in composite pressure vessels, *Compos. Struct.* 185 (2018) 573–583.
- [39] R. Rafiee, F. Reshad, S. Eidi, Stochastic analysis of functional failure pressures in glass fiber reinforced polyester pipes, *Mater. Des.* 67 (2015) 422–427.
- [40] R. Rafiee, Stochastic fatigue analysis of glass fiber reinforced polymer pipes, *Compos. Struct.* 167 (2017) 96–102.
- [41] S.S. Tomar, S. Zafar, M. Talha, W. Gao, D. Hui, State of the art of composite structures in non-deterministic framework: a review, *Thin-Walled Struct.* 132 (2018) 700–716.
- [42] S. Dey, T. Mukhopadhyay, S. Adhikari, Metamodel based high-fidelity stochastic analysis of composite laminates: a concise review with critical comparative assessment, *Compos. Struct.* 171 (2017) 227–250.
- [43] ISO E, Plastics—determination of tensile properties, 1997.
- [44] H. Touantji, S. Dempsey, Stress modeling of pipelines strengthened with advanced composites materials, *Thin-Walled Struct.* 39 (2001) 153–165.
- [45] ISO E, 527-4, Plastics—determination of tensile properties—part 4: test conditions for isotropic and orthotropic fibre-reinforced plastic composites, International Organization for Standardization (ISO), Geneva, Switzerland, 1997.
- [46] M.A. Sutton, J.J. Orteu, H. Schreier, *Image Correlation for Shape, Motion and Deformation Measurements: Basic Concepts, Theory and Applications*, Springer Science & Business Media, 2009.
- [47] B. Pan, K. Qian, H. Xie, A. Asundi, Two-dimensional digital image correlation for in-plane displacement and strain measurement: a review, *Meas. Sci. Technol.* 20 (2009) 062001.
- [48] Y. Dong, B. Pan, A review of speckle pattern fabrication and assessment for digital image correlation, *Exp. Mech.* 57 (2017) 1161–1181.
- [49] M.N. Vo, Z. Wang, L. Luu, J. Ma, Advanced geometric camera calibration for machine vision, *Opt. Eng.* 50 (2011) 110503.
- [50] L.A. Martins, F.L. Bastian, T.A. Netto, Structural and functional failure pressure of filament wound composite tubes, *Mater. Design* (1980–2015) 36 (2012) 779–787.
- [51] S.W. Tsai, E.M. Wu, A general theory of strength for anisotropic materials, *J. Compos. Mater.* 5 (1971) 58–80.
- [52] L. Novak, D. Novak, Polynomial chaos expansion for surrogate modelling: theory and software, *Beton-und Stahlbetonbau* 113 (2018) 27–32.
- [53] Á. Bautista-De Castro, L.J. Sánchez-Aparicio, P. Carrasco-García, L.F. Ramos, D. González-Aguilera, A multidisciplinary approach to calibrating advanced numerical simulations of masonry arch bridges, *Mech. Syst. Sig. Process.* 129 (2019) 337–365.
- [54] N. Wiener, The homogeneous chaos, *Am. J. Math.* 60 (1938) 897–936.
- [55] G. Blatman, B. Sudret, Adaptive sparse polynomial chaos expansion based on least angle regression, *J. Comput. Phys.* 230 (2011) 2345–2367.
- [56] B. Efron, T. Hastie, I. Johnstone, R. Tibshirani, Least angle regression, *Ann. Stat.* 32 (2004) 407–499.
- [57] G. Deman, K. Konakli, B. Sudret, J. Kerrou, P. Perrochet, H. Benabderrahmane, Using sparse polynomial chaos expansions for the global sensitivity analysis of groundwater lifetime expectancy in a multi-layered hydrogeological model, *Reliab. Eng. Syst. Saf.* 147 (2016) 156–169.
- [58] D. Lecompte, H. Sol, J. Vantomme, A. Habraken, Analysis of speckle patterns for deformation measurements by digital image correlation, *Int. Soc. Opt. Photon.* (2006) 63410E.
- [59] B. Pan, Z. Lu, H. Xie, Mean intensity gradient: an effective global parameter for quality assessment of the speckle patterns used in digital image correlation, *Opt. Lasers Eng.* 48 (2010) 469–477.
- [60] A.F. Ab Ghani, M.B. Ali, S. DharMalingam, J. Mahmud, Digital image correlation (DIC) technique in measuring strain using opensource platform Ncorr, *J. Adv. Res. Appl. Mech.* 26 (2016) 10–21.
- [61] P. Sasikumar, R. Suresh, P.K. Vijayaghosh, S. Gupta, Experimental characterisation of random field models for CFRP composite panels, *Compos. Struct.* 120 (2015) 451–471.
- [62] R.B. D'Agostino, *Goodness-of-fit-techniques*, CRC press, 1986.
- [63] H. Liu, *Pipeline Engineering*, CRC Press, 2003.
- [64] S. Marelli, B. Sudret, UQLab: A framework for uncertainty quantification in Matlab, *Vulnerability, Uncertainty, and Risk: Quantification, Mitigation, and Management* (2014) 2554–2563.
- [65] M.D. McKay, R.J. Beckman, W.J. Conover, Comparison of three methods for selecting values of input variables in the analysis of output from a computer code, *Technometrics* 21 (1979) 239–245.
- [66] D. Goldberg, *Genetic Algorithms in Search, Optimization & Machine Learning*, Addison-Wesley Publishing Company, Inc., 1989.
- [67] M. Mitchell, *An Introduction to Genetic Algorithms*, MIT Press, 1998.

Capítulo III

COMBINING DIGITAL IMAGE CORRELATION AND PROBABILISTIC APPROACHES FOR
THE RELIABILITY ANALYSIS OF COMPOSITE PRESSURE VESSELS

RESUMEN

El tercer trabajo publicado se plantea como una evolución del trabajo anterior, donde se implementa definitivamente la técnica del DIC2D integrando enfoques probabilísticos en la búsqueda de diseños fiables para una aplicación concreta como son los recipientes a presión elaborados con materiales compuestos (COPVs).

Este trabajo plantea consolidar los **objetivos** propuestos en esta tesis, así como avanzar un paso más en la técnica del DIC (*Digital Image Correlation*) para la extracción de las funciones de distribución (PDFs) de las variables mecánicas del composite, donde se pretende explotar al máximo la técnica de medida de campo completo. Una vez más las variables se seleccionarán a través de un estudio de Análisis Sensible. A su vez se adaptarán los modelos FEM al cálculo probabilístico para el diseño del COPV bajo criterios de fiabilidad.

En cuanto a la **metodología** empleada, este trabajo se sirvió de una versión mejorada del *Smartfire* para la calibración del DIC2D, técnica de donde se extraen medidas de deformación de campo completo y esto representa el gran salto respecto al capítulo previo, donde en lugar de emplear EV en un número limitado, se emplea la medida de campo completo.

Para el cálculo FEM se emplea de nuevo el software AbaqusTM que, gracias al lenguaje propio de programación Python, permite adaptar los modelos de manera más efectiva a la par que se integran las PDFs en el proceso cálculo.

La determinación de las variables más representativas se realiza a través de un análisis de sensibilidad global basado en el método de Sobol, donde para el cálculo de los conocidos como Índices de Sobol, se emplea el método de expansión de caos

polinomial. Finalmente se lleva a cabo el análisis estocástico, el cual se traslada a una dimensión mayor mediante la implementación del método *Semi Ramdon Field (o Random Variable)* método más riguroso, que permite trabajar con el campo completo de medida.

Como criterio de fallo para el diseño fiable se aplica el criterio de Tsai-Wu habitual en el caso de composites, donde el estudio de la propagación de las incertidumbres se lleva a cabo mediante el método de simulación *Latin Hypercube Sampling* (LHS).

En cuanto a los **resultados**, la calibración del DIC arroja un error cuadrático medio (RMSE) de 2.97% para los desplazamientos y del 0.04% para las deformaciones. Se generan dos modelos FEM, uno determinístico para el análisis de sensibilidad que indica que la variable que más influye (76%) es la deformación máxima principal seguida del módulo de Young (16%), y otro modelo probabilístico para el cálculo del coeficiente de seguridad, con una fiabilidad del 95% que muestra ser más conservador que el modelo determinístico.

Se puede concluir que el DIC es una técnica válida para obtener el campo completo de deformaciones de un material compuesto con altos niveles de precisión, y se confirma como una herramienta eficaz para el diseño de composites; donde la incorporación de métodos estocásticos al cálculo FEM, gracias a la fusión con el DIC, permite realizar diseños más fiables.

El empleo de métodos subrogados se muestra de gran eficacia para la implementación de las técnicas de análisis sensible como del RBDO.

Se logran implementar diferentes técnicas para alcanzar diseños fiables gracias a una estimación robusta de las incertidumbres asociadas al factor material. El empleo del campo completo implica un alto coste computacional cuyos tiempos de cálculo se presentan como inasumibles, lo que impediría que el empleo de esta técnica fuera viable, pero gracias a la combinación del análisis sensible junto a la metamodelización, se consigue una reducción drástica en los tiempos de cálculo, lo que posibilita que la metodología desarrollada pueda ser empleada y transferida al sector industrial por la fiabilidad de los resultados y razonables plazos de cálculo.

Available online at www.sciencedirect.com**ScienceDirect**journal homepage: <http://www.elsevier.com/locate/acme>**Original Research Article****Combining digital image correlation and probabilistic approaches for the reliability analysis of composite pressure vessels**

Roberto Garcia-Martin^a, Álvaro Bautista-De Castro^b, Luis Javier Sánchez-Aparicio^{b*}, José G. Fueyo^a, Diego Gonzalez-Aguilera^b

^a Department of Mechanical Engineering, University of Salamanca, Higher Polytechnic School of Zamora, Campus Viriato, Avenida Requejo, 33, 49022 Zamora, Spain

^b Department of Cartographic and Land Engineering, University of Salamanca, Higher Polytechnic School of Ávila, Hornos Caleros, 50, 05003 Ávila, Spain

ARTICLE INFO**Article history:**

Received 30 July 2018

Accepted 12 October 2018

Available online 14 November 2018

Keywords:

Composite material

Digital image correlation

Full-field strain

Random variable finite element

Stochastic analysis

ABSTRACT

The accuracy of reliability analysis of composite solutions depends on the robust estimation of the uncertainties associated with the mechanical properties of this material. On this basis, we propose a methodology able to exploit the full field strain data provided by the digital image correlation approach in order to extract the probabilistic density functions of the mechanical properties. These probabilistic density functions are complemented by a global sensitivity analysis based on the polynomial chaos expansion and a random variable approach, based on the latin hypercube sampling method, with the aim of obtaining a stochastic evaluation of composite pressure vessels.

© 2018 Politechnika Wrocławia. Published by Elsevier B.V. All rights reserved.

1. Introduction

Nowadays, composite materials couple a great part of everyday products such as components for vehicles, aircrafts, marine vessels, lightweight constructions, furniture or food containers among others [1–4]. These type of materials offer better resistance to environmental agents (specially in corrosive atmospheres), a remarkable fatigue endurance and high stiffness-to-weight and strength-to-weight ratios [5,6] and a high energy absorption [7–9]. These properties are specially

interesting in those prototypes devoted to the storage of liquefied petroleum or medical gases where the material used to constitute them is steel. Among the limitations of this metallic material are the problems related with corrosion, weight or between the manufacturing process and for which reinforced glass/carbon fibre polymer (GFPR/CFPR) is a potential alternative [10].

Whereas the design of a steel pressure vessel is properly defined and does not entail difficulties due to its homogeneity and isotropic behaviour, the design of composite pressure vessels is not trivial. The heterogeneous nature (e.g. the basic

* Corresponding author.

E-mail address: luisj@usal.es (L.J. Sánchez-Aparicio).

<https://doi.org/10.1016/j.acme.2018.10.001>

1644-9665/© 2018 Politechnika Wrocławia. Published by Elsevier B.V. All rights reserved.

Nomenclature

d	diameter of the circular spot
E	Young's Modulus
ν	Poisson's coefficient
H	height of the ROI
MIG	mean intensity gradient of the speckle pattern
$rand$	random factor to separate the speckle pattern spots
α	indices of the PCE
ψ_α	multivariate polynomial
$\hat{S}_i \hat{S}_i^t$	first-order and total Sobol's indices
step	separation between speckle pattern spots
W	width of the ROI

constituents of the composite material, the fibre orientation or the assembly and manufacturing processes [11], as well as the possibility of being orthotropic or fully anisotropic materials [12], demands the use of numerical simulation, by means of the finite element method (FEM), to study its mechanical behaviour. However, the use of these numerical simulations from a deterministic point of view (numerical simulations on which are adopted a unique variable for the different inputs) cannot provide suitable safety margins for the design of reinforced fibre polymer (FPR) structures [11]. Therefore, it is necessary to incorporate probabilistic approaches able to take into account the uncertainty related with the material, through the use of methods such as random variable models or the so-called random fields method [13]. These approaches take into account these uncertainties at different levels into the numerical model: from constituent levels (micro-scale), ply levels (meso-scale) to component levels (macro-scale) [13]. The use of these stochastic approaches offer advantages in terms of material utilization and would lead to a more accurate reliability estimation [11].

Therefore, the creation of accurate stochastic numerical simulations and the use of this product in an efficient way requires a comprehensive knowledge of the material behaviour. Generally, this evaluation is carried out by means of direct measurements through the use of linear variable differential transformers (LVDTs), laser transducers, extensometers and electrical resistance strain gauges [14–16]. The results of these techniques are highly affected by the presence of cracking, sliding or uneven load distributions without forgetting the local nature of these measurements (especially in the strain gauges) which are not particularly useful in detecting the global response of the material. Apart from these limitations, the use of these direct measurement systems may complicate the preparation of the test, entailing a high cost related to the use of the possible instrumentation (gauges or optical fibres) or to possible damage to sensors [15]. To overcome these drawbacks, several full-field indirect optical techniques have been developed such as Moiré interferometry [17], particle image velocimetry (PIV) [18] and, digital image correlation (DIC) [19]. This latter methodology has proved to be an efficient technique in composite materials, allowing the characterization of the mechanical properties of the materials, as well as for to studying the displacement and strain distribution during the experimental tests [14,15,20]. However, the full-field capacity of this technique, in displacements and strains, is not

exploited in most of the cases, using only part the data provided by two points (similar to an extensometer) to create the stress-strain curves and thus, to extract the mechanical properties of the material [14,15,20–22].

This paper therefore takes into account the influence of the uncertainties in the accurate numerical simulation of composite solutions, as well as the potential offered by the DIC approach: (i) accuracy; (ii) non-contact nature and (iii) full-field of displacements and strains. We propose a method for integrating the uncertainties presented in the mechanical properties of composite materials, extracted by means of the DIC approach, into probabilistic advanced numerical simulations with the aim of evaluating the safety of composite pressure vessels from a probabilistic point of view. To this end, the following structure was used: Section 1 is introduction; Section 2 describes the composite materials used, the digital image correlation method and the experimental methodology carried out in the specimens; Section 3 shows the experimental results obtained by the digital image correlation as well as the characterization of the mechanical properties of the material; Section 4 is dedicated to the integration of the data from the digital image correlation in probabilistic numerical simulations and finally Section 5 discusses the conclusions.

2. Materials and methods

2.1. Composite solution evaluated

Specimens used for the study consist of composite manufactured solutions made by an epoxy resin matrix Biresin CR82® with a hardener Biresin CH80-10® (Table 1) and E-Glass fibres composed by a fibre “Taffeta” Woven Roving EWR 300-1250® with a thickness of 0.3 mm (Table 2). The matrix was performed with a proportion of 158 g of resin and 42 g of catalyst for a specific quantity of 200 g.

Prior to performing the matrix, a wooden mould of dimensions 310 × 210 mm was manufactured, placing on it a perimeter tape with a thickness of 2 mm (red tape), in order to set this thickness in the subsequent manufactured specimens. Furthermore, a transparent film was placed on the wooden mould for demoulding (Fig. 1a).

A multilayer taffeta [0,90]S was performed (Fig. 1c). The first piece of the Woven Roving was placed and properly oriented on the surface of the wooden mould, impregnating it with the matrix (resin and catalyst) through the use of a brush. Subsequently, in the wooden mould we added eight more

Table 1 – Technical specifications of the epoxy resin used.

Mechanical properties	Value
Density (g/cm ³)	1.14
Flexural E-Modulus (MPa)	3600
Tensile E-Modulus (MPa)	3500
Flexural strength (MPa)	130
Elongation at maximum flexural strength (%)	4.6
Tensile strength (MPa)	75
Elongation at maximum tensile strength (%)	3.9
Water absorption (%)	0.23

Table 2 – Technical characteristics of fibres Woven Roving EWR 300-1250.

Glass type	E-Glass
Thickness (mm)	0.3
Density (warp × weft) (end/cm)	$4.6 \times 4.1 \pm 10\%$
Tex (warp × weft)	300×400
Moisture content (%)	0.1% at 20°C
Loss on ignition (%)	0.4–0.8
Width (cm)	125 ± 1
Weight (g/m^2)	300 ± 15
Weight per roll (kg)	50
Tensile strength (MPa)	3400
Elongation at maximum tensile strength (%)	4.5

layers (Fig. 1a), repeating the impregnation process with the matrix on each one of them. Once the nine fibre layers (the initial fibre layer and the eight fiber layers added) were in place, a paint roller was carefully used on each surface of the wooden mould to remove the surplus matrix in order to avoid displacements of the fibre layers. The time needed for adding the fibre layers on the wooden mould was 50 min.

All fibre layers were progressively pressed in order to achieve the desired thickness established by the red tape (2 mm). Thus, they were dried in a low-temperature furnace about 50°C for 5 h. As a result, a plate of epoxy resin with a symmetrical fibre reinforced oriented at 90° was obtained. Finally, from this plate a total of five composite specimens were extracted with the measures established by ISO guidelines [23] (Fig. 1b and c). These specimens were cut using a computer numerical control (CNC) machine.

2.2. Mechanical characterization of the composite solution: the 2D digital image correlation method

In order to characterize the mechanical properties of the composite solution previously shown, the 2D digital image

correlation (2D-DIC) approach was used. This method is an optical non-contact technique for measuring material deformations that uses image registration algorithms to track the relative displacements suffered by material points between a reference state (undeformed situation) and the subsequent deformed states during the mechanical tests (Fig. 2a).

For this tracking, it is necessary to acquire several images by means of a digital camera. Then, the reference image, which corresponds with the undeformed state, is split into smaller regions called subsets. These subsets are the features tracked along the different images by means of a cross-correlation coefficient, the Zero mean Normalized Cross-Correlation (ZNCC) being the most used index, since it presents insensitivity to illumination lighting noise [24].

During this tracking, it is assumed that the deformation of the subset can be represented as a linear combination of six degrees of freedom (translation in the x and y-direction, elongation in the x and y-direction and shear deformation in the x and y-direction) with respect to the reference subset (Fig. 2b).

At this point of the methodology, it has been possible to track the deformations suffered by all the subsets with pixel accuracy (cross correlation matching). This accuracy is due to the discrete nature of the digital image (with integer values that range from 0 to 255 in a 8 bits image). With the aim of obtaining a subpixel accuracy, the DIC method uses an iterative non-linear least square optimization scheme. During this optimization, an initial approximation uses the position tracked during the cross correlation stage, and then a b-spline interpolation scheme is used to pass from a discrete space of gray values to a continuous function. Among the types of b-splines methods available nowadays (from bicubic splines to biquintic b-splines), the biquintic b-spline is one of the most accurate [25].

Starting from the continuous space generated by means of the b-spline interpolation, the Inverse Composition Gauss-

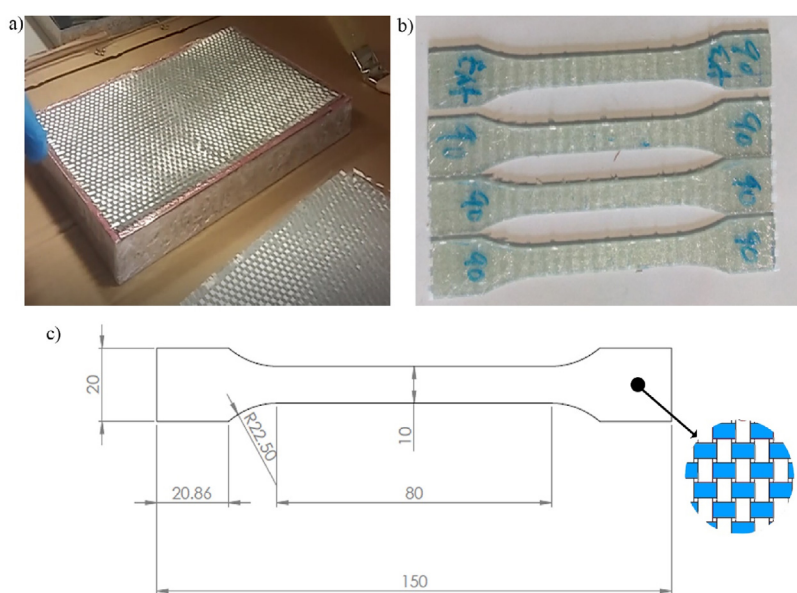


Fig. 1 – Composite solution manufactured: (a) wooden mould with fibre layers symmetrical oriented at 90° ; (b) composite specimens prepared for the experimental campaign and; (c) dimensions (in mm) according with the guideline BS EN ISO 527-5:2009 of the composite specimens with a detail of the taffeta configuration.

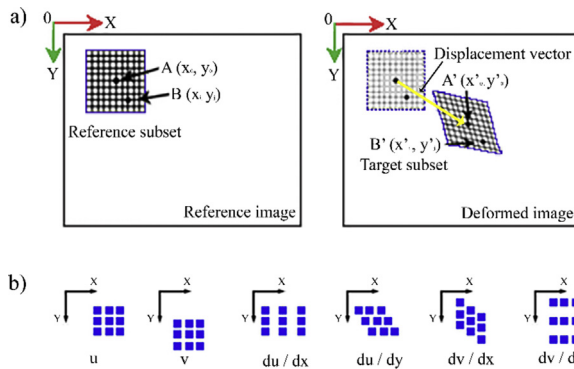


Fig. 2 – Graphical representation of the DIC approach: (a) evaluation of the displacement suffered by a subset and (b) degrees of freedom considered during the displacement analysis. u and v represents the translation of the subset in the x and y directions respectively; du/dx and du/dy the elongation of the subset in the x and y axis respectively and; dv/dy and dv/dx the shear deformation of the subset in the x and y axis respectively.

Newton method (IC-GN) was used to optimize the cost function. On each iteration, the IC-GN algorithm finds a small deformation of the reference subset (underdeformed image) that best fits the deformed reference subset, then, the shape function, defined by the six degrees of freedom (Fig. 2b), is updated [26]. This process is repeated until a convergence threshold is reached.

The procedure described above is repeated in all the subset that compose the image, allowing a full-field displacement to be obtained. It is worth mentioning that this process is complemented by the reliability guided method proposed by Pan [27]. This approach begins with a selected seed point and proceeds with the neighbour subset with highest ZNCC. Thanks to this, error propagation is avoided [27].

Additionally to the displacement, the DIC method can also determine the strains produced in specimens. In this case the gradients calculated during the previous step, by means of the IC-GN algorithm, are used to compute the Green-Lagrangian strain tensor. This method is applied over the entire region of interest (ROI) in order to obtain the corresponding strain field.

Complementary to the above mentioned and exposed in [24], an accurate extraction of displacements and strains requires the consideration of the following aspects: (i) a proper

preparation of the specimen surface and (ii) a geometrical calibration of the camera.

2.2.1. Specimen preparation

Under the basis defined previously, the success of the DIC approach depends strongly on the random intensity distribution of the ROI [28,29]. This intensity distribution must present distinct, unique, non-periodic and stable grayscale features, the so-called speckle pattern [28]. This speckle pattern can be natural (texture of the material) or artificial, the last one being the most robust and common [28]. For the present study case, and taking into account the absence of natural texture of the composite specimens, an artificial speckle pattern was applied following the approach proposed by Chen et al. [29].

In a first stage, a regular pattern of circular spots were generated, using as input the diameter of the circular spot (d) as well as the separation between circles (step). Then, this regular grid was perturbed with a random factor ($rand$). This perturbation avoids the generation of a isotropic pattern with preferential local features (Eqs. (1) and (2)) [29]. Finally, this speckle pattern was printed and applied, through the use of a transfer, on the surface of the specimen. It is worth mentioning that the specimen surface was treated previously with an elastic white primer, allowing us to optimize the contrast and adherence of the speckle pattern (Fig. 3).

$$x = x_i \pm \frac{1}{2} * rand * step \quad (1)$$

$$y = y_i \pm \frac{1}{2} * rand * step \quad (2)$$

where x, y are the coordinate of the center after the perturbation, x_i, y_i are the coordinates of the center before perturbation, $rand$ is a random factor from 0 to 1 and; $step$ is the distance between centers.

2.2.2. Camera calibration

The images captured by optical sensors suffer from lens distortion that can affect the final accuracy of the results. This error source can be minimized through the use of geometrical calibration algorithms which are able to remove the radial and tangential distortion induced by the lens system in the images acquired. In the present case, the calibration procedure defined by [30] was used. This method follows the next steps [30]: (i) detection of the control points in the raw images through the use of the edge detection and ellipse fitting method; (ii) optimization of the camera parameters and world coordinates of the control points using the Levenberg–

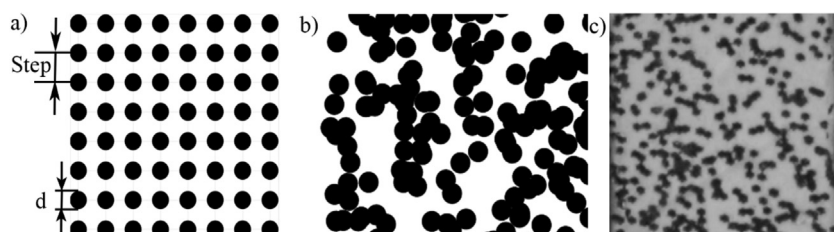


Fig. 3 – Speckle pattern design: (a) regular grid; (b) result of the random perturbation and (c) pattern captured by the camera.

Marquardt algorithm; (iii) extraction of the frontal images and the use of the calculated positions of the control points in the frontal images as an initial approximation in order to refine the positions for the subsequent process in the DIC method (subpixel interpolation and non-linear optimization); (iv) the reverse projection of the detected control points in the frontal images back to the raw images and (v) refinement of the camera parameters together with the world coordinates of the control points.

2.3. Data acquisition prototype

In order to carry out the DIC approach, an in-house acquisition prototype was developed. This prototype was built with the following components (Fig. 4): (i) a digital reflex camera Canon EOS 700D with a 60 mm prime macro-lens (Table 3); (ii) a programmable logic controller (PLC) composed by a Raspberry Pi 3® and a Monarco HAT®; (iii) a relay module with eight channels and (iv) a LED lighting unit with 50 W of power.

Regarding the PLC of the prototype, one of its analog inputs was connected with a load cell HBM K-U5-200K-D® of 200 KN from the traction testing machine MTS Alliance RF/200 establishing load set-points (from 0 kN to 10 kN in intervals of 0.5 kN). This test machine has a test speed comprised between 0.01 mm/min and 500 mm/min and an accuracy with an error between 1 N and 2 N, being suitable for the evaluation of the composite solution proposed. Then, these loads were synchronized through the PLC with the camera shots in order

Table 3 – Technical specifications of the digital reflex camera Canon EOS 700 D and the macro lens system used.

Canon EOS 700 D	
Sensor type	CMOS APS-C
Sensor size	22.3 × 14.9 mm ²
Crop factor	1.61
Pixel size	4.3 µm
Image size	5184 × 3456 px
Total pixels	18.5 Mpx
Focal length	60 mm
Closer focused distance	254 mm
Lens magnification	1:1 (life size)
Dimensions	133.1 × 99.8 × 78.8 mm

to obtain, in the same instant, an image and a load value. Thus, this data is registered through the PLC.

3. Experimental results

3.1. Tests setup

The mechanical characterization of the composite specimens developed in Section 2.1 was carried out by means of a 2D-DIC approach. With the aim of obtaining reliable results, a proper test set-up was considered, comprising the following stages: (i) the estimation of the distance and depth of field between the camera and the test specimen; (ii) the application of a speckle pattern on the tests specimens and (iii) the geometrical calibration of the camera.

The resolution of the DIC approach depends strongly on the Ground Sample Distance (GSD) of the images. However, if the camera is close regarding the target (surface with the speckle pattern of the specimen), the depth of field will be lower. On this basis, the acquisition system was placed at 1 m with respect to the traction testing machine (Fig. 5), achieving a GSD of 0.072 mm/px and a depth of field of 0.04 m (the aperture used was 7.1). It is worth mentioning that an ISO-100 and a shutter speed of 1/100 s were used to capture all the images, ensuring the best quality in terms of contrast and sharpness.

Concerning the texture of the specimens, an artificial speckle pattern was generated by means of the methodology proposed in Section 2.2.1. To this end, a regular grid with circular shapes was numerically created with a diameter (d) of 0.50 mm and a distance between the centers of the circles (step) of 1.22 mm. Then, this regular grid was perturbed adding to the horizontal and vertical coordinates of each blob a random displacement of 0.7 times the GSD ($rand$), resulting in a covering factor of 51% according with the range recommended by Lecompte et al. [31] (40–70%). Finally this speckle pattern was printed and applied on the surfaces of the tests specimens previously treated with an elastic white primer (Fig. 6).

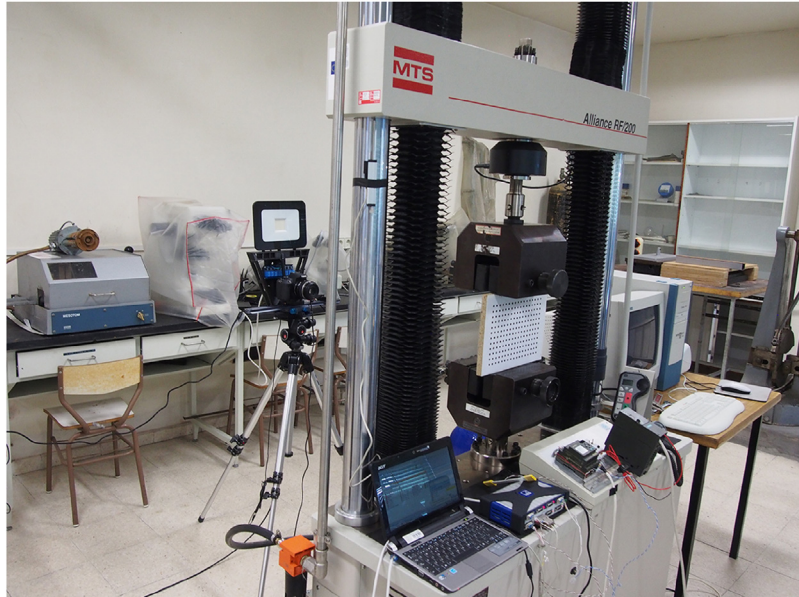
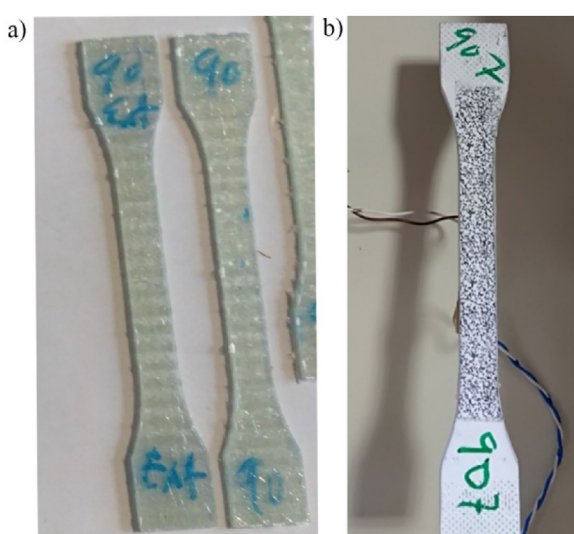
To validate the quality of the speckle pattern applied, the mean intensity gradient (MIG) was calculated as follows [32] (Eq. (3)). Higher MIG values suggest better gray distribution and thus imply lower errors in the final results. As a result an MIG of 46.8 was obtained, assuming it as an acceptable value regarding the quality evaluations of speckle patterns per-



Fig. 4 – Experimental prototype used during the traction tests in the specimens.

Table 4 – Results obtained from the mechanical characterization of the specimens.

Parameter	Mean	Covariance (%)	Lower bound	Upper bound
Young's Modulus (GPa)	27.00	4.82	23.90	29.80
Poisson's ratio (-)	0.21	33.25	0.18	0.23
Yield strain (mm/mm)	0.021	15.69	0.019	0.023

**Fig. 5 – Disposition of the data acquisition system with respect to the traction testing machine.****Fig. 6 – Composite specimens used during the experimental campaign: (a) natural texture of the tests specimens and (b) results after the application of the speckle pattern over the elastic white primer.**

formed with standard technology which usually present a MIG of 40 [32].

$$MIG = \sum_{i=1}^W \sum_{j=1}^H \frac{|\nabla f(x_{ij})|}{W * H} \quad (3)$$

where $|\nabla f(x_{ij})|$ is the local intensity gradient vector of a gray-scale image, W is the width of the ROI and H is the height of the ROI.

For the camera calibration, a flat panel composed of 10×7 ring patterns (70 control points) with a grid distance of 25.4 mm was used (Fig. 7a). During this stage, a total of 18 images of the flat panel in different positions were acquired (Fig. 7b). Finally, the calibration approach shown in Section 2.2.2 was applied, allowing the estimation of the intrinsic camera parameters. These parameters were used to undistort the images acquired during the tensile tests.

3.2. Full field displacements and strains

Taking into consideration the step-up previously shown, a total of five tensile tests were carried out following the BS EN ISO 527-5:2009 guidelines [23]. On each test, the stretching speed of the traction testing machine was fixed at 2 mm/min, acquiring a total of 20 images (one image each 200 N of traction force increment). It is worth mentioning that the first camera

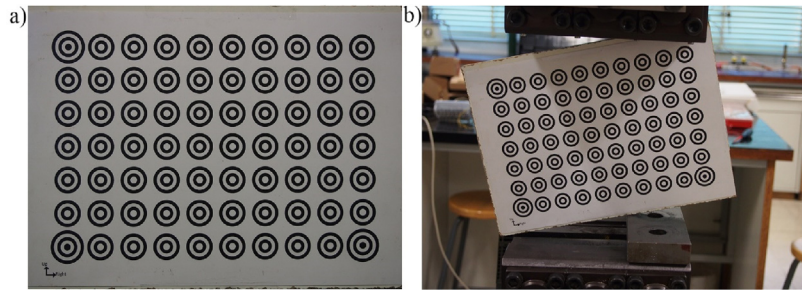


Fig. 7 – Geometrical calibration of the camera: (a) general view of the flat panel used for the calibration; (b) example of the positions used for the flat panel during the calibration.

shot was performed without load with the purpose of obtaining the reference image for the subsequent correlation process with the 2D-DIC method.

Then, each set of images were processed by means of the DIC approach defined in Section 2, using the open-source software Ncorr [33]. During this stage, a subset size of 50×50 pixels (approximately a square of 4 mm) with a step of 3 pixels was considered. This subset size ensures an adequate number of distinctive features for computing the ZNCC in each search window as well as a proper definition of the displacement field by means of linear shape functions (Fig. 2). As a result, it was possible to determine, on each test specimen, a full field of displacements (Fig. 8a) and strains (Fig. 8b and c).

Taking into consideration the type of test carried out, the state of stresses along the central area of the specimen can be considered constant and made up by an unique normal stress on the longitudinal direction. Therefore, if the material evaluated was homogeneous, the expected maximum principal strains will be constant. However, the results of the DIC analysis shown different maximum principal strains along the test specimen, highlighting the heterogeneous nature of the composite solution evaluated and thus the presence of different Young Modulus (Fig. 8b). Additional to this, it was possible to observe a variability in the minimum principal strain field suggesting the presence of a heterogeneous Poisson ratio (Fig. 8c). Both heterogeneities can be attributed

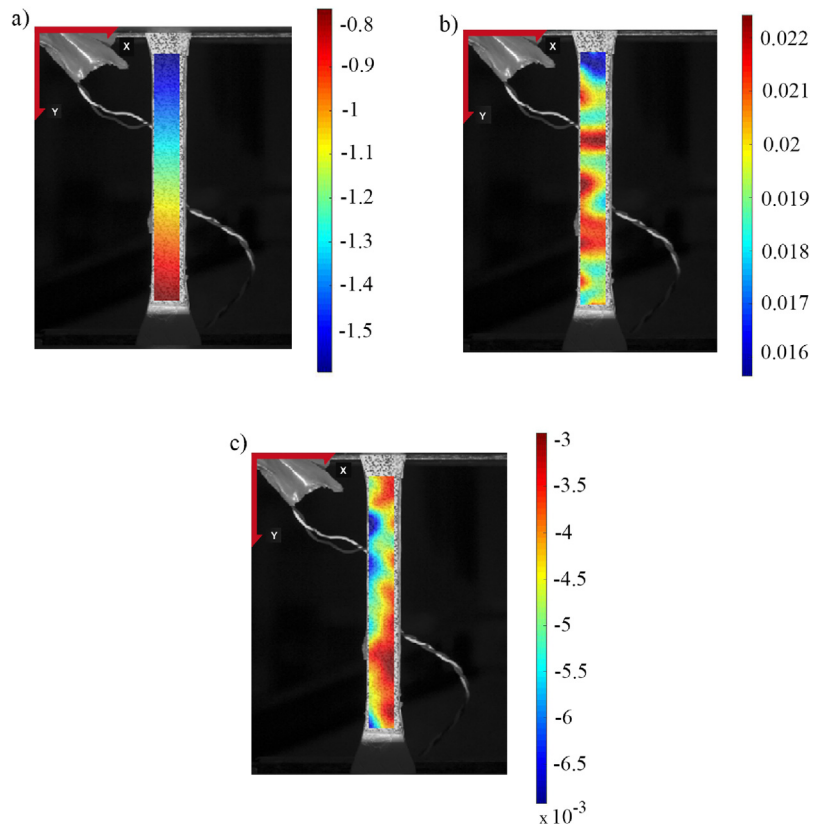


Fig. 8 – Detail of the displacements and strains obtained by the 2D-DIC method on the test specimens: (a) maximum displacements in mm in the y-axis direction; (b) maximum strains in the y-axis direction in mm/mm and (c) maximum strains in the x-axis direction in mm/mm.

to local variations during the production of the solution (small variations of the resin percentage in comparison with the fibre or small variations in the disposition of the fibres among other casuistics).

3.3. Accuracy assessment

With the aim of evaluating the accuracy provided by the 2D-DIC approach, in terms of displacements and strains, a LVDT (HBM TR50®) and a strain gauge (HBM-120 Ohm) were placed in one of the tests specimens used during the experimental method. Both sensors were connected with the data acquisition platform by means of the PLC system (Raspberry Pi-3® and Monarco HAT®). On the one hand, the data provided by the LVDT was contrasted with the displacements detected by the DIC approach between two fixed points (virtual extensometer) (Fig. 9a). It is worth mentioning that the application points of the virtual extensometer were the same than the measurement points of the LVDT in order to make the comparison reliable. On the other hand, the data provided by the strain gauge was compared with the strain obtained in the subset placed in the same area (Fig. 9a). During this comparison one image was captured each 100 N of Force (instead of the 200 N applied for the rest of the processes) with the aim of obtaining an enough

number of points to compare both strains before the failure of the strain gauge. In order to compare both strains the data provided by the strain gauge (engineering strains) was transformed to the Green-Lagragian strain tensor in order to be compared with the strain data provided by the 2D-DIC.

The data recorded from the extensometer and the strain gauges revealed an average discrepancy of 0.02 mm (0.32 pixels) for the displacements and 0.0002 mm/mm for the strains in the longitudinal direction regarding the displacements and the strains obtained by the 2D-DIC approach (Fig. 9b and c). These values correspond with a root-mean-square error (RMSE) of 2.97% for the displacements and a RMSE of 0.04% for the strains. Therefore, these lower discrepancies demonstrate the feasibility and accuracy of the 2D-DIC method as well as the data acquisition of the prototype.

3.4. Mechanical properties of the composite solution evaluated

The mechanical characterization of the composite solution can be carried out confronting the data provided by the virtual extensometers placed on the test specimen and the stresses captured by the DIC prototype (the strain–stress curve) (Figs. 9 and 10a). These stresses were the result of the force applied by

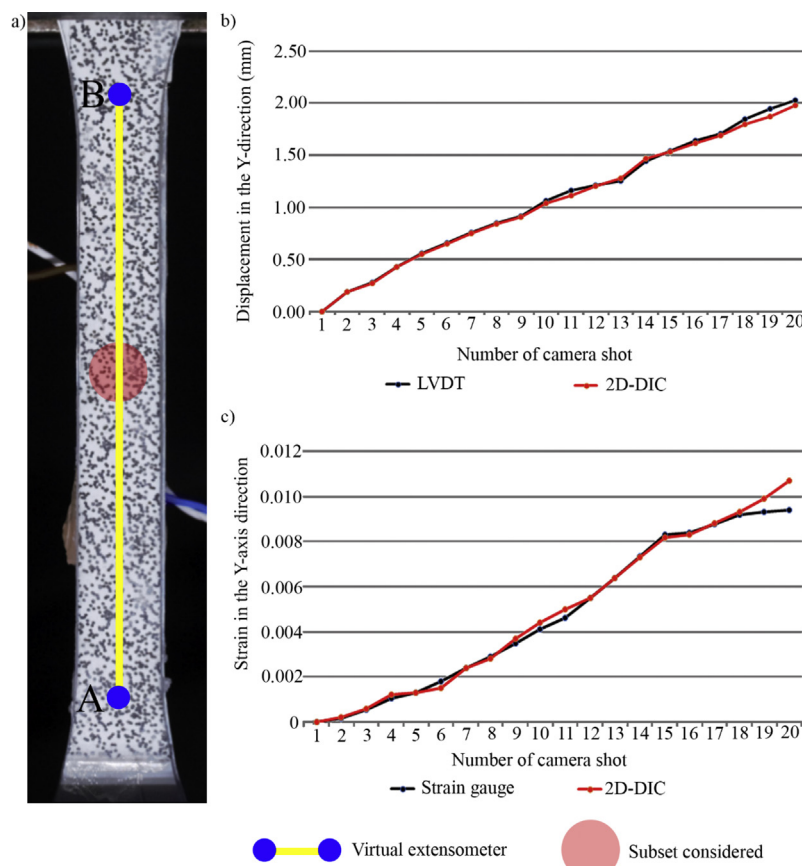


Fig. 9 – Results of the tensile test used to check the accuracy of the method: (a) location of the virtual extensometer and subset considered; (b) graphical comparison between the extensometer and the displacements obtained by the virtual extensometer through the 2D-DIC method and (c) graphical comparison between the strain gauge and the displacements obtained by the virtual extensometer through the 2D-DIC method.

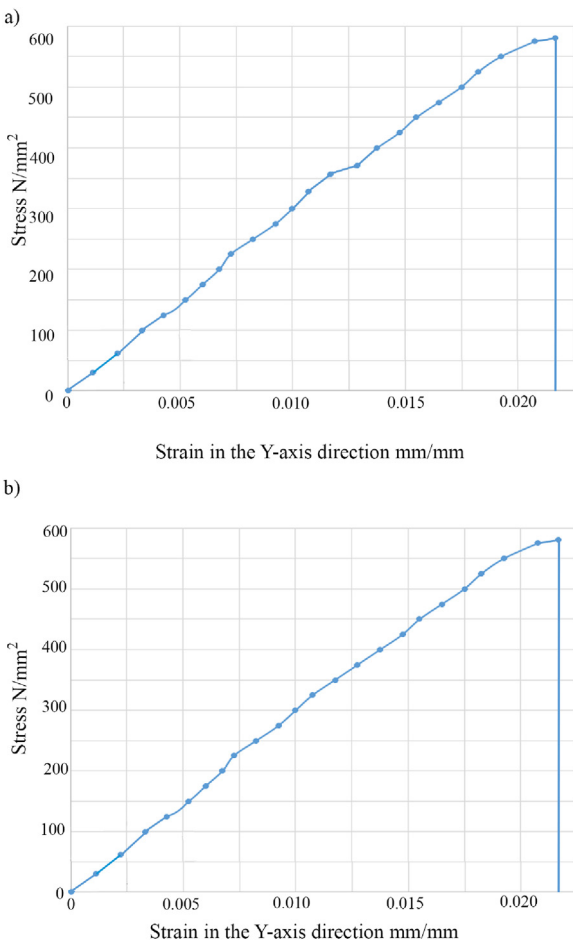


Fig. 10 – Example of a strain–stress curve obtained during the tensile tests: (a) strain–stress from the testing machine and; (b) strain–stress curve obtained from the virtual extensometers.

the press and the area of the test specimen ($10 \text{ mm} \times 2 \text{ mm}$). The strain–stress curves obtained by the press and the DIC approach shown a composite solution with a marked brittle behaviour (absence of plasticity) and a linear elastic behaviour (Fig. 10).

It is worth mentioning that the characterization of the material's mechanical properties by means of virtual extensometers allowed the proper definition of the composite solution from a deterministic point of view (considering the composite material as homogeneous). However, the results obtained by the DIC approach highlight the presence of a heterogeneous solution (Fig. 8).

Taking into account that one of the main advantages offered by the DIC approach is the full field strain characterization, it was possible to extract the probabilistic density distributions of each mechanical property that define the composite solution and thus capturing the heterogeneity shown by the material. To this end, the full-field strains obtained by the DIC approach were transformed into Young's Modulus and Poisson's ratios by means of a convolution process as follows (Fig. 11): (i) definition of the kernel matrix; (ii) convolution along the entire ROI defined by m steps along

the horizontal direction and n steps along the vertical direction; (iii) obtention of the Young's Modulus of each area evaluated confronting the maximum strain values obtained in each cycle by the convolution and the stress registered by the DIC prototype; (iv) evaluation of the Poisson's ratio by means of the relation between the maximum and minimum strain obtained by the convolution process. For the present study case, it was considered as kernel size similar to the size of the finite element used for the numerical simulations (50×50 pixels) and a step between kernels of 50 pixels in order to avoid overlaps.

Apart from the elastic properties of the composite solution, Young's Modulus and Poisson ratio, the maximum principal strain (yield strain) was calculated with the aim of defining properly the constitutive material model by means of the Tsai–Wu criterion [34]. To this end, a new ROI was defined on the observed failure area of each test specimen (Fig. 11). Then, it was applied the same procedure than those proposed for the extraction of the Elastic Modulus and Poisson ratio.

The parameters extracted by the convolution process previously defined allowed the creation of a population for each variable (Table 6). These parameters correspond to the material 0° mechanical properties. Because the number of layers and the direction of the reinforcement on each layer, they coincide with the mechanical properties of the material at 90° (Table 4).

With the aim of obtaining the probabilistic distribution function (PDF) of each variable a normality tests, by means of the Shapiro–Wilk approach, was carried out [35]. This test allowed us to characterize the populations into normal and non-normal distributions (Table 7). Finally, a curve fit method was performed with the aim of obtaining the PDFs. The candidate PDFs considered were Normal, Log-Normal, Weibull, Exponential and Uniform, obtaining normal distribution for the Young's Modulus and Poisson ratio and a Weibull distribution for the maximum principal strain (Table 5 and Fig. 12). These curves are consistent with the PDFs obtained in other experimental campaigns methodologies [13].

4. Numerical simulation combining DIC and stochastic approaches

4.1. Definition of the numerical model

In order to integrate the data provided by the DIC method with advance numerical simulations of composite pressure vessels, a prototype was created with the commercial finite element software ABAQUS®. This receptacle was designed with a semi-spherical shape in the upper and lower part and a cylindrical shape for the body of the container (Fig. 13). All these parts were designed with an internal radius of 16.5 mm and a constant thickness of 2 mm. For the body of the vessel, a height of 307 mm was considered.

Taking into consideration the geometrical model defined previously, two numerical meshes, composed of 10,368 first order quadrilateral shell elements (10,464 nodes and 62,784 degrees of freedom), were generated, namely (Fig. 14): (i) deterministic mesh and (ii) probabilistic mesh. While, the deterministic mesh considers the mechanical properties of the

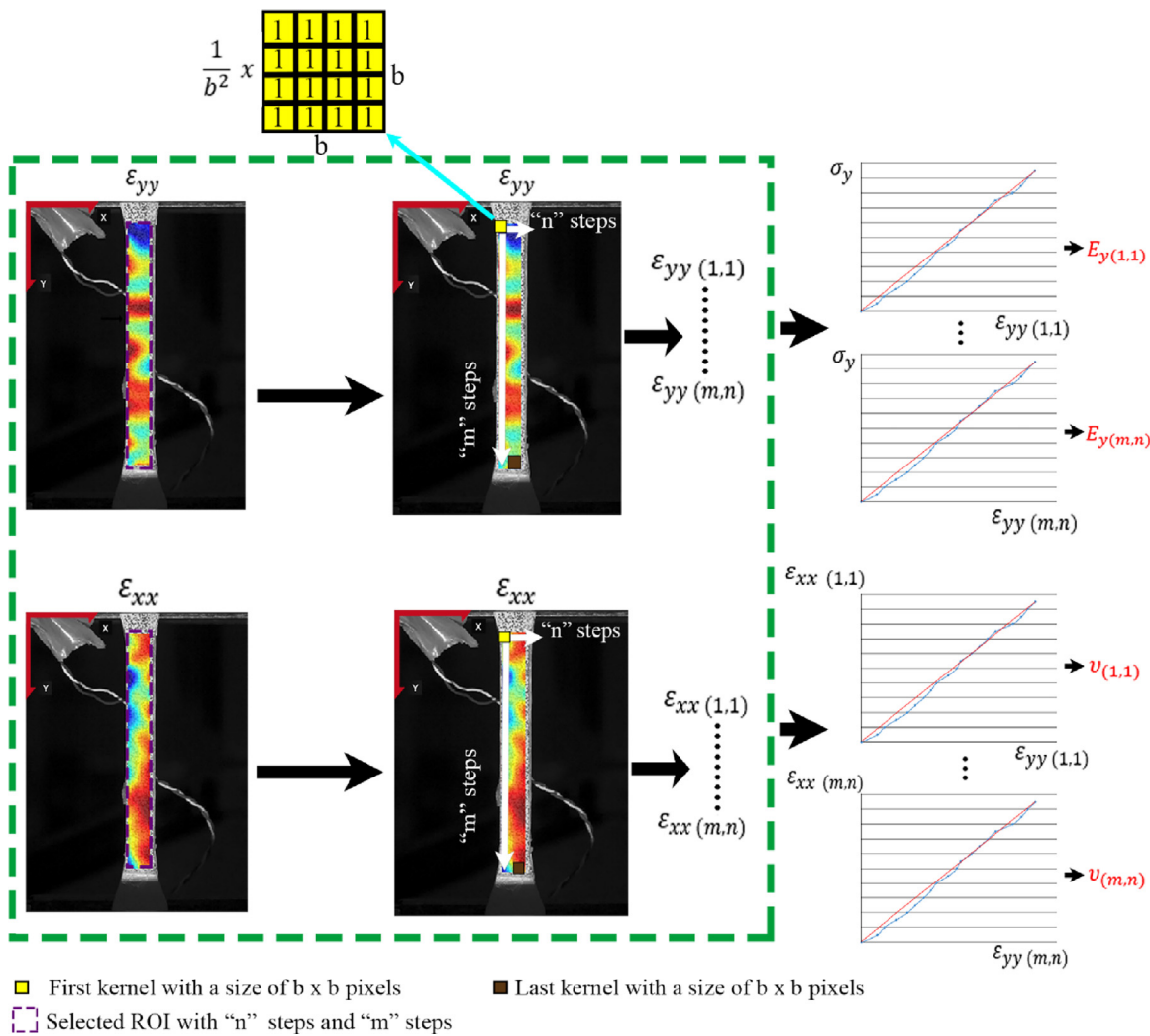


Fig. 11 – Proposed workflow to obtain the Young Modulus (E_y) and the Poisson ratios (v) of the specimens. The green line indicates one cycle on each deformed image.

composite material as unique and homogeneous, the probabilistic mesh represents the composite material as an heterogeneous material whose mechanical properties are extracted from the PDF obtained from the DIC approach (Fig. 12).

For all the numerical simulations, the following considerations were taken into account: (i) a uniform service pressure of 3 MPa according to guidelines [36]; (ii) a planar state of stresses without shear components (thin shell theory); (iii) a symmetrical Young's Modulus due to the symmetrical disposition of the fibres (Fig. 1) and; (iv) a failure criterion based on the Tsai-Wu theory [34].

4.2. Global sensitivity analysis

4.2.1. Polynomial chaos expansion and the Sobol' method

Prior to the numerical evaluation, a sensitivity analysis was carried out with the aim of evaluating the influence of the input parameters in the model response (Tsai-Wu failure criterion). Among the variety of methods used in sensitivity analysis, one of the most common and robust is the Sobol' method [37,38]. This method is based on the decomposition of the response variance as a sum of contributions related to each input parameter through the Sobol's indices, which are usually assessed through the use of Monte Carlo (MC) simulations.

Table 5 – Probabilistic distribution functions of the elastic modulus, Poisson's ratio and strain in the y-axis direction of the specimens.

Parameter	Distribution	p-Value	Mean (Normal)/A (Weibull)	Deviation (Normal)/B (Weibull)
Young's Modulus (GPa)	Normal	0.99	27.11	1.24
Poisson's ratio (-)	Normal	0.97	0.21	0.03
y-Axis strain (mm/mm)	Weibull	0.21	0.02	14.74

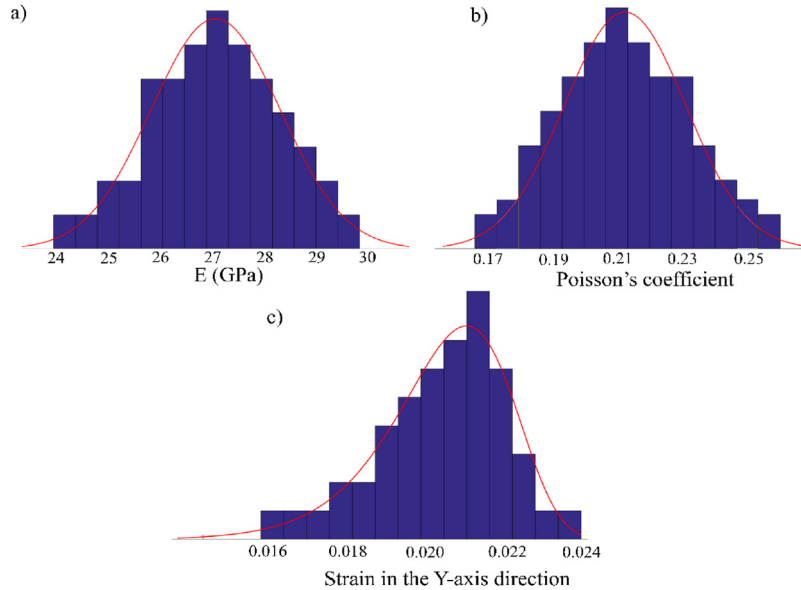


Fig. 12 – Graphical representation of the probabilistic distribution functions of each parameter: (a) normal distribution of the elastic modulus; (b) normal distribution of the Poisson's coefficient and (c) Weibull distribution of the maximum principal strain.

However, the MC simulations require thousand of simulations to achieve reliable results [39]. Considering this topic, there is an alternative that offers reliable results with lower computational cost: the so-called surrogate models. The main advantages of these models are their compactness and their analytical scalability, allowing to approximate the input-output response of a complex system with a low number of inputs.

From the present study case, the polynomial chaos expansion (PCE) metamodel was used. This strategy approximates the computational model through a set of orthonormal polynomials of the input parameters (Eq. (4)) [40]. Complementary to this, a least-angle regression and a least-square minimization were used with the aim of determining the coefficients of the polynomials (Eq. (4)) [41].

$$\tilde{f} = \sum_{\alpha \in A} y_\alpha \psi_\alpha(X) \quad (4)$$

where \tilde{f} is the surrogate model, $\alpha = \{\alpha_1 \dots \alpha_d\}$ are the indexes of the PCE, A is the set of indexes α which correspond to the truncation scheme, $X = (X_1, X_2, \dots, X_d)$ is the multivariate vec-

tor of the input parameters considered and finally, ψ_α is the multivariate polynomial.

In order to validate the accuracy of the metamodel, the leave-one-out error (LOO) was used [42,43]. Once the metamodel was built and validated, the first and total Sobol's indices were calculated through Eqs. (5) and (6), respectively.

$$\hat{S}_i = \frac{\sum_{\alpha \in A_i} \hat{y}_\alpha^2}{\sum_{\alpha \in A, \alpha \neq i} \hat{y}_\alpha^2} \quad \text{where } A_i = \{\alpha \in A : \alpha_i > 0, \alpha_j \neq i = 0\} \quad (5)$$

$$\hat{S}_i^t = \frac{\sum_{\alpha \in A_i^T} \hat{y}_\alpha^2}{\sum_{\alpha \in A, \alpha \neq i} \hat{y}_\alpha^2} \text{af}; \quad \text{where } A_i^T = \{\alpha \in A : \alpha_i > 0\} \quad (6)$$

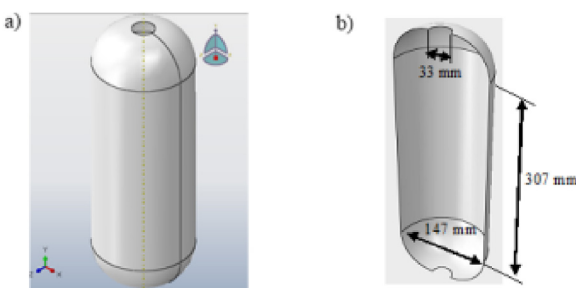


Fig. 13 – Pressure vessel evaluated: (a) general view and (b) cross section.

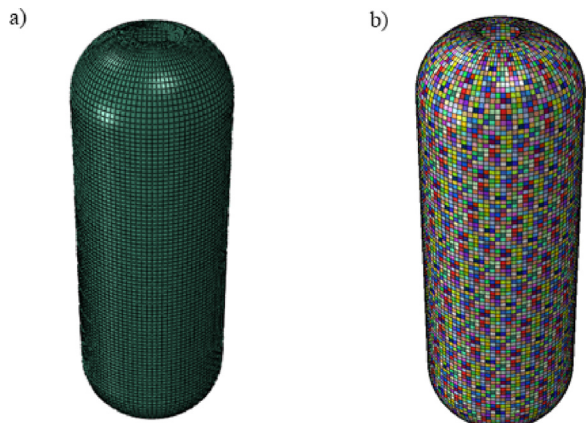


Fig. 14 – Numerical meshes considered: (a) deterministic mesh and (b) probabilistic mesh. The size of the elements was 4 mm, corresponding with the subset size used during the DIC tests. In different colours the materials considered for each numerical simulation.

where \hat{S}_i and \hat{S}_i^t are the first-order and total Sobol's indices of the output variable i , \hat{y} and α are the coefficients and indices of the PCE respectively and A is the subset of the input variables.

4.2.2. Results obtained from the global sensitivity analysis

Taking into account the methodology described in the previous section, a global sensitivity analysis was performed over the deterministic mesh, considering as input variables those obtained by the DIC approach, namely: (i) Young Modulus; (ii) Poisson's coefficient and (iii) maximum principal strain.

Once these set of variables were, different PCE-metamodels were built in order to assess the Sobol's indices of the output: the Tsai-Wu factor. During these assessments different sample sizes were considered with the purpose of obtaining the best ratio between the number of samples and the consistency of the metamodel. These samples were obtained through the use of the latin hypercube sampling (LHS) method [44] taking into account the PDF of each variable (Table 5 and Fig. 12).

The results revealed that the optimum design of experiment (DoE) of the metamodel was 200, showing a LOO error of 1.44×10^{-4} (Table 6) and a constant value in the different Sobol's indexes (Table 7).

From the Sobol's analysis it is possible to conclude that the uncertainties associated with the Tsai-Wu factor are mainly due to the maximum principal strain (e_{11}) (Fig. 15). This variable influences approximately 76% of the total variation of this factor, being consistent with the formulation of the Tsai-Wu criterion [34]. Also, it is possible to observe a high sensitivity of the Young's Modulus (E) in the final results, which influences 16% of the uncertainty of the Tsai-Wu factor. The Poisson ratio is the less sensitive variable (Fig. 15). It is worth mentioning that the First Order Sobol indexes were similar to the total Sobol indexes, suggesting that there is no interaction between variables (Fig. 15).

4.3. Stochastic analysis

Taking into consideration that the safety of a composite pressure vessel is guaranteed when the Tsai-Wu factor is lower than 1, a robust numerical analysis passes through the use of a stochastic approach able to integrate the uncertainty of the inputs, obtained by means of the DIC approach, in order to determine the probability of having a specific range of Tsai-Wu factors. On this basis, the Semi Random Field method (random variable approach) proposed by [45] was adopted (Fig. 16). In this approach, each element of the numerical

Table 7 – Total Sobol's indices obtained of the output variable (Tsai-Wu failure criterion) of the pressure vessel during the global sensitivity analysis.

Number of samples obtained with the LHS	Total Sobol's indices		
	Elastic modulus	Poisson's coefficient	Maximum principal strain
25	0.17	0.06	0.77
50	0.21	0.05	0.74
100	0.17	0.08	0.75
200	0.16	0.08	0.76
300	0.16	0.08	0.76
400	0.16	0.08	0.76

model adopts random values of the variables (Young's Modulus, Poisson's coefficient and maximum principal strain) according to the probability density functions obtained by means of the DIC approach (Fig. 12 and Table 5).

Considering that the input uncertainties in the output values in complex system can be written as exposed bellow (Eq. (7)), the probability of having a value lower than a pre-establish threshold can be defined by means of the complementary cumulative distribution function (CCDF) (Eqs. (7) and (8)).

$$Y_i = f(D_i * X_i) \quad (7)$$

$$\text{prob}(y > Y) = \int_{S_{SU}} \delta Y [f(x)] \text{pdf}_u(X) dV_{SU} \quad (8)$$

where f represents the numerical model, X_i the input vector; D_i the distribution associated with each element of the numerical model and Y_i the model's predictions.

It is worth mentioning that the value of this integral is not trivial, requiring the use of approximation methods such as the Fourier amplitude sensitivity test (FAST) or the Monte Carlo simulation. For the present study case, the LHS method was used to estimate the propagation and analysis of the uncertainty of the output values [46]. Specifically, a total of 500 samples were used to create the PDF and the CCDF of the Tsai-Wu values (Fig. 17).

Considering a value of 0.95 as an acceptable probability level, the most unfavourable case during the design of this pressure vessel will be 0.54 (maximum admissible pressure of 5.56 MPa), meanwhile in the most favourable case, the pressure vessel will have a value of 0.39 (maximum admissible pressure of 7.69 MPa), with 0.46 and 6.52 MPa being the most probable value for the Tsai-Wu and the maximum pressure respectively (Fig. 17a). These results contrast with those obtained by means of a deterministic model (numerical model generated with the average values of each variable), for which a Tsai-Wu factor of 0.37 was obtained (Fig. 17b). These values threw a maximum admissible pressure of 8.10 MPa. In this case, the maximum pressure is achieved at the same time in all those elements placed close to the nozzle's hole in the

Table 6 – LOO error in the output variable (Tsai-Wu failure criterion) for different sizes of the DoE.

Number of samples obtained with the LHS	LOO error
25	11.1
50	0.98
100	1.22×10^{-3}
200	1.44×10^{-4}
300	1.58×10^{-5}
400	4.10×10^{-6}

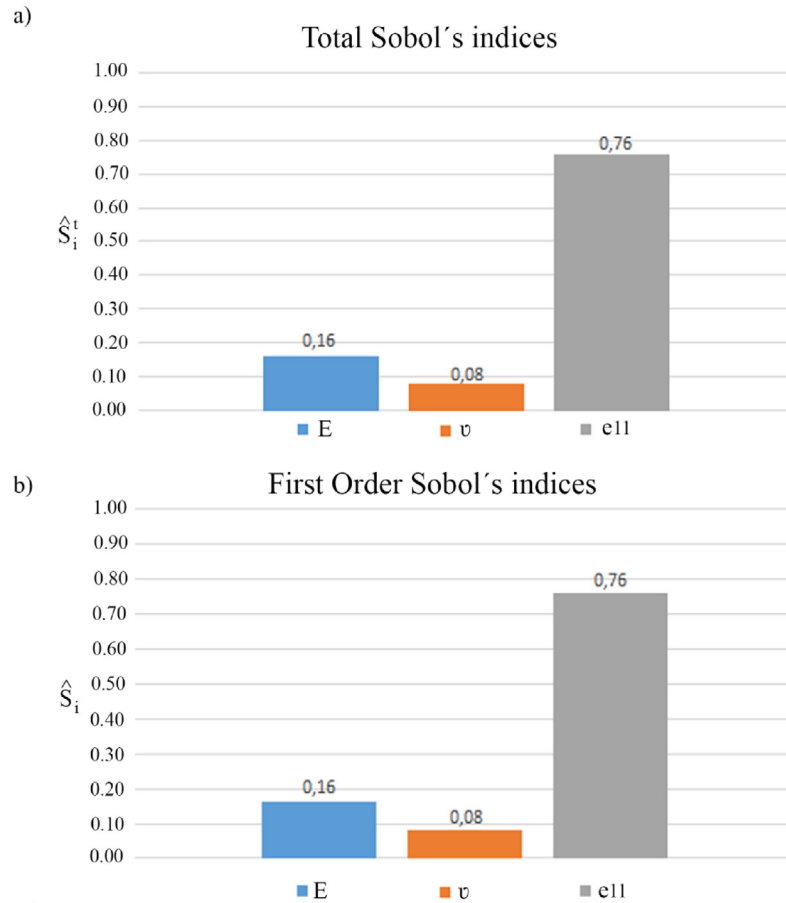


Fig. 15 – Results obtained from the PCE metamodel: (a) total Sobol indices (\hat{S}_i^t) and (b) first Order Sobol indices (\hat{S}_i).

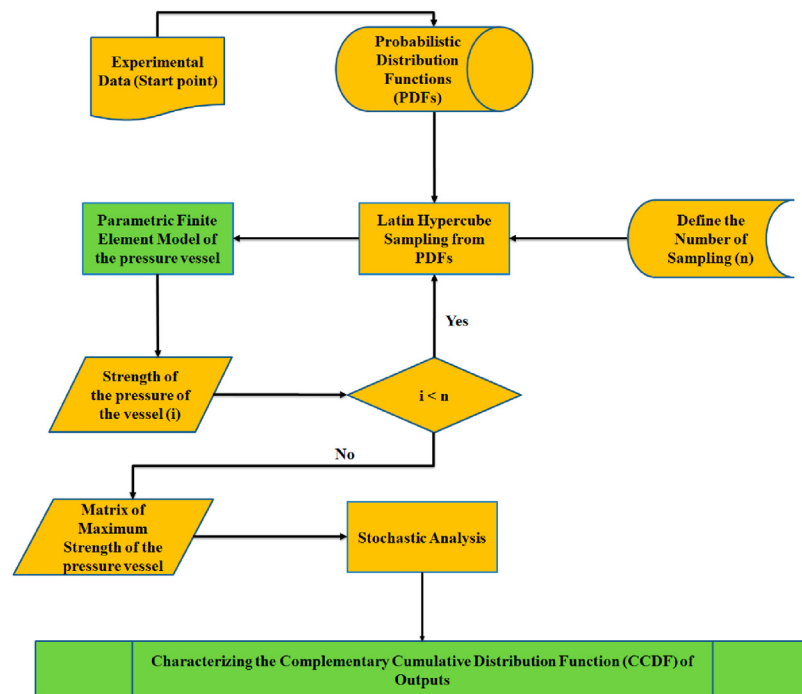


Fig. 16 – Workflow adopted for the stochastic evaluation of the composite pressure vessel.

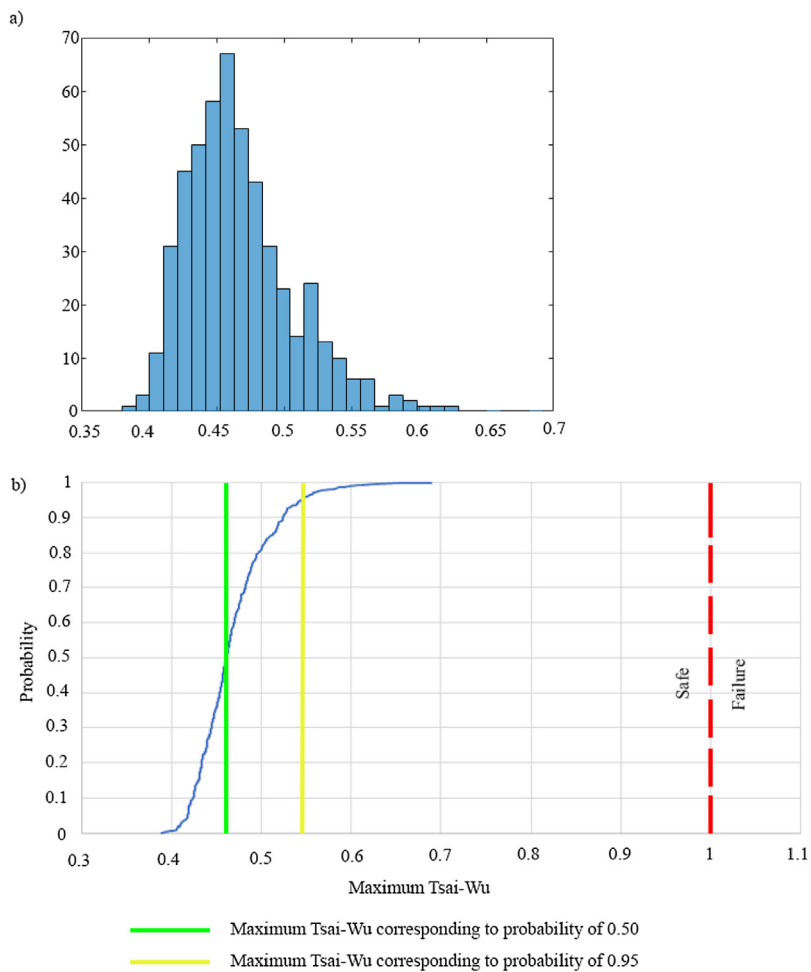


Fig. 17 – Results of the semi-random field simulation: (a) complementary cumulative density function and (b) probabilistic density function.

spherical part of the vessel (Fig. 18a). In contrast with this, the

probabilistic model obtained a random distribution of the

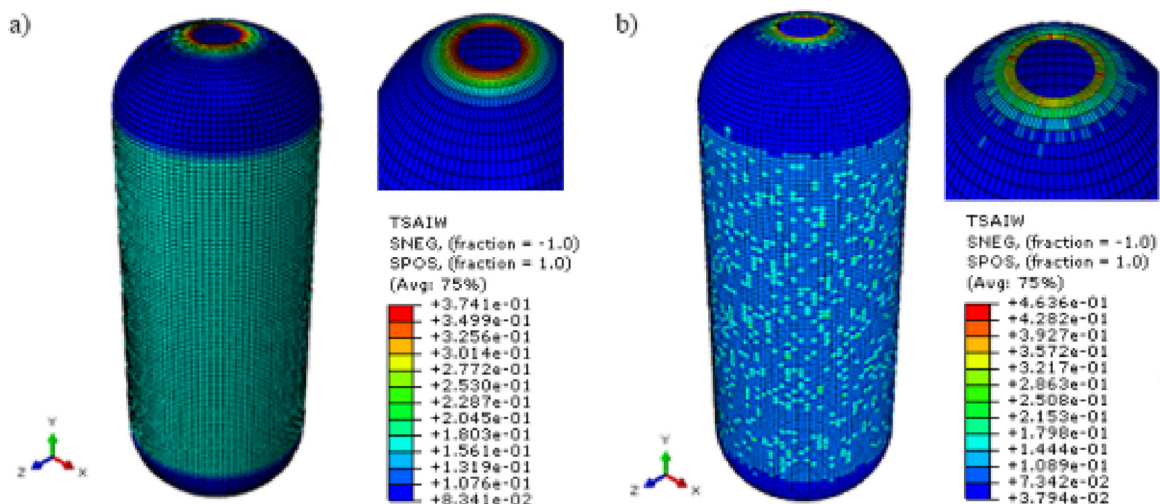


Fig. 18 – Numerical results: (a) deterministic model built with the average values and (b) example of a sample used during the probabilistic analysis.

Tsai-Wu factor, highlighting the probability of a random fracture which depends of the local mechanical properties of the composite material (Fig. 18b).

5. Conclusions

This paper proposes a methodology based on the combination of the 2D digital image correlation method with probabilistic approaches, based on random variable strategy, with the purpose of obtaining a reliability analysis of composite pressure vessels. To this end, it is proposed a methodology able to exploit the full field data provided by the 2D digital image correlation method with the aim of obtaining the probabilistic density function of each material property, namely: (i) Young's Modulus; (ii) Poisson's ratio and; (iii) Yield Strain. Then, and with the aim of integrating this data into an advanced numerical framework, two finite element models of a pressure vessel prototype were built: (i) a deterministic model and; (ii) a probabilistic model. On the one hand, the deterministic model was used to study the influence of the input uncertainties in the output values (Tsai-Wu safety factor), suggesting that the Tsai-Wu factor is mainly influenced by the maximum strain and the Young Modulus. On the other hand, the probabilistic model was used to study, from a stochastic point of view, the safety factor of the pressure vessel prototype, adopting to this end a Monte Carlo strategy based on the Latin Hypercube Sampling method. This approach, fed by the probabilistic functions, threw more conservative values than for the deterministic one. These differences can be attributed, mainly, to the uncertainties in the maximum principal strain with an average value of 0.021 mm/mm and a covariance value of 15.69%, specially in the union between the vessel's body and the vessel's nozzle. In this area, the fracture in the deterministic model is obtained at the same time on all points, meanwhile in the probabilistic model is obtained in one point (area with the worst mechanical properties). Taking into consideration the results obtained during the experimental campaign, future works will be focused on the following fields: (i) on the use of the full field data provided by DIC for the estimation of the correlation functions needed for the creation of random fields models in composite materials; (ii) on the improvement of the methodology used to design the speckle pattern including additional restriction that improve the heterogeneity of the gray level values and thus increase the MIG value of the ROI; (iii) the integration of the 3D DIC approach for the validation of the solution developed by the stochastic strategy shown in this paper.

Conflict of interest

None declared.

Ethical statement

This material has not been published in whole or part elsewhere.

The manuscript is not currently being considered for publication in another journal.

All authors have been personally and actively involved in substantive work leading to the manuscript.

Funding body

This work was financed by ERDF funds through the V Sudoe Interreg program within the framework of the COMPRESSer project, Ref. SOE2/P1/E0643 and the TCUE action SICMES supported by the Foundation University of Salamanca.

Acknowledgments

The authors would like to thank the V Sudoe Interreg program and the TCUE action SICMES.

REFERENCES

- [1] M. Delogu, L. Zanchi, C. Dattilo, M. Pierini, Innovative composites and hybrid materials for electric vehicles lightweight design in a sustainability perspective, Mater. Today Commun. 13 (2017) 192–209, <https://doi.org/10.1016/j.mtcomm.2017.09.012>.
- [2] A. Vicario, S.S. Ramanan, S. Arun, 3.4 Composites in Missiles and Launch Vehicles, 2018.
- [3] L. Sutherland, A review of impact testing on marine composite materials: Part I – marine impacts on marine composites, Compos. Struct. (2017), <https://doi.org/10.1016/j.compstruct.12.073>.
- [4] R.F. Gibson, A review of recent research on mechanics of multifunctional composite materials and structures, Compos. Struct. 92 (2010) 2793–2810, <https://doi.org/10.1016/j.compstruct.2010.05.003>.
- [5] R. Rafiee, M.A. Torabi, Stochastic prediction of burst pressure in composite pressure vessels, Compos. Struct. 185 (2018) 573–583, <https://doi.org/10.1016/j.compstruct.2017.11.068>.
- [6] L.J. Sánchez-Aparicio, L.F. Ramos, J. Sena-Cruz, J.O. Barros, B. Riveiro, Experimental and numerical approaches for structural assessment in new footbridge designs (SFRSCC-GFPR hybrid structure), Compos. Struct. 134 (2015) 95–105, <https://doi.org/10.1016/j.compstruct.2015.07.041>.
- [7] N. Movahedi, E. Linul, Mechanical properties of light expanded clay aggregated (LECA) filled tubes, Mater. Lett. 217 (2018) 194–197, <https://doi.org/10.1016/j.matlet.2018.01.078>.
- [8] E. Linul, L. Marsavina, J. Kováčik, Collapse mechanisms of metal foam matrix composites under static and dynamic loading conditions, Mater. Sci. Eng.: A 690 (2017) 214–224, <https://doi.org/10.1016/j.msea.2017.03.009>.
- [9] T. Fiedler, M. Taherishargh, L. Krstulović-Opara, M. Vesenjak, Dynamic compressive loading of expanded perlite/aluminum syntactic foam, Mater. Sci. Eng.: A 626 (2015) 296–304, <https://doi.org/10.1016/j.msea.2014.12.032>.
- [10] R. Rafiee, On the mechanical performance of glass-fibre-reinforced thermosetting-resin pipes: a review, Compos. Struct. 143 (2016) 151–164, <https://doi.org/10.1016/j.compstruct.2016.02.037>.
- [11] S. Sriramula, M.K. Chryssanthopoulos, Quantification of uncertainty modelling in stochastic analysis of FRP

- composites, Compos. Part A: Appl. Sci. Manufact. 40 (2009) 1673–1684, <https://doi.org/10.1016/j.compositesa.2009.08.020>.
- [12] J.N. Reddy, *Mechanics of Laminated Composite Plates and Shells: Theory and Analysis*, CRC Press, 2004.
- [13] P. Sasikumar, R. Suresh, P. Vijayaghosh, S. Gupta, Experimental characterisation of random field models for CFRP composite panels, Compos. Struct. 120 (2015) 451–471, <https://doi.org/10.1016/j.compstruct.2014.10.023>.
- [14] O. Orell, J. Vuorinen, J. Jokinen, H. Kettunen, P. Hytönen, J. Turunen, et al., Characterization of elastic constants of anisotropic composites in compression using digital image correlation, Compos. Struct. 185 (2018) 176–185, <https://doi.org/10.1016/j.compstruct.2017.11.008>.
- [15] M. Tekieli, S. De Santis, G. de Felice, A. Kwiecień, F. Roscini, Application of digital image correlation to composite reinforcements testing, Compos. Struct. 160 (2017) 670–688, <https://doi.org/10.1016/j.compstruct.2016.10.096>.
- [16] S. Sharifi, S. Gohari, M. Shariftehshizi, R. Alebrahim, C. Burvill, Y. Yahya, et al., Fracture of laminated woven GFRP composite pressure vessels under combined low-velocity impact and internal pressure, Arch. Civil Mech. Eng. 18 (2018) 1715–1728, <https://doi.org/10.1016/j.acme.2018.07.006>.
- [17] M.A. Seif, U.A. Khashaba, R. Rojas-Oviedo, Measuring delamination in carbon/epoxy composites using a shadow moiré laser based imaging technique, Compos. Struct. 79 (2007) 113–118, <https://doi.org/10.1016/j.compstruct.2005.11.039>.
- [18] P. Callaway, M. Gilbert, C.C. Smith, Influence of backfill on the capacity of masonry arch bridges, in: Proceedings of the Institution of Civil Engineers: Bridge Engineering, ICE Publishing, 2012 147–157, <https://doi.org/10.1680/bren.11.00038>.
- [19] F. Hild, S. Roux, Digital image correlation: from displacement measurement to identification of elastic properties – a review, Strain 42 (2006) 69–80, <https://doi.org/10.1111/j.1475-1305.2006.00258.x>.
- [20] H.C. Biscaia, N. Franco, C. Chastre, Development of a simple bond-slip model for joints monitored with the DIC technique, Arch. Civil Mech. Eng. 18 (2018) 1535–1546, <https://doi.org/10.1016/j.acme.2018.06.009>.
- [21] L.J. Sánchez-Aparicio, A. Villarino, J. García-Gago, D. González-Aguilera, Photogrammetric, geometrical, and numerical strategies to evaluate initial and current conditions in historical constructions: a test case in the church of San Lorenzo (Zamora, Spain), Remote Sensing 8 (2016), <http://dx.doi.org/10.3390/rs8010060.60>.
- [22] T. Gajewski, T. Garbowksi, Calibration of concrete parameters based on digital image correlation and inverse analysis, Arch. Civil Mech. Eng. 14 (2014) 170–180, <https://doi.org/10.1016/j.acme.2013.05.012>.
- [23] ISOB, *Plastics – Determination of Tensile Properties*, 1997.
- [24] B. Pan, K. Qian, H. Xie, A. Asundi, Two-dimensional digital image correlation for in-plane displacement and strain measurement: a review, Meas. Sci. Technol. 20 (2009) 062001, <http://dx.doi.org/10.1088/0957-0233/20/6/062001>.
- [25] L. Luu, Z. Wang, M. Vo, T. Hoang, J. Ma, Accuracy enhancement of digital image correlation with B-spline interpolation, Opt. Lett. 36 (2011) 3070–3072, <https://doi.org/10.1364/OL.36.003070>.
- [26] J. Blaber, B. Adair, A. Antoniou, Ncorr: open-source 2D digital image correlation matlab software, Exp. Mech. 55 (2015) 1105–1122, <http://dx.doi.org/10.1007/s11340-015-0009-1>.
- [27] B. Pan, Reliability-guided digital image correlation for image deformation measurement, Appl. Opt. 48 (2009) 1535–1542, <https://doi.org/10.1364/AO.48.001535>.
- [28] Y. Dong, B. Pan, A review of speckle pattern fabrication and assessment for digital image correlation, Exp. Mech. 57 (2017) 1161–1181, <http://dx.doi.org/10.1007/s11340-017-0283-1>.
- [29] Z. Chen, G. Quan, F. Zhu, X. He, A method to transfer speckle patterns for digital image correlation, Meas. Sci. Technol. 26 (2015) 095201, <http://dx.doi.org/10.1088/0957-0233/26/9/095201>.
- [30] M.N. Vo, Z. Wang, L. Luu, J. Ma, Advanced geometric camera calibration for machine vision, Opt. Eng. 50 (2011) 110503, <https://doi.org/10.1117/1.3647521>.
- [31] D. Lecompte, H. Sol, J. Vantomme, A. Habraken, Analysis of speckle patterns for deformation measurements by digital image correlation, in: SPECKLE06: Speckles, From Grains to Flowers: International Society for Optics and Photonics, 2006, 63410E, <https://doi.org/10.1117/12.695276>.
- [32] B. Pan, Z. Lu, H. Xie, Mean intensity gradient: an effective global parameter for quality assessment of the speckle patterns used in digital image correlation, Opt. Lasers Eng. 48 (2010) 469–477, <https://doi.org/10.1016/j.optlaseng.2009.08.010>.
- [33] A. Ab Ghani, M. Ali, S. Dharmalingam, J. Mahmud, *Digital Image Correlation (DIC) Technique in Measuring Strain Using Opensource Platform Ncorr*, 2016.
- [34] S.W. Tsai, E.M. Wu, A general theory of strength for anisotropic materials, J. Compos. Mater. 5 (1971) 58–80, <https://doi.org/10.1177/002199837100500106>.
- [35] S.S. Shapiro, M.B. Wilk, An analysis of variance test for normality (complete samples), Biometrika 52 (1965) 591–611, <http://dx.doi.org/10.2307/2333709>.
- [36] Certificación AEdNy, *UNE-EN 3-8: extintores portátiles de incendios. Requisitos adicionales a la Norma Europea EN 3-7 para la construcción resistencia a la presión y los ensayos mecánicos para extintores con una presión máxima admisible igual o inferior a 30 bar*, AENOR, 2007.
- [37] IyM. Sobol', On sensitivity estimation for nonlinear mathematical models, Matematich. Model. 2 (1990) 112–118.
- [38] F. Zhu, Q. Zhou, F. Wang, X. Yang, Spatial variability and sensitivity analysis on the compressive strength of hollow concrete block masonry wallets, Construct. Build. Mater. 140 (2017) 129–138, <https://doi.org/10.1016/j.conbuildmat.2017.02.099>.
- [39] B. Sudret, Global sensitivity analysis using polynomial chaos expansions, Reliab. Eng. Syst. Saf. 93 (2008) 964–979, <https://doi.org/10.1016/j.ress.2007.04.002>.
- [40] R. Ghanem, P. Spanos, *Stochastic Finite Elements: A Spectral Approach*, revised edition, Dover Publications, New York, 2003.
- [41] G. Blatman, B. Sudret, Adaptive sparse polynomial chaos expansion based on least angle regression, J. Comput. Phys. 230 (2011) 2345–2367, <https://doi.org/10.1016/j.jcp.2010.12.021>.
- [42] M. Stone, Cross-validatory choice and assessment of statistical predictions, J. R. Stat. Soc. Ser. B (Methodol.) (1974) 111–147.
- [43] S. Geisser, The predictive sample reuse method with applications, J. Am. Stat. Assoc. 70 (1975) 320–328.
- [44] M.D. McKay, R.J. Beckman, W.J. Conover, Comparison of three methods for selecting values of input variables in the analysis of output from a computer code, Technometrics 21 (1979) 239–245, <https://doi.org/10.1080/00401706.1979.10489755>.
- [45] E. Moradabadi, D.F. Laefer, J.A. Clarke, P.B. Lourenço, A semi-random field finite element method to predict the maximum eccentric compressive load for masonry prisms, Construct. Build. Mater. 77 (2015) 489–500, <https://doi.org/10.1016/j.conbuildmat.2014.12.027>.
- [46] J.C. Helton, F.J. Davis, Latin hypercube sampling and the propagation of uncertainty in analyses of complex systems, Reliab. Eng. Syst. Saf. 81 (2003) 23–69, [https://doi.org/10.1016/S0951-8320\(03\)00058-9](https://doi.org/10.1016/S0951-8320(03)00058-9).

Conclusiones y Trabajo Futuro

La presente Tesis Doctoral focaliza el esfuerzo en avanzar en el diseño en el ámbito de la Ingeniería Mecánica a través de las técnicas de la Geomática.

Las investigaciones realizadas durante el desarrollo de esta Tesis Doctoral han permitido acometer satisfactoriamente los objetivos planteados y realizar una aportación en un amplio espectro. Este abarca desde la fase inicial del diseño en ingeniería, como es la caracterización de materiales, hasta la fase final que acomete la determinación de los coeficientes de seguridad del producto desarrollado. Esta aportación ha sido materializada a través de la publicación en revistas especializadas de impacto de los resultados frutos de la presente investigación.

A continuación, se comentan más detalladamente las conclusiones y contribuciones derivadas de este trabajo, en relación a los objetivos previamente marcados, así como las líneas de trabajo futuras suscitadas por los resultados obtenidos.

1. Conclusiones

- *Definir un sistema de medida de bajo coste.*

Se ha logrado desarrollar un sistema de adquisición de datos denominado *Smartfire* basado en plataformas de bajo coste (Arduino y Raspberry-pi), el cual ha demostrado estar dotada de la precisión requerida para llevar a cabo ensayos de tipo mecánico.

A mayores se ha logrado combinar con éxito señales de tipo mecánico con señales externas de otra naturaleza (temperatura, humedad, etc) bajo una aplicación informática basada en tecnología de inteligencia artificial (*soft agents systems*). Concretamente para monitorización y vigilancia, que sumado a las capacidades de comunicación del *Smartfire* amplía las posibilidades futuras de los resultados de la presente investigación.

- *Implementar una técnica de no contacto para la caracterización de materiales compuestos.*

La Correlación Digital de Imágenes ha probado ser una técnica de amplia potencialidad en la evaluación mecánica de materiales, específicamente en materiales altamente tecnológicos como son los materiales compuestos, objeto de este trabajo. De esta manera se posiciona como una estrategia no destructiva, sin contacto y de bajo coste capaz de competir con los sistemas tradicionales tales como las galgas extensiométricas o extensómetros.

- *Explotar los datos ofrecidos por el método DIC para la extracción de las funciones de distribución de las variables mecánicas de composites.*

Se ha conseguido explotar con éxito la técnica de correlación digital de imágenes 2D obteniéndose los datos de campo completo de los parámetros mecánicos de los materiales compuestos; módulo de Young, coeficiente de Poisson, etc. Esto permite avanzar en el diseño mecánico basado en el empleo de composites adoptando enfoques probabilísticos, de tal manera que estos resultados se presentan como más precisos que los arrojados por los enfoques más tradicionales basados en enfoques determinísticos.

- *Integración de Análisis Sensible para la determinación de parámetros críticos.*

Se ha conseguido con éxito incorporar al cálculo el análisis sensible para la determinación de las variables que más afectan al diseño; esto supone un avance en las áreas de conocimiento implicadas, tal que permite una mejor comprensión del comportamiento del material a la par que se reducen los costes computacionales.

- *Generar modelos FEM alimentados mediante DIC y adaptados a procesos de cálculo de tipo estocástico.*

Se avanza en el conocimiento y diseño de modelos basados en el método de elementos finitos, integrando los datos proporcionados por la técnica del DIC en los modelos FEM.

Gracias al conocimiento generado sobre el lenguaje de programación *Python*, se ha conseguido la implementación de variables de tipo probabilístico en los citados modelos, lo que supone un avance al pasar de un cálculo determinístico a uno de tipo estocástico.

- *Evaluar la aplicabilidad de métodos de subrogación o metamodelos para la reducción del coste computacional en simulaciones probabilísticas.*

La metamodelización o implementación de métodos subrogados ha demostrado ser un método eficaz a la hora de reproducir la respuesta mecánica de los elementos a analizar, y se presenta como una herramienta de gran utilidad en estrategias de optimización.

La reducción de tiempos de cálculo alcanzada permite afrontar el cálculo de elementos mecánicos elaborados con materiales compuestos bajo condiciones de tipo probabilístico, que de otra forma sería inasumible. A mayores se ha logrado desarrollar metamodelos con un número de ensayos relativamente bajo.

- *Implementar técnicas de Ingeniería robusta basada en modelos de fiabilidad en el diseño de elementos presurizados.*

Se ha conseguido optimizar el diseño de elementos presurizados gracias a la implementación de la técnica RBDO. A través de la implementación de algoritmos genéticos se seleccionan aquellas soluciones que, siendo fiables se elaboran con el menor consumo de material.

La obtención de diseños fiables se consigue vía ingeniería robusta basada en modelos de fiabilidad, asistida por la implementación de métodos subrogados.

2. Trabajos futuros.

Las técnicas empleadas a lo largo de esta tesis han permitido llevar a buen puerto la investigación desarrollada, cuyo fin era el de resolver las cuestiones planteadas y superar los retos que surgían a medida que el trabajo avanzaba. No obstante, y como consecuencia del avance técnico y metodológico se plantean nuevos retos y posibilidades, lo cual deja abierta las puertas a seguir profundizando en el tema planteado a la par que se buscan nuevas utilidades a la tecnología desarrollada.

Uno de los primeros resultados de este trabajo, el *Smartfire*, ha suscitado gran interés tanto en el entorno industrial más cercano como a nivel internacional. Por lo tanto, se ha planteado proteger la tecnología mediante patente, a la par que seguir trabajando en un desarrollo más robusto de cara a la transferencia tecnológica, sin perder el objetivo de tecnología de bajo coste y gran precisión, fusionándola con tecnologías propias del internet de las cosas (IoT) como p.e. la tecnología Lora.

Se pretende continuar explotando los resultados de campo completo proporcionados por el DIC, avanzando en el cálculo basado en procesos estocásticos implementando la técnica de *Random Fields*.

Otro de los trabajos futuros a acometer es aplicar todo el conocimiento generado a la técnica del *Filament Winding*. La implementación en la línea de investigación de esta técnica supone nuevas variables a la par que nuevas posibilidades, p.e. variar la naturaleza del Liner, lo que permitirá aumentar el rango de aplicaciones.

El siguiente paso natural de esta tesis es dar el salto del DIC2D al DIC3D. Esto supone un reto interesante y lleno de posibilidades tal que permitirá verificar los diseños realizados a nivel macro, a la par que avanzar en conocimiento del material. Por ejemplo, hoy en día el coeficiente de Poisson sólo se determina en la dirección principal estimándose en las otras direcciones debido a la dificultad de obtenerlo por técnicas convencionales; resolver esta cuestión supondrá un avance en la caracterización de los composites.

Bibliografía

- AEMAC. (2005). *Actas del VI congreso nacional de materiales compuestos* (Universidad Politécnica de Valencia, Ed.). Valencia.
- Arunkumar, S., Eshwara Moorthy, P. R., & Karthik, N. (2020). Design optimization of horizontal pressure vessel. *Materials Today: Proceedings*. <https://doi.org/10.1016/j.matpr.2020.02.314>
- Ashby, M. F. (2011). *Chapter 5 - Materials Selection—The Basics* (M. F. B. T.-M. S. in M. D. (Fourth E. Ashby, Ed.). <https://doi.org/10.1016/B978-1-85617-663-7.00005-9>
- Askeland, D. R. (2001). *Ciencia e ingeniería de los materiales* (Cuarta edi). Madrid: Paraninfo.
- ASME BPVC-VIII. Boiler and Pressure Vessel Code*. (2019).
- Barton, R. R., & Meckesheimer, M. (2006). Chapter 18 Metamodel-Based Simulation Optimization. In S. G. Henderson & B. L. B. T.-H. in O. R. and M. S. Nelson (Eds.), *Simulation* (Vol. 13, pp. 535–574). [https://doi.org/10.1016/S0927-0507\(06\)13018-2](https://doi.org/10.1016/S0927-0507(06)13018-2)
- Bautista-De Castro, Á., Sánchez-Aparicio, L. J., Carrasco-García, P., Ramos, L. F., & González-Aguilera, D. (2019). A multidisciplinary approach to calibrating advanced numerical simulations of masonry arch bridges. *Mechanical Systems and Signal Processing*, 129, 337–365. <https://doi.org/10.1016/j.ymssp.2019.04.043>
- Biscaia, H. C., Franco, N., & Chastre, C. (2018). Development of a simple bond-slip model for joints monitored with the DIC technique. *Archives of Civil and Mechanical Engineering*, 18(4), 1535–1546. <https://doi.org/10.1016/j.acme.2018.06.009>
- Callaway, P., Gilbert, M., & Smith, C. C. (2012). Influence of backfill on the capacity of masonry arch bridges. *Proceedings of the Institution of Civil Engineers - Bridge Engineering*, 165(3), 147–157. <https://doi.org/10.1680/bren.11.00038>
- Canal, J. P., Micuzzi, A., Logarzo, H., Terlisky, A., Toscano, R., & Dvorkin, E. (2019). On the finite element modeling of COPVs. *Computers & Structures*, 220, 1–13. <https://doi.org/10.1016/j.compstruc.2019.04.007>
- CC Technologies, I. (Ed.). (2002). *Corrosion Cost and Preventive Strategies in the United States [Summary]*. Retrieved from <https://rosap.ntl.bts.gov/view/dot/39217>
- Chen, S., Chen, W., & Lee, S. (2010). Level set based robust shape and topology optimization under random field uncertainties. *Structural and Multidisciplinary Optimization*, 41(4), 507–524. <https://doi.org/10.1007/s00158-009-0449-2>

- Chung, F. T. H., Li, M. H., Lee, L. L., & Starling, K. E. (1985). An accurate equation of state for carbon dioxide. *Journal of Chemical Engineering of Japan*, 18(6), 490–496. <https://doi.org/10.1252/jcej.18.490>
- Cohen, D. (1997). Influence of filament winding parameters on composite vessel quality and strength. *Composites Part A: Applied Science and Manufacturing*, 28(12), 1035–1047. [https://doi.org/10.1016/S1359-835X\(97\)00073-0](https://doi.org/10.1016/S1359-835X(97)00073-0)
- Cordero Martínez, A. (2017). *Diseño óptimo robusto de topología de estructuras continuas con isolíneas y algoritmos genéticos*. Universidad Politécnica de Cartagena.
- Cui, Z., Liu, Q., Sun, Y., & Li, Q. (2020). On crushing responses of filament winding CFRP/aluminum and GFRP/CFRP/aluminum hybrid structures. *Composites Part B: Engineering*, 200, 108341. <https://doi.org/10.1016/j.compositesb.2020.108341>
- D., T. M., D., E. C., & Masoud, R.-R. (2006). Reliability-Based Optimization of Fiber-Reinforced Polymer Composite Bridge Deck Panels. *Journal of Structural Engineering*, 132(12), 1898–1906. [https://doi.org/10.1061/\(ASCE\)0733-9445\(2006\)132:12\(1898\)](https://doi.org/10.1061/(ASCE)0733-9445(2006)132:12(1898))
- Dan M. Frangopoulou. (2008). *Structural Design Optimization Considering Uncertainties* (1st Edito; M. P. Yannis Tsompanakis, Nikos D. Lagaros, Ed.). <https://doi.org/10.1201/b10995>
- das Neves Carneiro, G., & Conceição António, C. (2019). Global optimal reliability index of implicit composite laminate structures by evolutionary algorithms. *Structural Safety*, 79, 54–65. <https://doi.org/https://doi.org/10.1016/j.strusafe.2019.03.001>
- Delogu, M., Zanchi, L., Dattilo, C. A., & Pierini, M. (2017). Innovative composites and hybrid materials for electric vehicles lightweight design in a sustainability perspective. *Materials Today Communications*, 13, 192–209. <https://doi.org/10.1016/j.mtcomm.2017.09.012>
- Díaz, J., Cid Montoya, M., & Hernández, S. (2016). Efficient methodologies for reliability-based design optimization of composite panels. *Advances in Engineering Software*, 93, 9–21. <https://doi.org/10.1016/j.advengsoft.2015.12.001>
- Dong, Y. L., & Pan, B. (2017). A Review of Speckle Pattern Fabrication and Assessment for Digital Image Correlation. *Experimental Mechanics*, 57(8), 1161–1181. <https://doi.org/10.1007/s11340-017-0283-1>
- Duell, J. M., Wilson, J. M., & Kessler, M. R. (2008). Analysis of a carbon composite overwrap pipeline repair system. *International Journal of Pressure Vessels and Piping*, 85(11), 782–788. <https://doi.org/10.1016/j.ijpvp.2008.08.001>
- Enoma, N., & Zingoni, A. (2020). Analytical formulation and numerical modelling for multi-shell toroidal pressure vessels. *Computers & Structures*, 232, 105811. <https://doi.org/10.1016/j.compstruc.2017.07.013>
- Fleischer, J., Teti, R., Lanza, G., Mativenga, P., Möhring, H.-C., & Caggiano, A. (2018). Composite materials parts manufacturing. *CIRP Annals*, 67(2), 603–626. <https://doi.org/10.1016/j.cirp.2018.05.005>

- Gabriel, P. F., Verly, J. G., Piater, J. H., & Genon, A. (2003). The state of the art in multiple object tracking under occlusion in video sequences. *Advanced Concepts for Intelligent Vision Systems*, 166–173.
- Ger, G. S., Hwang, D. G., Chen, W. Y., & Hsu, S. E. (1988). Design and fabrication of high performance composite pressure vessels. *Theoretical and Applied Fracture Mechanics*, 10(2), 157–163. [https://doi.org/https://doi.org/10.1016/0167-8442\(88\)90007-9](https://doi.org/https://doi.org/10.1016/0167-8442(88)90007-9)
- Gibson, R. F. (2010). A review of recent research on mechanics of multifunctional composite materials and structures. *Composite Structures*, 92(12), 2793–2810. <https://doi.org/10.1016/j.compstruct.2010.05.003>
- Hackworth, M. R., & Henshaw, J. M. (2000). A pressure vessel fracture mechanics study of the aluminum beverage can. *Engineering Fracture Mechanics*, 65(5), 525–539. [https://doi.org/10.1016/S0013-7944\(99\)00144-7](https://doi.org/10.1016/S0013-7944(99)00144-7)
- Hild, F., & Roux, S. (2006). Digital Image Correlation: from Displacement Measurement to Identification of Elastic Properties – a Review. *Strain*, 42(2), 69–80. <https://doi.org/10.1111/j.1475-1305.2006.00258.x>
- Hoffmann, K. (1974). *Applying the Wheatstone bridge circuit*. HBM Germany.
- Hua, T., Xie, H., Wang, S., Hu, Z., Chen, P., & Zhang, Q. (2011). Evaluation of the quality of a speckle pattern in the digital image correlation method by mean subset fluctuation. *Optics & Laser Technology*, 43(1), 9–13. <https://doi.org/10.1016/j.optlastec.2010.04.010>
- Informe anual SEDIGAS*. (2018).
- ISO 15649 Industrias de petróleo y gas natural - Tuberías*. (2001).
- J.Massa, J.Giro, A. G. (2015). *Compendio de Cálculo estructural II*. FCEFyN-UNC.
- Kendall, D. (2007). Building the future with FRP composites. *Reinforced Plastics*, 51(5), 26–33. [https://doi.org/10.1016/S0034-3617\(08\)70131-0](https://doi.org/10.1016/S0034-3617(08)70131-0)
- Koziol, J. A. (1987). Book Reviews:Goodness-of-Fit Techniques Ralph B. D'Agostino, Michael A. Stephens (Eds.) New York : Marcel Dekker, 1986. xviii + 560 pp. *Journal of Educational Statistics*, 12(4), 412–416. <https://doi.org/10.3102/10769986012004412>
- Lee, H. Y., & Jeong, J. Y. (2020). Quantification of conservatism in pressure vessel design subjected to long-term creep conditions as per ASME Section VIII division 2. *International Journal of Pressure Vessels and Piping*, 180(January), 104039. <https://doi.org/10.1016/j.ijpvp.2019.104039>
- Lopez, R., & Beck, A. (2012). Reliability-Based Design Optimization Strategies Based on FORM: A Review. *Journal of the Brazilian Society of Mechanical Sciences and Engineering*, 34, 506–514. <https://doi.org/10.1590/S1678-58782012000400012>
- Luu, L., Wang, Z., Vo, M., Hoang, T., & Ma, J. (2011). Accuracy enhancement of digital image correlation with B-spline interpolation. *Opt. Lett.*, 36(16), 3070–3072. <https://doi.org/10.1364/OL.36.003070>

- Marelli, S., & Sudret, B. (n.d.). UQLab: A Framework for Uncertainty Quantification in Matlab. In *Vulnerability, Uncertainty, and Risk* (pp. 2554–2563). <https://doi.org/10.1061/9780784413609.257>
- Mazurkiewicz, L., Tomaszewski, M., Malachowski, J., Sybilski, K., Chebakov, M., Witek, M., ... Dmitrienko, R. (2017). Experimental and numerical study of steel pipe with part-wall defect reinforced with fibre glass sleeve. *International Journal of Pressure Vessels and Piping*, 149, 108–119. <https://doi.org/10.1016/j.ijpvp.2016.12.008>
- Miravete, A. (2011). *Materiales compuestos Vol. 1 y 2* (Miravete, Ed.).
- Miyamoto, K., & Minamiguchi, H. (1995). *Composite prepreg and tennis rackets using the same*. Google Patents.
- Moustapha, M., & Sudret, B. (2019). Surrogate-assisted reliability-based design optimization: a survey and a unified modular framework. *Structural and Multidisciplinary Optimization*, 60(5), 2157–2176. <https://doi.org/10.1007/s00158-019-02290-y>
- Nicolich, M. (1993). Pressure vessel manufacturing: Mechanical analysis of gas bottles with convex end-plates. *International Journal of Pressure Vessels and Piping*, 55(3), 423–433. [https://doi.org/10.1016/0308-0161\(93\)90061-W](https://doi.org/10.1016/0308-0161(93)90061-W)
- Ochola, R. O., Marcus, K., Nurick, G. N., & Franz, T. (2004). Mechanical behaviour of glass and carbon fibre reinforced composites at varying strain rates. *Composite Structures*, 63(3), 455–467. [https://doi.org/10.1016/S0263-8223\(03\)00194-6](https://doi.org/10.1016/S0263-8223(03)00194-6)
- Orell, O., Vuorinen, J., Jokinen, J., Kettunen, H., Hytönen, P., Turunen, J., & Kanerva, M. (2018). Characterization of elastic constants of anisotropic composites in compression using digital image correlation. *Composite Structures*, 185, 176–185. <https://doi.org/10.1016/j.compstruct.2017.11.008>
- Padaui, T., & Enrique, A. (2013). *Algoritmo para calcular esfuerzos y criterios de falla de Tsai-Hill, Tsai-Wu, Hashim y Hashim-Rotem en agujeros circulares en laminados de fibra de vidrio*.
- Rafiee, R. (2016). On the mechanical performance of glass-fibre-reinforced thermosetting-resin pipes: A review. *Composite Structures*, 143, 151–164. <https://doi.org/10.1016/j.compstruct.2016.02.037>
- Rafiee, R. (2017). Stochastic fatigue analysis of glass fiber reinforced polymer pipes. *Composite Structures*, 167, 96–102. <https://doi.org/10.1016/j.compstruct.2017.01.068>
- Rafiee, R., Reshadi, F., & Eidi, S. (2015). Stochastic analysis of functional failure pressures in glass fiber reinforced polyester pipes. *Materials & Design*, 67, 422–427. <https://doi.org/10.1016/j.matdes.2014.12.003>
- Rafiee, R., & Torabi, M. A. (2018). Stochastic prediction of burst pressure in composite pressure vessels. *Composite Structures*, 185, 573–583. <https://doi.org/10.1016/j.compstruct.2017.11.068>
- Reddy, J. N. (2003). *Mechanics of laminated composite plates and shells: theory and analysis*. CRC press.

- Sampson, R. C. (1970). A stress-optic law for photoelastic analysis of orthotropic composites. *Experimental Mechanics*, 10(5), 210–215. <https://doi.org/10.1007/BF02324034>
- Sasikumar, P., Suresh, R., Vijayaghosh, P. K., & Gupta, S. (2015). Experimental characterisation of random field models for CFRP composite panels. *Composite Structures*, 120, 451–471. <https://doi.org/10.1016/j.compstruct.2014.10.023>
- Schuëller, G. I., & Jensen, H. A. (2008). Computational methods in optimization considering uncertainties – An overview. *Computer Methods in Applied Mechanics and Engineering*, 198(1), 2–13. <https://doi.org/10.1016/j.cma.2008.05.004>
- Seif, M. A., Khashaba, U. A., & Rojas-Oviedo, R. (2007). Measuring delamination in carbon/epoxy composites using a shadow moiré laser based imaging technique. *Composite Structures*, 79(1), 113–118. <https://doi.org/10.1016/j.compstruct.2005.11.039>
- Shamsuddoha, M., Islam, M. M., Aravindhan, T., Manalo, A., & Lau, K. tak. (2013). Effectiveness of using fibre-reinforced polymer composites for underwater steel pipeline repairs. *Composite Structures*, 100, 40–54. <https://doi.org/10.1016/j.compstruct.2012.12.019>
- Sutton, H. S.-J. O. A. (2009). *Image Correlation for Shape, Motion and Deformation Measurements*. <https://doi.org/10.1007/978-0-387-78747-3>
- Sutton, M. A., Wolters, W. J., Peters, W. H., Ranson, W. F., & McNeill, S. R. (1983). Determination of displacements using an improved digital correlation method. *Image and Vision Computing*, 1(3), 133–139. [https://doi.org/10.1016/0262-8856\(83\)90064-1](https://doi.org/10.1016/0262-8856(83)90064-1)
- Takeuchi, T., Kakubo, Y., Matsukawa, Y., Nozawa, Y., Toyama, T., Nagai, Y., ... Suzuki, M. (2014). Effects of thermal aging on microstructure and hardness of stainless steel weld-overlay claddings of nuclear reactor pressure vessels. *Journal of Nuclear Materials*, 452(1), 235–240. <https://doi.org/10.1016/j.jnucmat.2014.04.003>
- Tekieli, M., De Santis, S., de Felice, G., Kwiecień, A., & Roscini, F. (2017). Application of Digital Image Correlation to composite reinforcements testing. *Composite Structures*, 160, 670–688. <https://doi.org/10.1016/j.compstruct.2016.10.096>
- The world factbook field listing: pipelines.* (2013). Retrieved from Central Intelligence Agency (USA)
- UNE-EN 764 *Equipos a presión*. (2015).
- Vanegas Useche, L., & Arias Maya, L. (2004). Falla De Los Materiales Compuestos Laminados. *Scientia et Technica*, 2(25), 113–118. <https://doi.org/10.22517/23447214.7215>
- Vasiliev, V. V., & Morozov, E. (2001). *Mechanics and Analysis of Composite Materials*.
- Velosa, J. C., Nunes, J. P., Antunes, P. J., Silva, J. F., & Marques, A. T. (2009). Development of a new generation of filament wound composite pressure cylinders. *Composites Science and Technology*, 69(9), 1348–1353. <https://doi.org/10.1016/j.compscitech.2008.09.018>

- Venkateshwar Reddy, C., Ramesh Babu, P., Ramnarayanan, R., & Das, D. (2017). Mechanical Characterization Of Unidirectional Carbon And Glass/Epoxy Reinforced Composites For High Strength Applications. *Materials Today: Proceedings*, 4(2, Part A), 3166–3172. <https://doi.org/10.1016/j.matpr.2017.02.201>
- Viguié, J., Dumont, P. J. J., Orgéas, L., Vacher, P., Desloges, I., & Mauret, E. (2011). Surface stress and strain fields on compressed panels of corrugated board boxes. An experimental analysis by using Digital Image Stereocorrelation. *Composite Structures*, 93(11), 2861–2873. <https://doi.org/10.1016/j.compstruct.2011.05.018>
- Wang, C. H., & Duong, C. N. (2016). *Chapter 2 - Failure criteria* (C. H. Wang & C. N. B. T.-B. J. and R. to C. A. S. Duong, Eds.). <https://doi.org/10.1016/B978-0-12-417153-4.00002-5>
- Yang, M., Zhang, D., & Han, X. (2020). New efficient and robust method for structural reliability analysis and its application in reliability-based design optimization. *Computer Methods in Applied Mechanics and Engineering*, 366, 113018. <https://doi.org/10.1016/j.cma.2020.113018>
- Zhu, G., Sun, G., Li, G., Cheng, A., & Li, Q. (2018). Modeling for CFRP structures subjected to quasi-static crushing. *Composite Structures*, 184, 41–55. <https://doi.org/10.1016/j.compstruct.2017.09.001>

Anexo I

INDEXACIÓN Y FACTOR DE IMPACTO DE LAS PUBLICACIONES CIENTÍFICAS

Artículo 1: Smartfire, Intelligent platform for monitoring fire extinguishers and their building environment

Revista	Sensor
URL	https://www.mdpi.com/journal/sensors
Editorial	MDPI
Factor de impacto	3.275
JCR	
SJR 2019	0.65
Quartil	Q1
Ranking	10/63



Artículo 2: Combining digital image correlation and probabilistic approaches for the reliability analysis of composite pressure vessels

Revista	Construction and Building Materials
URL	https://www.journals.elsevier.com/construction-and-building-materials
Editorial	Elsevier
Factor de impacto	4.419
JCR	
SJR 2019	1.491
Quartil	Q1
Ranking	10/174



Artículo 3: Digital image correlation and reliability-based methods for the design and repair of pressure pipes through composite solutions

Revista	Archives of Civil and Mechanical Engineering
URL	http://www.elsevier.com/locate/acme
Editorial	Elsevier
Factor de impacto	3.672
JCR	
SJR 2019	0.947
Quartil	Q1
Ranking	22/130

